University of Florida
Civil and Coastal Engineering
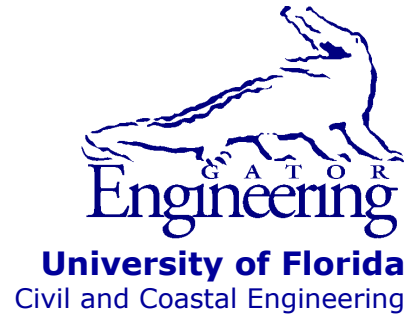
Final Report   March 2017

Distribution Factors for Construction Loads and Girder Capacity Equations

Principal investigator:
Gary R. Consolazio, Ph.D.

Graduate research assistant:
Jeffrey M. Honig

Department of Civil and Coastal Engineering
University of Florida
P.O. Box 116580
Gainesville, Florida 32611

DISCLAIMER

The opinions, findings, and conclusions expressed in this publication are those of the authors and not necessarily those of the State of Florida Department of Transportation.

SI (MODERN METRIC) CONVERSION FACTORS
*APPROXIMATE CONVERSIONS **TO** SI UNITS*

SYMBOL	WHEN YOU KNOW	MULTIPLY BY	TO FIND	SYMBOL
LENGTH				
in	inches	25.4	millimeters	mm
ft	feet	0.305	meters	m
yd	yards	0.914	meters	m
mi	miles	1.61	kilometers	km
AREA				
in^2	square inches	645.2	square millimeters	mm^2
ft^2	square feet	0.093	square meters	m^2
yd^2	square yard	0.836	square meters	m^2
ac	acres	0.405	hectares	ha
mi^2	square miles	2.59	square kilometers	km^2
VOLUME				
fl oz	fluid ounces	29.57	milliliters	mL
gal	gallons	3.785	liters	L
ft^3	cubic feet	0.028	cubic meters	m^3
yd^3	cubic yards	0.765	cubic meters	m^3
NOTE: volumes greater than 1000 L shall be shown in m^3				
MASS				
oz	ounces	28.35	grams	g
lb	pounds	0.454	kilograms	kg
T	short tons (2,000 lb)	0.907	Megagrams	Mg (or "t")
TEMPERATURE (exact degrees)				
ºF	Fahrenheit	5(F-32)/9 or (F-32)/1.8	Celsius	ºC
FORCE and PRESSURE or STRESS				
kip	1,000 pound force	4.45	kilonewtons	kN
lbf	pound force	4.45	newtons	N
lbf/in^2	pound force per square inch	6.89	kilopascals	kPa
ksi	kips force per square inch	6.89	Megapascals	MPa

TECHNICAL REPORT DOCUMENTATION PAGE

1. Report No.	2. Government Accession No.	3. Recipient's Catalog No.

4. Title and Subtitle	5. Report Date
Distribution factors for construction loads and girder capacity equations	March 2017
	6. Performing Organization Code
	8. Performing Organization Report No.

7. Author(s)	
Gary R. Consolazio, Jeffrey M. Honig	2017/124011

9. Performing Organization Name and Address	10. Work Unit No. (TRAIS)
University of Florida	
Department of Civil and Coastal Engineering	11. Contract or Grant No.
365 Weil Hall, P.O. Box 116580	BDV31-977-46
Gainesville, FL 32611-6580	

12. Sponsoring Agency Name and Address	13. Type of Report and Period Covered
Florida Department of Transportation	
Research Management Center	Final Report
605 Suwannee Street, MS 30	
Tallahassee, FL 32399-0450	14. Sponsoring Agency Code

15. Supplementary Notes

16. Abstract

During the process of constructing a highway bridge, there are several construction stages that warrant consideration from a structural safety and design perspective. The first objective of the present study was to use analytical models of prestressed concrete girders (Florida-I Beams) at multiple stages of construction to update previously developed capacity equations for wind load and gravity load. Updated analytical bridge models were developed that accounted for a revised definition of lateral girder sweep—one that accounted for both maximum allowable fabrication tolerance as well as transverse thermal gradients (i.e., thermally induced sweep). Subsequently, analytical parametric studies were conducted to update—using the revised definition of sweep—previously developed girder capacity equations. The updated capacity equations take into consideration different Florida-I Beam cross-sections, span lengths, wind loads, skew angles, and brace stiffnesses.

A second objective in this study was to use finite element analyses of partially constructed bridge systems—consisting of multiple Florida-I Beam (FIBs) with construction loads—to quantify distribution factors for interior and exterior girder end shear forces and maximum girder moments. A large-scale parametric study was conducted with consideration of different Florida-I Beam cross-sections, span lengths, girder spacing, deck overhang widths, skew angles, number of girders, number of braces, and bracing configurations (K-brace and X-brace) to quantify shear and moment distribution factor data. These data were subsequently used to develop empirical construction stage distribution factor (*DF*) equations at multiple levels of design conservatism.

17. Key Words	18. Distribution Statement
Distribution factor, construction load, thermal sweep, girder stability, wind load	No restrictions.

19. Security Classif. (of this report)	20. Security Classif. (of this page)	21. No. of Pages	22. Price
Unclassified	Unclassified	127	

Form DOT F 1700.7 (8-72). Reproduction of completed page authorized

ACKNOWLEDGEMENTS

EXECUTIVE SUMMARY

During the process of constructing a highway bridge, there are several construction stages that warrant consideration from a structural safety and design perspective. The first objective of the present study was to use analytical models of prestressed concrete girders (Florida-I Beams) at multiple stages of construction to update previously developed capacity equations for wind load and gravity load. Updated analytical bridge models were developed that accounted for a revised definition of lateral girder sweep—one that accounted for both maximum allowable fabrication tolerance as well as transverse thermal gradients (i.e., thermally induced sweep). Subsequently, analytical parametric studies were conducted to update—using the revised definition of sweep—previously developed girder capacity equations. The updated capacity equations take into consideration different Florida-I Beam cross-sections, span lengths, wind loads, skew angles, and brace stiffnesses.

A second objective in this study was to use finite element analyses of partially constructed bridge systems—consisting of multiple Florida-I Beam (FIBs) with construction loads—to quantify distribution factors for interior and exterior girder end shear forces and maximum girder moments. A large-scale parametric study was conducted with consideration of different Florida-I Beam cross-sections, span lengths, girder spacing, deck overhang widths, skew angles, number of girders, number of braces, and bracing configurations (K-brace and X-brace) to quantify shear and moment distribution factor data. These data were subsequently used to develop empirical construction stage distribution factor (*DF*) equations at multiple levels of design conservatism.

TABLE OF CONTENTS

LIST OF FIGURES

LIST OF TABLES

CHAPTER 1
INTRODUCTION

1.1 Background

During the process of constructing a highway bridge, there are several construction stages that warrant consideration from a structural safety and design perspective. Initially, individual girders are lifted by crane and placed into position atop flexible bearing pads located on the bridge supports (e.g., abutments or piers). The most critical phase of construction, with regard to stability, is after girder placement (prior to the casting of the deck), when girders are supported only by bearing pads and can be subject to high lateral wind loads.

The stage at which wind loading is often most critical occurs when the first girder is erected. At this stage of construction, other girders are not present to brace against, hence the initial girder can only be anchored to the pier at the ends. For bridge designs in which girder stability is a primary concern, girder erection can sometimes be scheduled to minimize the exposure period for the initial girder, so that—statistically—it is less likely that peak wind forces will occur. However, meeting such a schedule is not always feasible, and adverse weather conditions cannot necessarily be anticipated. For example, strong afternoon thunderstorms can form rapidly in Florida during the summer months. In such situations, it is important to be able to assess in advance whether anchor bracing will be needed to prevent girder collapse under the effects of wind loads.

Furthermore, placement of all girders into their final position constitutes another distinct structural stage that must be assessed for safety. In this structural configuration, it is typical for temporary braces (Figure 1.1) to be installed between the individual girders to form a more stable structural unit (Consolazio and Edwards, 2014). Additionally, one or more girders may also be anchored to the bridge supports (Consolazio et al., 2013). Structurally, the system at this stage consists of individual girders, bearing pads, braces, potentially anchors, and support structures (i.e., substructures).

Figure 1.1 Prestressed concrete girders braced together for stability

After continued construction progress, another key stage will be reached wherein stay-in-place (SIP) forms have been installed between the girders and overhang formwork (and associated overhang support brackets) have been eccentrically attached to the exterior (fascia) girders of the bridge. Loading conditions at this stage consist primarily of vertical 'construction loads' that are associated with the process of placing the wet (non-structural) concrete deck

(Figure 1.2) and finishing it with a finishing machine (i.e., a 'bridge paver'). During deck placement, most of the construction loads are applied eccentrically to overhang formwork and to stay-in-place forms. Consequently, both interior and exterior girder moments and end shear forces produced by construction loads must be considered in the bridge design process. Furthermore, several geometric parameters influence the magnitude and distribution of maximum girder moments and girder end shears that are caused by construction loads.

Figure 1.2 Bridge construction loads

1.2 Objectives

One objective of the present study was to use analytical models of prestressed concrete girders (Florida-I Beams), at multiple stages of construction, to update previously developed capacity equations (Consolazio et al., 2013) for wind load and gravity load. Specifically, the analytical models were updated to account for a revised definition of sweep—one that included not only fabrication sweep, but also thermally-induced sweep. An additional objective was to use finite element analysis models of partially constructed bridge systems—consisting of multiple Florida-I Beam (FIBs)—with construction loads applied (Consolazio and Edwards, 2014) to quantify interior and exterior girder end shear forces and maximum girder moments. Computed end shear forces and maximum moments were subsequently used to develop empirical construction stage distribution factor (*DF*) equations.

1.3 Scope of work

- Revise sweep definition: In FDOT project BDK75-977-33 (Consolazio et al., 2013), results from multiple analytical parametric studies were used to develop simplified girder-capacity and bridge-capacity equations. Girder sweep values were intended to account for fabrication tolerances, limited to ⅛ in. for every 10 ft of girder length, and not to exceed 1.5 in. In the present study, a literature review was conducted to develop an updated definition of initial girder sweep—one in which the effects of transverse thermal gradients (i.e., thermal sweep) were added and the previously imposed maximum limit of 1.5 in. removed.

- Update previously-developed individual-girder and multi-girder (system) capacity equations: Using the revised definition of sweep, analysis procedures and finite element models of unanchored FIB bridge girders with wind loads were used to revise the BDK75-977-33 equation for unanchored-girder wind capacity [$P_{max,0}$, reported as Eqn. (8.2) in Consolazio et al. (2013)]. Additionally, the equation for 'baseline' unanchored two-girder strut-braced system buckling capacity in zero-wind [C_0, reported as Eqn. (9.2) in Consolazio et al. (2013)] was updated to reflect the revised definition of sweep. A limited-scope parametric study was subsequently conducted to ensure that the equation for multi-girder moment-resisting-braced system capacity [C, reported as Eqn. (9.23) in Consolazio et al. (2013)], supplemented by the updated baseline equation (C_0) remained conservative relative to corresponding capacities computed using finite element analyses.

- Develop distribution factor equations: Bridge modeling and analysis procedures were developed and used to conduct a large-scale construction-load parametric study—covering typical ranges of possible bridge system configurations. Girder end shear forces and maximum moments due to superimposed construction loads were quantified and subsequently used to develop empirical distribution factor (DF) equations.

CHAPTER 2
PHYSICAL DESCRIPTION OF BRIDGES DURING CONSTRUCTION

2.1 Introduction

Girder types under investigation in this study were Florida-I Beams (FIBs), a group of standard cross-sectional shapes of varying depths that are commonly employed in Florida bridge designs. These beams are typically cast offsite, transported to the construction site, then lifted into position one-at-a-time by crane, where they are placed on elastomeric bearing pads and braced together for stability. In this chapter, a physical description of the 'construction-stage' structures under consideration will be provided along with definition of relevant terminology.

2.2 Geometric parameters

The term *girder system* will be used to refer to a group of two or more FIBs braced together in an evenly spaced row (Figure 2.1). In addition to span length and lateral spacing, several additional geometric parameters define the shape and placement of the girders within a system:

- Grade: Longitudinal incline of the girders, typically expressed as a percentage of rise per unit of horizontal length (Figure 2.2).
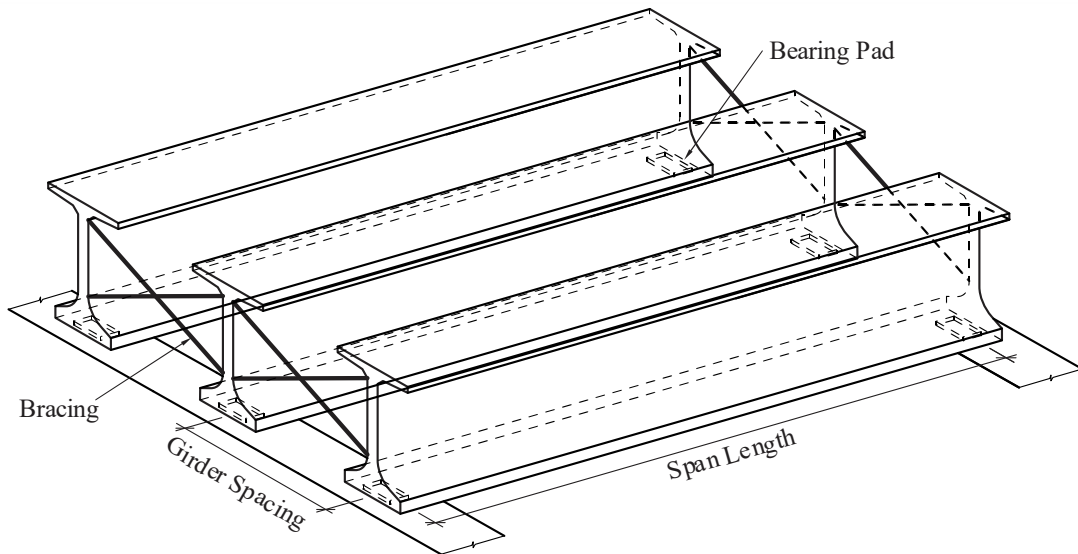
Figure 2.1 Girder system
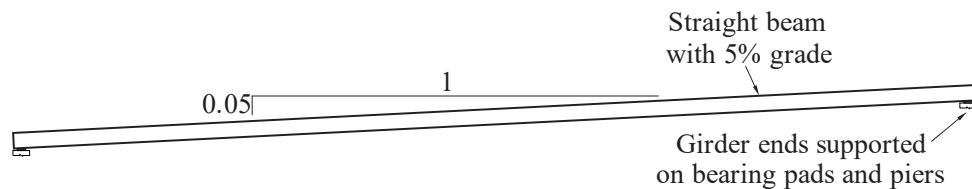
Figure 2.2 Definition of grade (elevation view)

- Cross-slope: The transverse incline (slope) of the deck, expressed as a percentage, which results in girders that are staggered vertically (Figure 2.3).
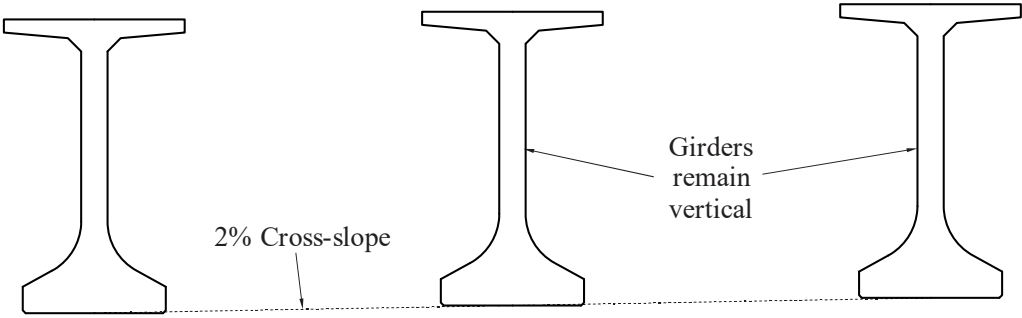
Figure 2.3 Definition of cross-slope (section view)

- Skew angle: Longitudinal staggering of girders, due to pier caps that are not perpendicular to the girder axes (Figure 2.4).
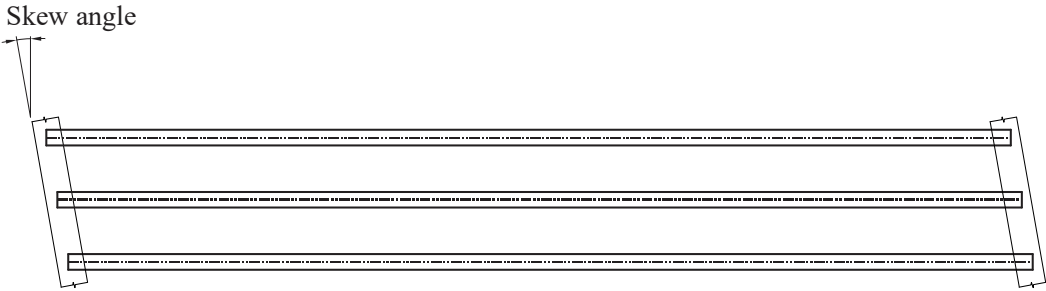
Figure 2.4 Definition of skew (plan view)

- Camber: Vertical bowing of the girder (Figure 2.5) due to prestressing in the bottom flange; expressed as the maximum vertical deviation from a perfectly straight line connecting one end of the girder to the other.
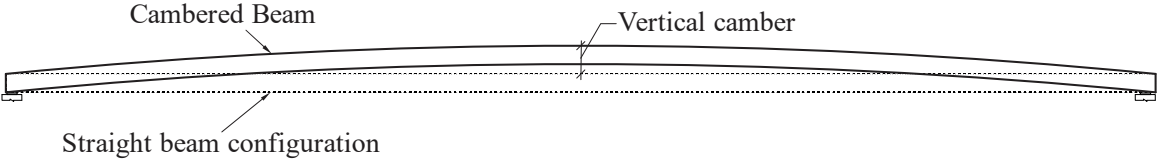
Figure 2.5 Definition of camber (elevation view)

- Sweep: Lateral bowing of the girder (Figure 2.6), expressed as the maximum horizontal deviation from a perfectly straight line connecting one end of the girder to the other.

Straight beam configuration

Lateral sweep

Beam with sweep imperfection
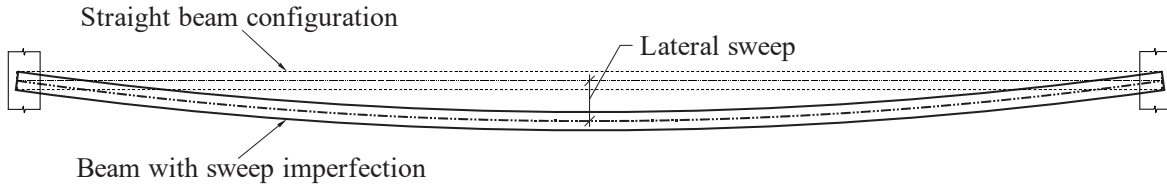
Figure 2.6 Definition of sweep (plan view)

2.3 Bearing pads

FIB bridge girders rest directly on steel-reinforced elastomeric bearing pads which are the only points of contact between the girder and the substructure. There is generally sufficient friction between the pad and other structural components so that any movement of a girder relative to the substructure (with the exception of vertical uplift) must displace the top surface of the pad relative to the bottom surface. As a result, the girder support conditions in all six degrees of freedom (three translations, and three rotations) can be represented as finite stiffnesses that correspond to the equivalent deformation modes of the pad. These deformation modes fall into four categories: shear, compression (axial), rotation (e.g., roll), and torsion. Bearing pad stiffnesses in this study were quantified using calculation procedures developed and experimentally validated in a previous study (BDK75-977-33, Consolazio et al., 2013) for typical Florida bridge bearing pads.

2.4 Bracing

As adjacent girders are erected during the bridge construction process, girder-to-girder braces (henceforth referred to simply as *braces*) are used to connect the girders together into a single structural unit. At a minimum, braces are installed near the ends of the girders (close to the supporting piers); such braces are referred to as *end-span braces*. In addition, *intermediate-span braces* spaced at unit fractions (1/2, 1/3, 1/4) of the girder length may also be included. For example, quarter-point (1/4 span) bracing divides the girder into four (4) equal unbraced lengths (Figure 2.7).
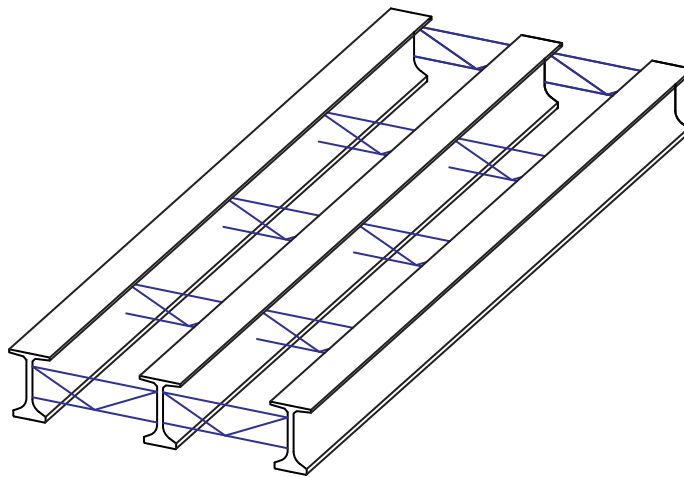
Figure 2.7 Girder system with quarter-point bracing

When skew is present, brace point locations are longitudinally offset (Figure 2.8) between adjacent girders because *FDOT Design Standard No. 20005: Prestressed I-Beam Temporary Bracing* (FDOT, 2014a) requires that all braces be placed perpendicular to the girders.
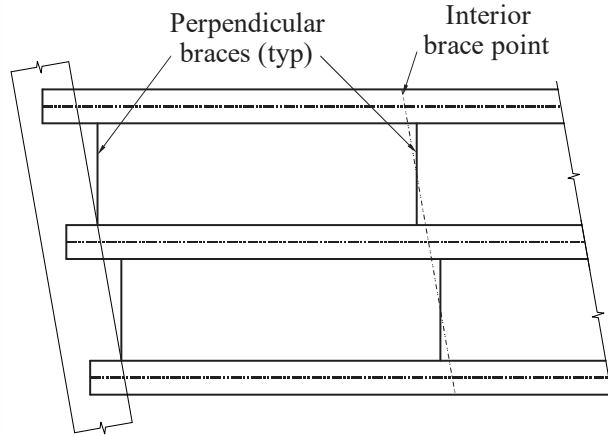
Figure 2.8 Perpendicular brace placement on skewed bridge (plan view)

Braces are typically constructed from timber or steel members, but individual brace designs are left to the discretion of the contractor, so a variety of different bracing configurations are possible. Common types of braces used in practice in Florida include X-braces (Figure 2.9a) and K-braces (Figure 2.9b). Braces are typically attached to the girders using bolted connections or welded to cast-in steel plates.

(a)   (b)
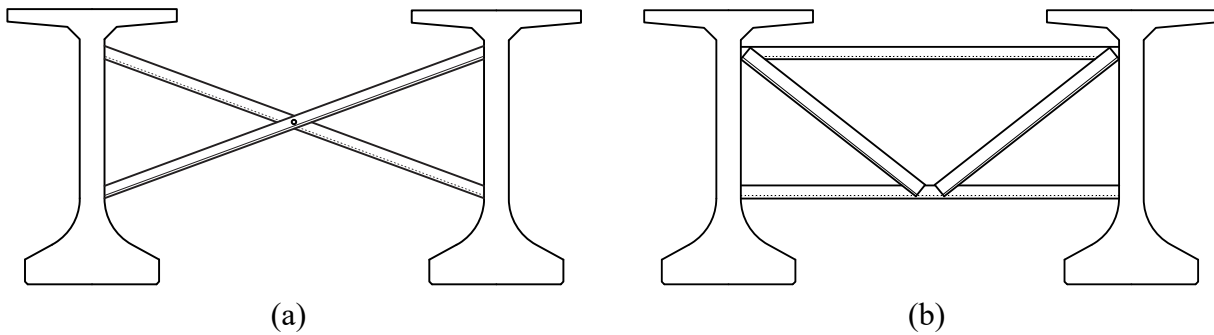
Figure 2.9 Common brace types: (a) X-brace; (b) K-brace

CHAPTER 3
GIRDER SWEEP INCLUDING THERMAL GRADIENT EFFECTS

3.1 Introduction

A primary objective of the present study involved revising previously developed girder capacity equations (for wind load and gravity load) to account for a revised definition of girder sweep. Previous girder capacity equations were developed from finite element analysis (FEA) models used in BDK75-977-33 (Consolazio et al., 2013), where girder capacity was reached when a girder (or girder system) became unstable. Lateral deflection, and ultimately instability of the analytical models was initiated by the introduction of girder imperfections (i.e., sweep). In the present study, the definition of girder sweep has been revised by removing the previously imposed maximum fabrication limit of 1.5 in. and by including the effects of transverse thermal temperature gradients (i.e., thermal sweep).

3.2 Literature review: thermal sweep

In Lee (2010), equations for determining maximum vertical and lateral deflections caused by solar-induced thermal gradients were presented for four (4) typical AASHTO-PCI bridge girder types. Lee used finite element heat transfer models, validated using experimental test data, to calculate non-linear temperature gradients for prestressed concrete girders of varying cross-sectional shapes. Each finite element model incorporated environmental conditions that included the solar radiation level (based on geographic location), ambient air temperature, and wind speed. By imposing 'extreme' environmental conditions (determined from monthly averages of data recorded over a 30 year period) on each finite element model, Lee computed transverse non-linear temperature gradients in the top flange, web, and bottom flange of four (4) typical AASHTO-PCI bulb-tee bridge girders. Primary environmental conditions employed in the study were established for the Atlanta, Georgia geographical area. However, to further assess temperature gradients for different geographical locations, Lee also evaluated extreme environmental conditions for seven (7) additional cities, distributed across the continental United States. Of the eight (8) cities considered, Atlanta, Georgia was closest in proximity to the state of Florida, therefore data for Atlanta were used in the present study (BDV31-977-46) to quantify thermally induced sweep values for Florida FIB girder sections.

Using both experimentally measured temperature data as well gradients computed from finite element thermal analyses, Lee (2012) also proposed a set of simplified transverse temperature gradients (replicated in Figure 3.1) for the top flange, web, and bottom flange of prestressed concrete girders. Using the proposed simplified gradients, maximum transverse deflection (i.e., sweep) induced by thermal gradients can be calculated for general bridge girder shapes and arbitrary span lengths by employing procedures such as moment-curvature analysis.
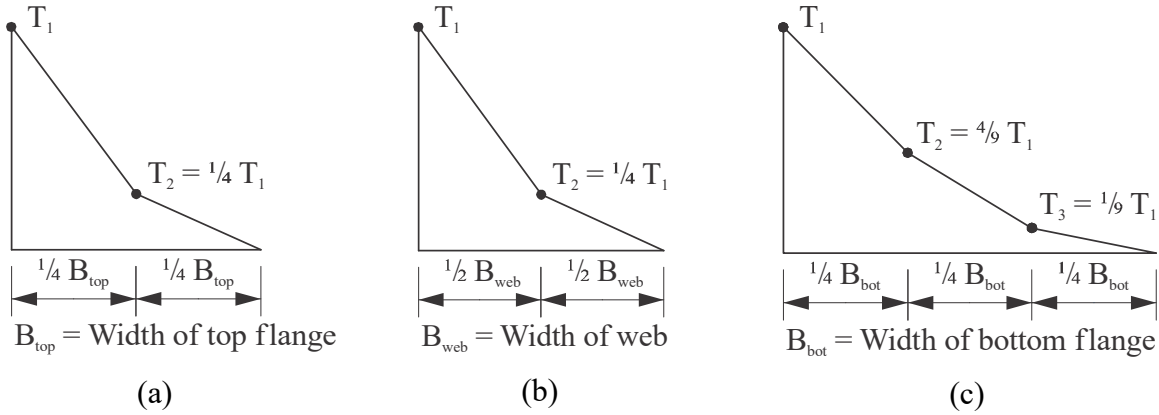
Figure 3.1 Transverse thermal gradients of prestressed concrete bridge girders
proposed by Lee (2012): (a) Top flange; (b) Web; (c) Bottom flange

To assess the accuracy of both the maximum thermal sweep equations and the simplified thermal gradients, thermal sweep data were analytically computed using the equations proposed by Lee, and then compared to experimentally measured thermal sweep data published in the literature. Experimental data used in this evaluation process were obtained from an investigation of a bridge collapse in Arizona (CTL Group, 2007), and from research conducted for the Georgia DOT (Hurff, 2010). After computing tolerance limits on fabrication-related sweep imperfection, as set forth in the PCI Bridge Design Manual (2011), Hurff (2010) demonstrated that maximum experimentally measured thermal sweep was as much as 48% of the maximum allowable fabrication sweep. In a separate experimental study, measured sweep data reported by the CTL Group indicated a maximum thermal sweep of 0.65 in. for a 114 ft girder. At this magnitude, thermal sweep was approximately 46% of the allowable fabrication sweep for a girder of the same length. Analytical sweep values computed using the maximum sweep equations proposed by Lee (2010) were found to be in good agreement with the experimental data reported by Hurff (2010) and the CTL Group (2007).

The simplified gradients proposed by Lee (2012) were derived from non-linear temperature gradients computed from finite element thermal analyses (FEA) of typical BT-63 and Type-V girder cross-sections. Each such simplified gradient (Figure 3.2a) consisted of a descending 'left side' branch corresponding to the side of the girder directly exposed to solar radiation, and an ascending 'right side' branch corresponding to secondary solar heating. To ensure that conservatively large predictions of maximum thermal sweep were obtained for prestressed concrete bridge girders, the rise in temperature on the 'right side' of the FEA gradients was omitted from the simplified gradients proposed by Lee (2012, Figure 3.2b). Lateral sweeps computed using these simplified ('left side' only) gradients will produce larger (i.e., more conservative) thermal sweep quantities than those computed using the more complex, two-sided gradients. To avoid introducing excess-conservatism into the thermal sweeps calculated in the present study, an approximate 'right side' ascending branch was added to the simplified ('left side' only) gradients proposed by Lee (2012). Using the two-sided non-linear FEA temperature gradients documented by Lee (2010), a temperature ratio (λ) was computed as:

$$\lambda = \frac{T_{R,FEA}}{T_{1,FEA}} \tag{3.1}$$

An approximate 'right side' linear ascending branch (Figure 3.2c) of the gradient was then defined as maximizing at temperature $T_{R,SIMP}$ (Figure 3.2c) where:

$$T_{R,SIMP} = \lambda \left(T_{1,SIMP} \right) \tag{3.2}$$

and $T_{1,SIMP}$ is the maximum 'left side' temperature from the simplified gradients proposed by Lee (2012). The simplified gradient proposed by Lee (2012) for the bottom flange also omitted an ascending right side branch; therefore, a quantity, $T_{R,SIMP}$, was similarly approximated for the bottom flange in the same fashion as described above. Combining this 'ascending branch approximation' together with the simplified gradients from Figure 3.1, produced final gradients for top flange, web, and bottom flange (Figure 3.3) that were used in the present study.

Lee (2010) determined that winter and summer seasonal conditions produced the maximum and minimum transverse thermal movements, respectively. Because winter conditions produced the largest thermal movements, for conservativism, Lee (2010) recommended that winter temperature gradient data (e.g., $T_{1,SIMP}$) be used in computing prestressed concrete bridge girder thermal sweep. As noted earlier, the gradients quantified by Lee were based on 'extreme' environmental (seasonal) conditions in Atlanta, Georgia. Florida, however, is located in a more temperate climate (environment) than Atlanta, Georgia. Consequently, to avoid introducing excess conservatism into the calculation of thermal sweep for Florida-I Beams, an average of the winter and summer thermal sweeps proposed by Lee was used in the present study.

Before applying this approach to the calculation of thermal sweep values for FIB girders, it was first applied to the BT-63 girder cross-section studied by Lee to ensure that suitable results were obtained. For purposes of comparing results from the different approaches, a 'sweep ratio' was defined as the maximum thermal sweep divided by the maximum allowable fabrication sweep. Using the maximum thermal sweep equations provided in Lee (2010), calculations were performed for a BT-63 girder at varying span lengths for winter conditions, summer conditions, and the average of these two (Figure 3.4, lines). Next, thermal gradients were formed per Figure 3.3, applied to the BT-63 cross-section for various span lengths, and thermal sweep ratios were computed (Figure 3.4, symbols). Examining the 'average of winter and summer' data in Figure 3.4, it is evident that there is good agreement between the BT-63 results derived from detailed thermal FEA analyses (the Lee 2010 data) and the 'Lee (2012) plus approximate ascending branch' approach proposed herein. Based on these results, the latter approach (i.e., Figure 3.3) was deemed to be suitable for use in computing thermal sweep data for Florida-I Beam sections at varying span lengths.

BT-63 temperature gradient per Lee (2010)

$T_{1,FEA}$

$T_{R,FEA}$

(a)
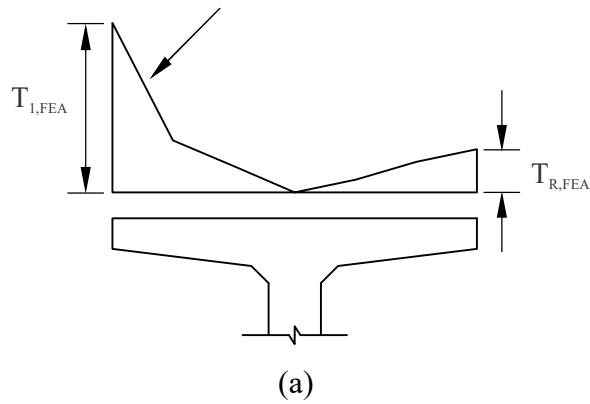
Simplified temperature gradient proposed by
Lee (2012) for prestressed concrete bridge girders

$T_{1,SIMP}$

(b)
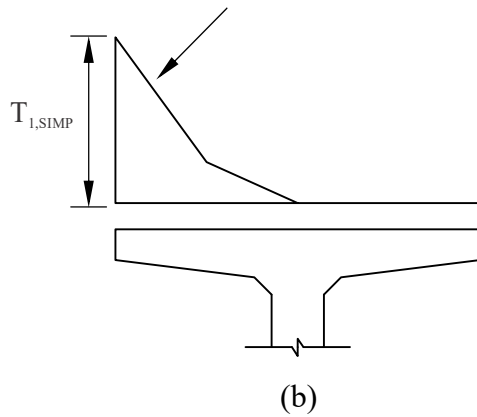
Simplified temperature gradient proposed by
Lee (2012) supplemented by additional
approximated ascending branch to $T_{R,SIMP}$

$T_{1,SIMP}$

$T_{R,SIMP}$

(c)
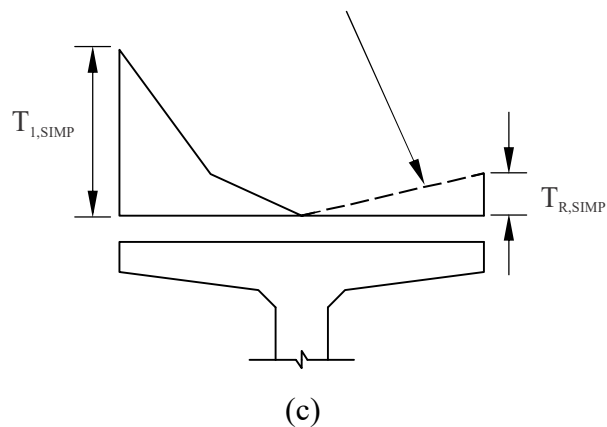
Figure 3.2 Top flange transverse thermal gradient:
(a) From finite element analysis of a typical BT-63 girder (Lee, 2010);
(b) Simplified gradient proposed by Lee (2012);
(c) Approximated right side ascending branch (BDV31-977-46)
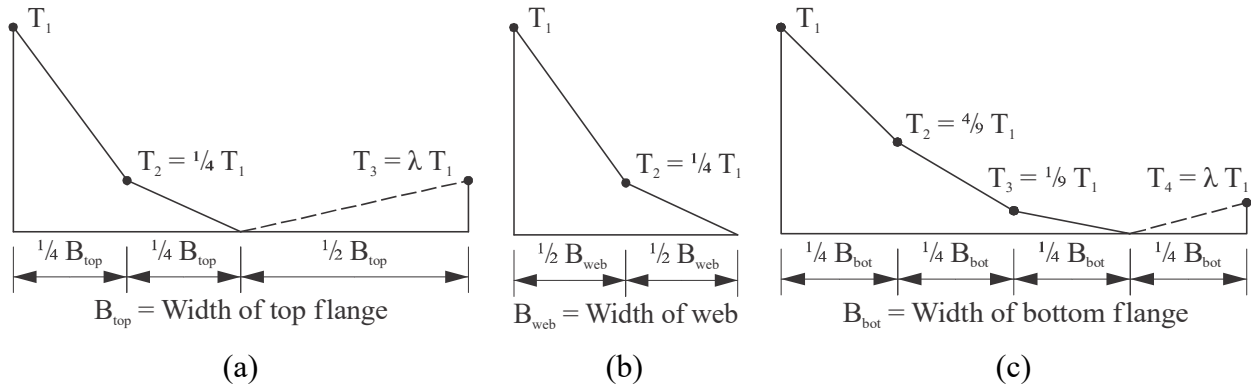
Figure 3.3 Transverse thermal gradients for FIB bridge girders:
(a) Top flange; (b) Web; (c) Bottom flange
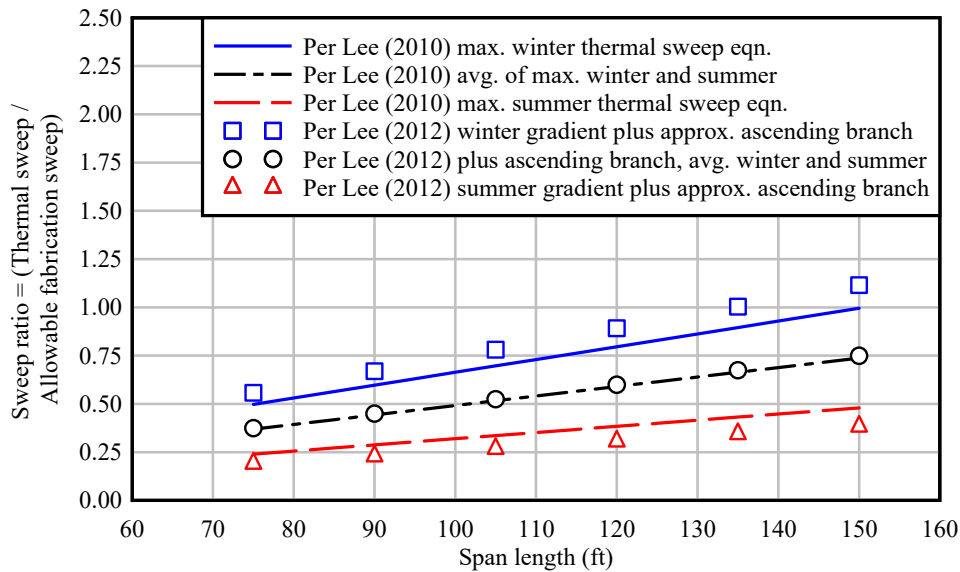
Figure 3.4 Comparison of sweep ratios computed for BT-63 girder (at varying span lengths) as
computed using different methods

3.3 Thermal sweep for Florida-I Beams

Total thermal sweep deflections were calculated for each Florida-I Beam (FIB) cross-sectional shape—at multiple span lengths (minimum practical, intermediate, and maximum practical)—using the gradient formation approach described above and using moment-curvature analysis (see Appendix B). For each pair of FIB section type and span length, upper and lower bounding values of thermal sweep (Figure 3.5) were calculated using winter temperature data (Lee, 2012) and summer temperature data (Lee, 2010). Subsequently, the total thermal sweep deflections were converted into thermal 'sweep ratios' (Figure 3.6) by dividing by the allowable fabrication sweep. Partially as a consequence of the fact that all FIB sections have the same top and bottom flange width and geometry, the computed sweep ratios were found to correlate to span length in an approximately linear manner. Based on this observation, individual linear best-

fit relationships between thermal sweep ratio and span length were constructed from the winter sweep data and summer sweep data. A seasonally averaged Florida-I Beam (FIB) thermal sweep ratio relationship (Figure 3.6) was then constructed by averaging the best fit winter and summer curves. Functionally, this relationship has the form:

$$sr_{FIB} = 0.00572L - 0.05927 \qquad (3.3)$$

where sr_{FIB} is the seasonally averaged FIB sweep ratio, and L is the span length in ft. To compute *total* lateral sweep imperfections for use in girder stability analyses, thermal sweep was superimposed with the maximum allowable fabrication sweep as:

$$s = s_{fabrication} + s_{thermal} = \left(1 + sr_{FIB}\right)s_{fabrication} \qquad (3.4)$$

Substituting Eqn. (3.3) into Eqn. (3.4), and defining maximum allowable fabrication sweep specified in the PCI Bridge Design Manual (2011) as ⅛ in. for every 10 ft of girder length, the total lateral sweep used in the present study for FIB girders was:

$$s_{FIB} = \left(1 + \left(0.00572L - 0.0593\right)\right)\left(L/10\right)\left(1/8''\right) \qquad (3.5)$$

which can be mathematically simplified to:

$$s_{FIB} = \left(0.941 + 0.00572L\right)\left(L/10\right)\left(1/8''\right) \qquad (3.6)$$

where s_{FIB} is the total sweep (lateral imperfection) in inches, and L is the span length in ft.
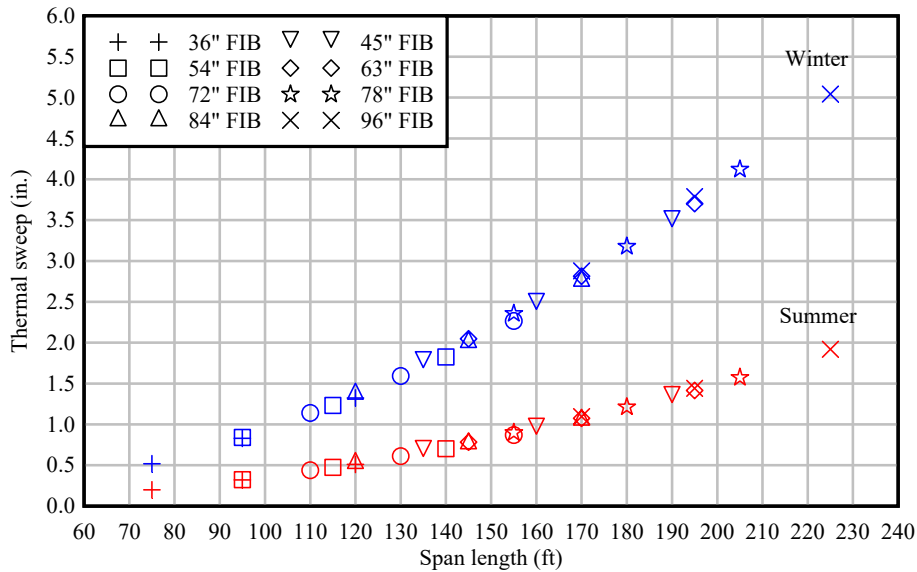
Figure 3.5 Thermal sweep data for FIB sections

13
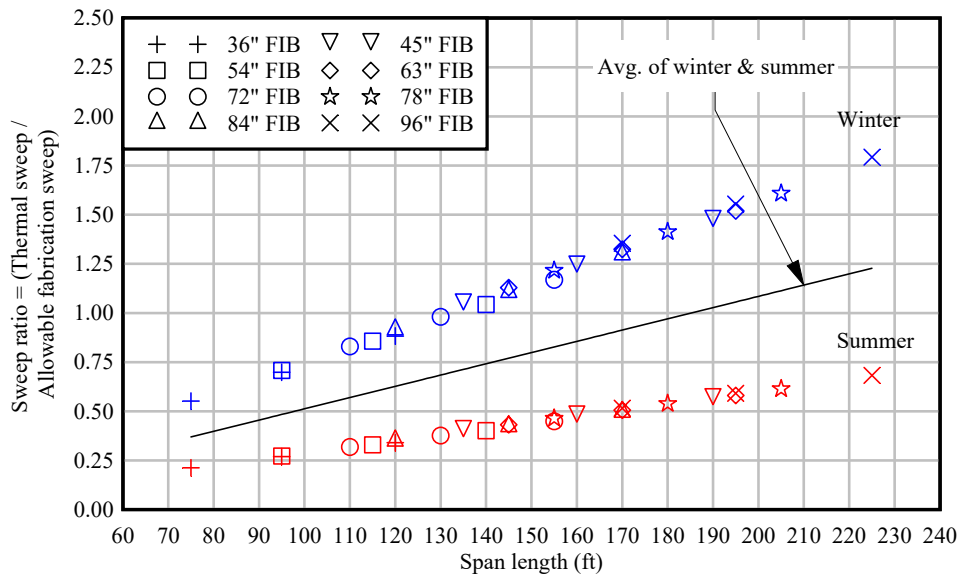
Figure 3.6 Thermal sweep ratios for FIB sections

CHAPTER 4
DEVELOPMENT OF UNANCHORED SINGLE-GIRDER WIND CAPACITY EQUATION

4.1 Introduction

To update previously developed girder capacity equations—considering the revised definition of sweep—systems of FIB girders were modeled (Figure 4.1) and structurally analyzed using the ADINA (2016) finite element analysis code. The models incorporated bearing pad support stiffnesses, and were capable of capturing buckling behavior of FIBs, while remaining computationally efficient enough that thousands of parametric analyses could be performed. Models analyzed in the present study were developed in a semi-automated fashion by extending a modeling methodology developed in a previous study (BDK75-977-33, Consolazio et al., 2013) to include the revised definition of sweep.

In the global coordinate system employed in the models, X corresponded to the transverse direction, Y to the longitudinal direction, and Z to the vertical direction. A local girder coordinate system (u,v,w) was also used corresponding to the same directions, with the origin at one end of the girder at the centroid of the cross-section. Girder buckling capacities were quantified using geometrically-nonlinear large-displacement analyses in which static loads were applied in incremental steps, taking into account the deformed state of the structure at each load step. Instability was initiated by introducing girder fabrication imperfections (i.e., sweep) into the models, so that each load step (load increment) caused the models to deform to ever greater levels. By analyzing the load-displacement results (using a modified Southwell analysis; see Consolazio et al., 2013), it was possible to determine when girder displacements began growing asymptotically, indicating a collapse.
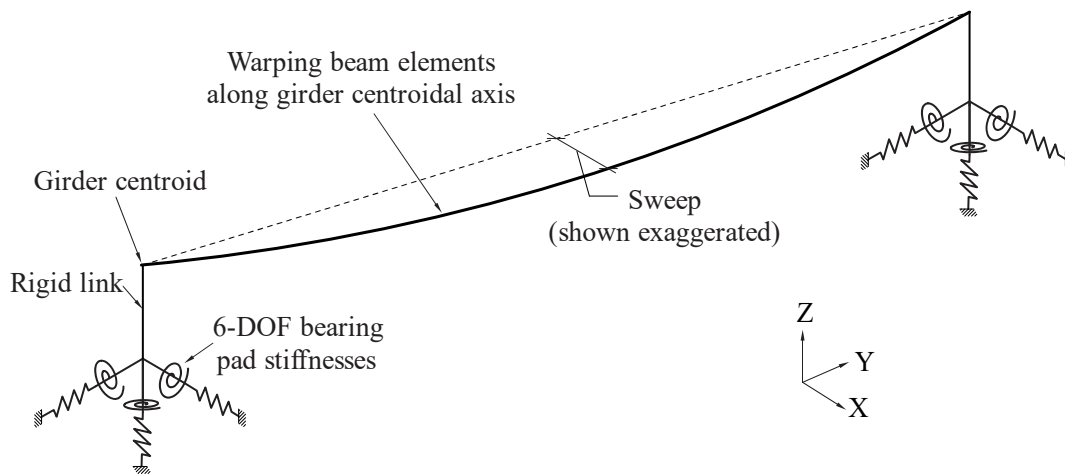
Figure 4.1 Finite element model of a single FIB (isometric view)

4.2 Modeling of bridge girders

Each bridge girder was modeled using *warping beams*, an advanced beam element formulation provided by ADINA (2016) that incorporates degrees of freedom representing torsionally-induced out-of-plane warping of the cross-section. Warping beams are primarily intended for modeling thin-walled sections for which warping effects can significantly affect

structural response, but they also have several additional refinements that make them superior to standard Hermitian beam elements for buckling analysis applications. For example, offsets between the shear center and the centroid of asymmetric cross-sections are accounted for automatically, and the kinematic formulation of the element includes coupling between bending and torsional deformation modes.

Warping beams require the calculation of a comprehensive set of cross-sectional properties, several of which require knowledge of the *warping function*, which cannot be calculated in closed-form (for complex shapes) and must therefore instead be solved for numerically. Details relating to the section properties previously calculated in BDK75-977-33 for FIB cross-sectional shapes are included in Appendix A of the present report.

Construction sweep tolerances implemented in the present study (BDV31-977-46) were determined from Eqn. (3.6), which includes maximum allowable fabrication imperfections limited to ⅛ in. for every 10 ft of girder length and an additional superimposed thermal sweep. To ensure conservative calculations of buckling capacity, all FIBs were modeled with the maximum allowable sweep (u_{max}), as determined from span length and Eqn. (3.6). Geometrically, sweep was implemented using a sinusoidal function (Figure 4.2) with the maximum allowable sweep at midspan, so that the lateral deviation, u, at any position, v, along the girder length was:

$$u(v) = u_{max} \sin\left(\frac{\pi v}{L}\right)$$ (4.1)
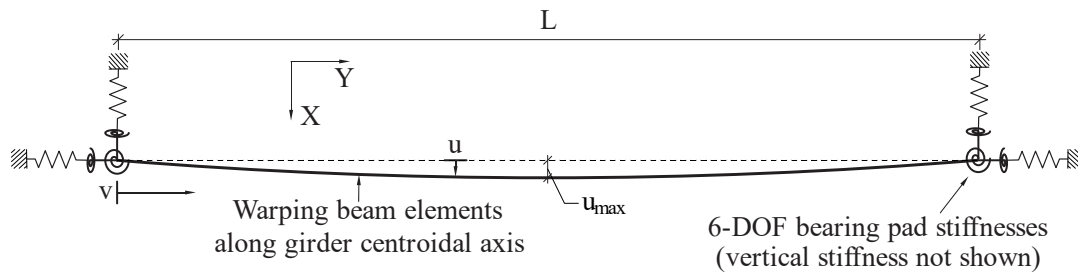
Figure 4.2 Representation of sweep in FIB model (plan view)

During early phases of constructing a bridge, the deck is not present and hence the weight of the deck is not yet present. Consequently, the girders will have more camber at this stage than they will have in the completed configuration of the bridge (when deck self-weight is active). It was therefore important to represent the 'deck-free' girder camber condition in the models, because the additional elevation of the girder center of gravity reduces buckling capacity by a small amount. In BDK75-977-33, to establish maximum probable girder camber for use in model development, trial beam designs were produced for all eight (8) FIB cross-sections with the goal of maximizing camber. This was accomplished by placing all prestressing tendons as low as possible in the bottom flange and finding the span length at which camber was maximized. Long-term creep effects were ignored and it was further assumed that cracking did not occur. From these calculations, it was determined that 3.25 in. was a reasonable upper bound camber for FIB girders during construction.

It is important to recognize that the measured camber of a bridge girder in the field is a superposition of two independent deflections: an upward deflection caused by prestress forces and a downward deflection caused by the self-weight of the girder. The initial (undeformed)

geometry of a finite element model should represent its free-body state, prior to the application of any external loads, including gravity loads. Therefore, it was necessary to add additional camber to the models to offset the expected self-weight deflection. In other words, the geometric camber included in the finite elements models represented *only the upward deflection caused by prestressing* so that after self-weight was applied to the model, the total deflection would match the camber that would be measured in the field. As a result, each girder model was assigned a maximum geometric camber (w_{max}) of:

$$w_{max} = 3.25 \text{ in.} + \frac{5A\gamma L^4}{384EI} \tag{4.2}$$

where A is the girder cross-sectional area, γ is the unit weight of the concrete, L is the span length, E is the elastic modulus, and I is the strong-axis moment of inertia.

Because geometric camber in the models represented upward deflections caused by straight prestressing tendons (which generate a constant internal moment throughout the length of the beam), the girder camber was implemented with a parabolic shape (Figure 4.3) so that the vertical deviation, w, at any point, v, along the girder length was:

$$w(v) = 4w_{max} \left[\left(\frac{v}{L} \right) - \left(\frac{v}{L} \right)^2 \right] \tag{4.3}$$
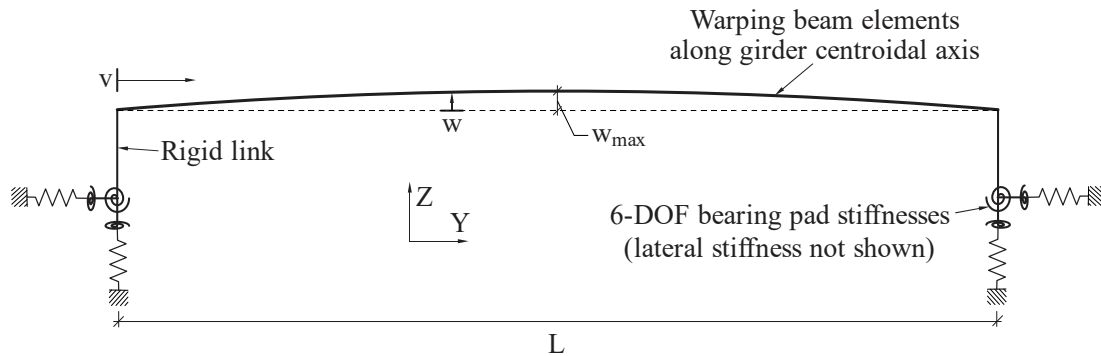
Figure 4.3 Representation of camber in FIB model (elevation view)

4.2.1 Modeling of end supports

Girder support stiffnesses were modeled with six (6) geometrically linear springs to represent the stiffness of the bearing pad in each degree of freedom, with each spring corresponding to one of the four (4) main deformation modes of the pad: shear, axial, torsion, and roll (Figure 4.4). Pad stiffnesses were computed using the methods discussed in Consolazio et al. (2013).

4.2.2 Bearing pad selection

Seven (7) standard types of elastomeric bearing pad are provided in *Design Standard No. 20510: Composite Elastomeric Bearing Pads – Prestressed Florida-I Beams* (FDOT, 2012a) for use with FIBs. During design, selection of the type of pad that will be used in a particular bridge

is based on thermal expansion and live load deflection limit states of the completed bridge, neither of which can be predicted based solely on girder dimensions (cross-sectional and span length). As such, it is not appropriate to assume that for each FIB type, there is a specific corresponding type of bearing pad that would be utilized. Hence, in BDK75-977-33 and in the present study, it was conservatively assumed that the pad type with the lowest roll stiffness (which will produce the lowest buckling capacity) would be used in conjunction with all FIB types. After calculating the roll stiffness of every standard FDOT FIB pad type, using the grillage method discussed in Consolazio et al. (2013), the Type J bearing pad was selected for use.
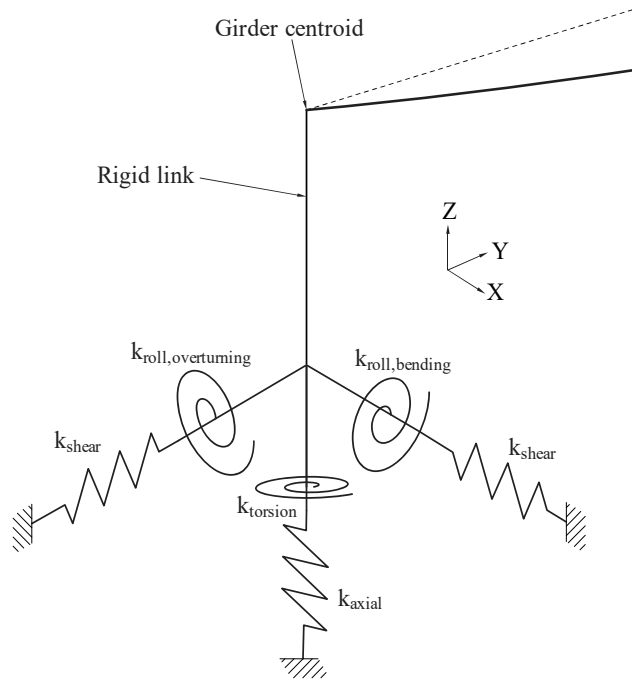
Figure 4.4 Bearing pad stiffness springs in FIB model (isometric view)

4.2.3 Axial load selection

The amount of axial load applied to a bearing pad does not change the initial linear portion of the roll stiffness curve, but it does affect the moment required to initiate girder roll-off from the pad. Reducing the compressive axial load on a pad reduces the moment that is required to cause girder roll-off. Additionally, reducing girder span length reduces girder self-weight which, in turn, reduces the axial loads on the bearing pads. Therefore, to be conservative in this study, the minimum length ranges for each FIB shape were determined from design aids in *Instructions for Design Standard No. 20010: Prestressed Florida-I Beams* (IDS 20010; FDOT, 2012b) and the minimum expected axial pad load was calculated for each FIB shape. (These calculations assumed that the girders were simply supported. Additionally, the effects of wind uplift forces were conservatively ignored). Using this process, a single worst-case (minimized) roll stiffness curve was calculated for each type of FIB, resulting in a total of seven (7) bearing pad moment-rotation curves.

4.2.4 Girder slope selection

Overturning (roll) pad stiffness is reduced by the presence of girder slope, which can arise from a combination of girder camber and bridge grade. According to *Instructions for Design Standard No. 20510: Composite Elastomeric Bearing Pads – Prestressed Florida-I Beams* (IDS 20510; FDOT, 2012c), the maximum expected slope angle in the *completed bridge* is 0.0125 rad, because if this angle is exceeded, beveled bearing plates must be installed to eliminate slope. Therefore, the maximum expected camber *prior to the casting of the deck* is the sum of 0.0125 rad and any camber-induced slope that is negated by the downward deflection under the weight of the deck and other superimposed dead loads (SDL). After a series of trial beam design calculations was performed in BDK75-977-33, it was determined that a reasonable upper limit for the SDL-negated slope was 0.01 rad. Additionally, AASHTO LRFD (2010) recommends an "allowance for uncertainties" of 0.005 rad with regard to bearing pad slope angle. The maximum completed slope of 0.0125 rad, the SDL-negated slope of 0.01 rad, and the slope uncertainty of 0.005 rad combined for a total maximum slope angle of 0.0275 rad. This was conservatively rounded up to a slope angle of 0.03 rad, which was used to compute the bearing pad overturning roll stiffness curves.

4.2.5 Load application to individual bridge girders

Two types of structural loads were included in the models: wind and gravity. Lateral wind loads, calculated for each girder using the design drag coefficients proposed in Consolazio et al. (2013) for FIBs, were applied to the girder elements as tributary nodal loads (Figure 4.5a). Small overturning moments were also applied at each node to compensate for the eccentricity between the centroid of the cross-section (where the nodes and elements were located) and the center of pressure (where the lateral load was assumed to act on the girder) (Figure 4.5b). Wind loads were always applied in the direction of increasing girder sweep.
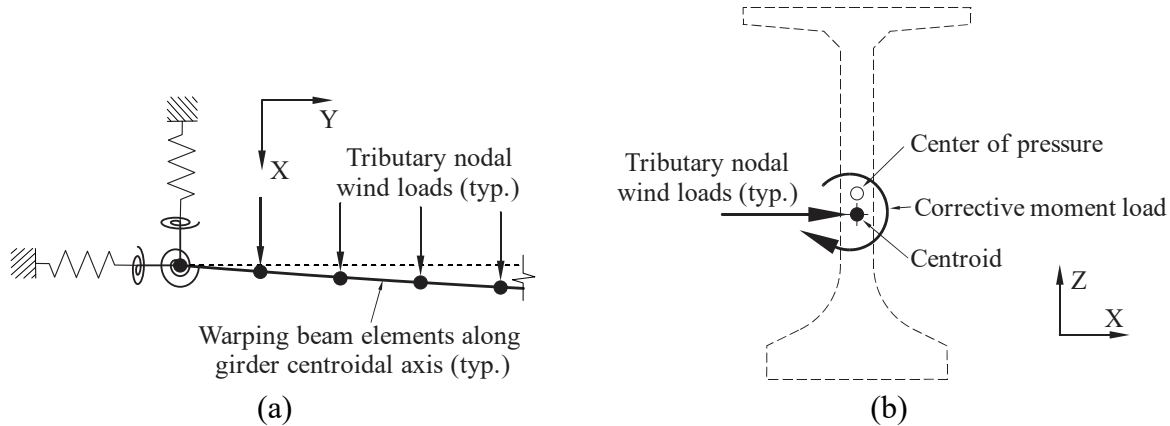
Figure 4.5 Representation of wind load in structural models:
(a) Lateral nodal loads (top view); (b) Overturning moments (section view)

Gravity load was applied as a vertical 'acceleration load' (i.e., a mass-proportional body force) in units of *g*, the acceleration due to gravity, so that a load of 1 g represented the self-weight of the girder. In field conditions, girders are always subjected to a constant gravity load of 1 g. However, in the structural models analyzed in this study, gravity loading was used to initiate

instability. After wind loads were applied, gravity load was linearly ramped up—beyond 1 g if possible—until girder instability occurred. Subsequently, the capacity of the system was expressed as a gravity load (in g), which can also be thought of as a capacity-to-demand ratio. For example, if a system became unstable at a gravity load of 1.5 g, then the ratio of capacity (1.5 g) to demand (1 g) was 1.5.

4.3 Parametric study of unanchored individual bridge girders

Using the updated sweep Eqn. (3.6), a parametric study was performed using ADINA to analyze finite element models of single unanchored Florida-I Beams (FIBs) over a range of span lengths. Each stability analysis in the parametric study was performed for the purpose of quantifying the maximum lateral wind load that could be applied before girder instability occurred. For each model, the *vertical* load carrying capacity was evaluated several times at different *lateral* wind pressures, iterating until the vertical capacity was within 1% of 1 g (i.e., girder self-weight). The resulting wind pressure for each case was denoted as the lateral *wind capacity* of that girder.

4.3.1 Selection of parameters

Girder parameters that were varied in the parametric study were the FIB cross-section depth (in.) and span length (ft). All eight (8) standard FIB cross-sections were included in the study, with depths ranging from 36 in. to 96 in. In BDK75-977-33 (Consolazio et al., 2013), bridge grade was found to have negligible effect on wind capacity; therefore in the present study, all analyses were performed at a level (0%) grade.

Material properties assumed for the prestressed concrete FIBs were $f_c' = 8.5$ ksi, unit weight = 150 pcf, and Poisson's ratio = 0.2. Using these values and equations provided in PCI (2010), the concrete elastic modulus was computed to be E = 5589 ksi. It should be noted that in BDK75-977-33 (Consolazio et al., 2013), the concrete strength was assumed to be $f_c' = 6.5$ ksi (with corresponding E = 4887 ksi). In a related follow-up study, BDK75-977-70 (Consolazio and Edwards, 2014), the concrete strength was adjusted to $f_c' = 8.5$ ksi to better represent typical conditions in Florida bridge construction practice. In the present study, the updated value of $f_c' = 8.5$ ksi was retained.

Span length ranges for each FIB section used in the parametric study were in accordance with those determined previously in BDK75-977-33. Maximum and minimum span lengths were based on design aids included in *Instructions for Design Standard No. 20010: Prestressed Florida-I Beams* (IDS 20010; FDOT, 2012b). This document provides estimated span lengths (Table 4.1) for FIBs with different lateral spacings, based on representative bridge design calculations. Maximum span lengths were based on a girder spacing of 6 ft and an environment classified as "Moderately Aggressive", while minimum lengths assumed a 12-ft girder spacing and an "Extremely Aggressive" environment. Additionally, per FDOT request, maximum span lengths 10 ft longer than the maximums considered in BDK75-977-33 were added to the parametric study. Span lengths were incremented at 5-ft intervals over the final chosen ranges (Table 4.1).

Table 4.1 Span length ranges for FIBs

	Values from IDS 20010		
	Min length (ft)	**Max length (ft)**	**Final range**
36″ FIB	80	105	75–120
45″ FIB	98	126	95–140
54″ FIB	113	142	110–155
63″ FIB	124	155	120–170
72″ FIB	142	173	135–190
78″ FIB	151	182	145–195
84″ FIB	159	191	155–205
96″ FIB	175	208	170–225
Spacing	12 ft	6 ft	
Environment	Extremely aggressive	Moderately aggressive	

4.3.2 Updated wind capacity of a single unanchored girder

The relationships between wind capacity and span length, as previously determined in BDK75-977-33 (without inclusion of thermal sweep), and as determined in the present parametric study (with inclusion of thermal sweep) are compared in Figure 4.6. As expected, including thermal sweep had the effect of reducing wind load capacities, particularly at longer span lengths. Also, similar to the BDK75-977-33 results, capacity data from the present study indicated that span length was the strongest predictor of wind capacity. Girder depth was found to have a secondary influence in that increasing the depth decreased the wind capacity (due to the increased 'sail area').

In BDK75-977-33, the data shown in Figure 4.6a were used to construct the following wind capacity equation [cited as Eqn. (8.2) in Consolazio et al. (2013)]:

$$P_{max,0} = 123e^{\frac{-L}{100}}\left(1+15e^{\frac{-D}{22}}\right) - 750e^{\frac{-D}{16}} - 16 \tag{4.4}$$

where $P_{max,0}$ is the wind capacity in psf, L is the span length in ft, and D is the FIB cross-section depth in inches. Using 1) the general 'functional form' of Eqn. (4.4), 2) the updated capacity data shown in Figure 4.6b, and 3) an improved curve-fitting process, the following updated wind capacity equation for unanchored girders was constructed:

$$P_{max,0} = 63e^{\frac{-L}{55}}\left(\frac{1}{3}+15e^{\frac{-D}{79}}\right) - 34e^{\frac{-D}{72}} - \frac{1}{8} \tag{4.5}$$

where $P_{max,0}$ is the wind capacity in psf, L is the span length in ft, and D is the FIB cross-section depth in inches.
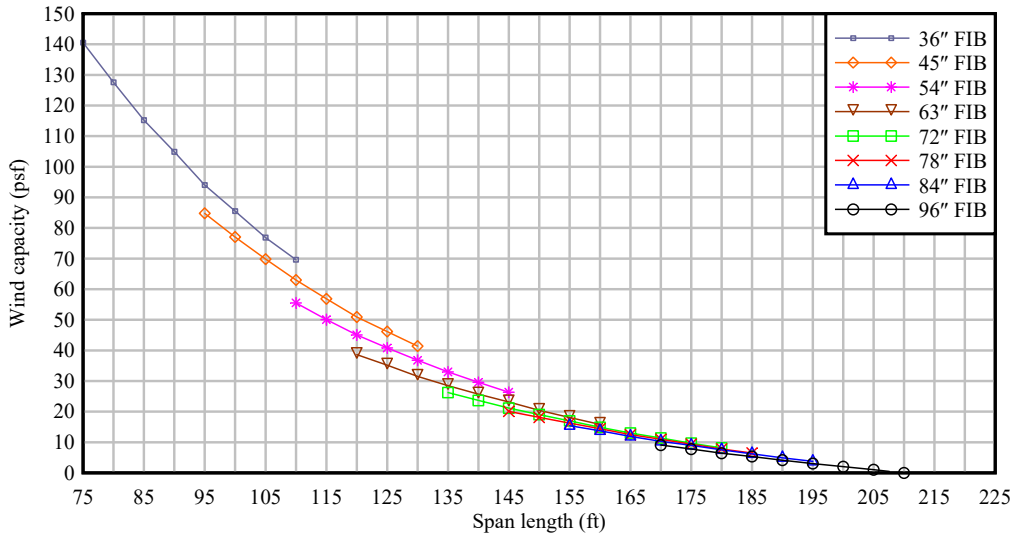
(a)
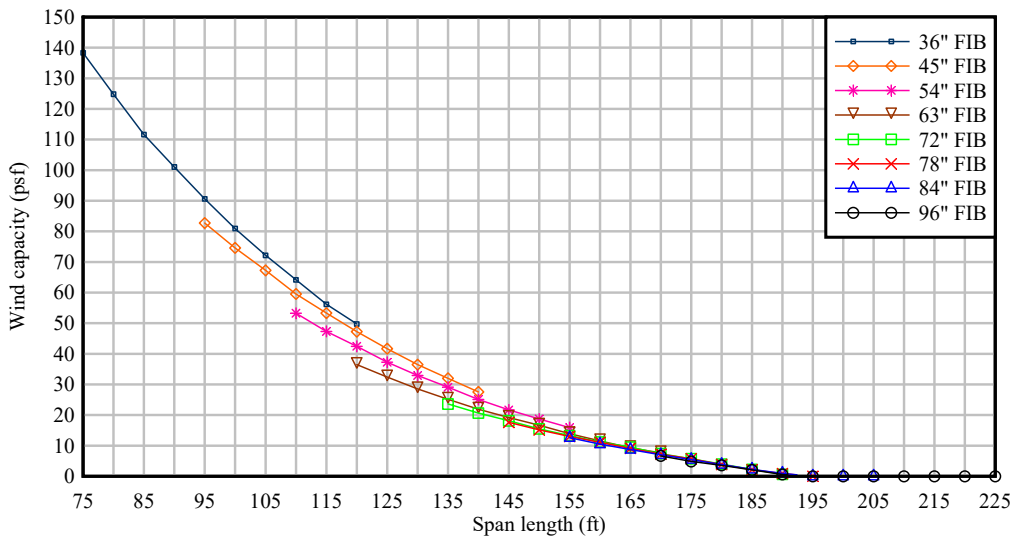
(b)

Figure 4.6 Wind capacities for unanchored FIBs:
(a) Data from BDK75-977-33 (without inclusion of thermal sweep);
(b) Data from present study (with inclusion of thermal sweep)

When forming Eqn. (4.4) in BDK75-977-33, a multi-stage curve fitting process was used in which individual curves were initially fit to the capacity vs. span-length data for each FIB type, followed by a subsequent curve fitting process that was applied to the coefficients from the individual FIB fits. In contrast, when forming Eqn. (4.5) in the present study, error in the curve fitting process was *simultaneously* minimized across the entire data set (i.e., all span lengths and all girder types/depths shown in Figure 4.7b) at one time. (Subsequent to this process, minor adjustments were made to the fitting coefficients to ensure conservative capacities were obtained for all data points in the data set). As Figure 4.7 indicates, the updated 'simultaneous' fitting process yielded a capacity equation that fit the trends in the underlying data better than did the original equation developed in BDK75-977-33.

22
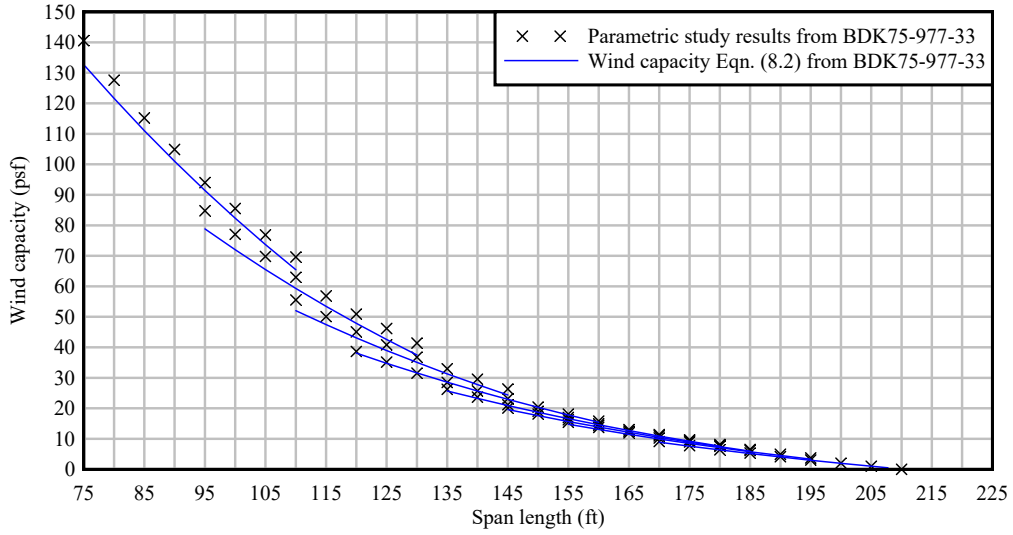
(a)
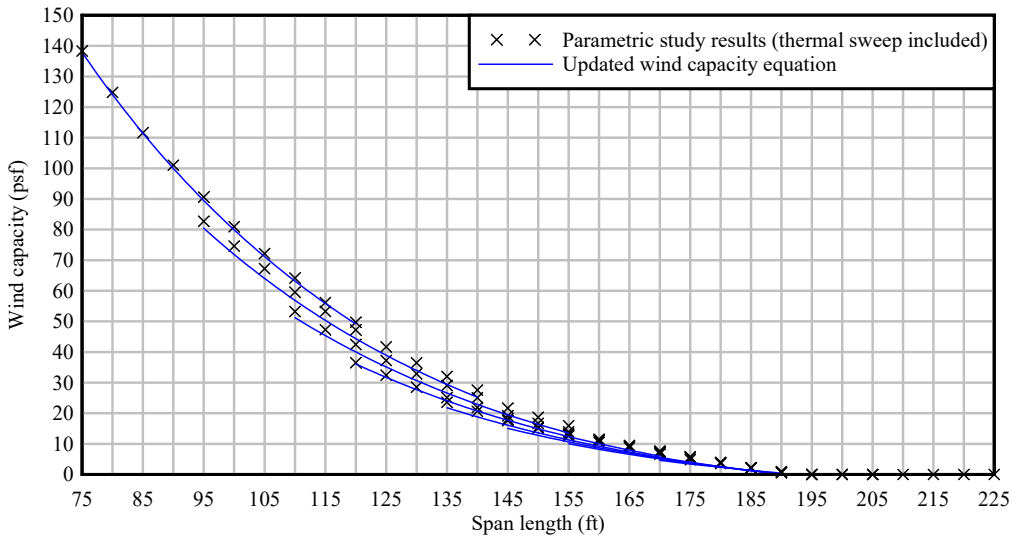
(b)

Figure 4.7 Wind capacity of an unanchored FIB:
(a) Data from Figure 4.6a and Eqn. (4.4) [i.e., Eqn. (8.2) from BDK75-977-33];
(b) Data from Figure 4.6b and Eqn. (4.5) developed in present study

23

CHAPTER 5
DEVELOPMENT OF UNANCHORED STRUT-BRACED TWO-GIRDER BUCKLING CAPACITY EQUATION

5.1 Introduction

To develop an updated unanchored strut-braced two-girder buckling capacity (C_0) equation—accounting for the revised definition of sweep—multi-girder systems of FIBs were modeled and analyzed using ADINA (2016). Structural modeling techniques used in the present study matched those previously developed in BDK75-977-33 (Consolazio et al., 2013). For the convenience of the reader, a summary is provided below of material in Consolazio et al. (2013) that is pertinent to the development of a revised baseline capacity (C_0) equation.

5.2 Review of multi-girder system-related information from BDK75-977-33

5.2.1 Preliminary sensitivity studies

In BDK75-977-33, several system parameters were identified as having negligible influence on system capacity. Consequently, these parameters were not varied in the final parametric studies. The parameters were:

- Bridge grade: All analyses were performed on girder models with level (0%) grade.

- Cross-slope: Multi-girder models had a default −2% cross-slope.

Preliminary studies revealed that braces were naturally divided into two categories that had very different effects on system behavior: *strut braces* and *moment-resisting braces*. As a result, separate parametric studies were performed for each brace category.

5.2.2 Strut braces

Top struts and parallel struts (Figure 5.1) are both examples of strut braces, which include (but are not limited to) all brace designs consisting solely of horizontal compression members. In BDK75-977-33, it was found that all strut brace designs are essentially interchangeable with regard to lateral stability. That is, a girder system braced with top struts has the same capacity as an otherwise identical system braced instead with parallel struts (or any other type of strut brace). As a result, the capacity of a strut-braced system is also insensitive to girder spacing (which only affects the length—and thus the axial stiffness—of the strut members).
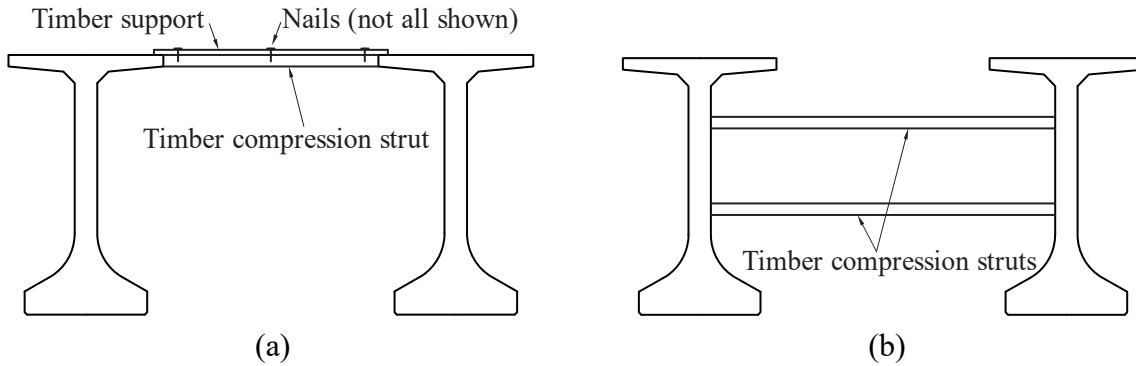
Figure 5.1 Examples of strut bracing: (a) Top strut; (b) Parallel struts

Strut braces can be defined (or identified) by their lack of resistance to girder overturning. In a small-displacement (geometrically linear) analysis of a system with zero bearing pad rotational stiffness, a strut with ideal pin connections forms a collapse mechanism (Figure 5.2) that allows the connected girders to rotate freely in unison. Therefore, struts can only provide stability by coupling the girders together, and resistance to collapse is primarily provided by the roll stiffness of the anchors and, to a lesser extent, the roll stiffness of the bearing pad supports.
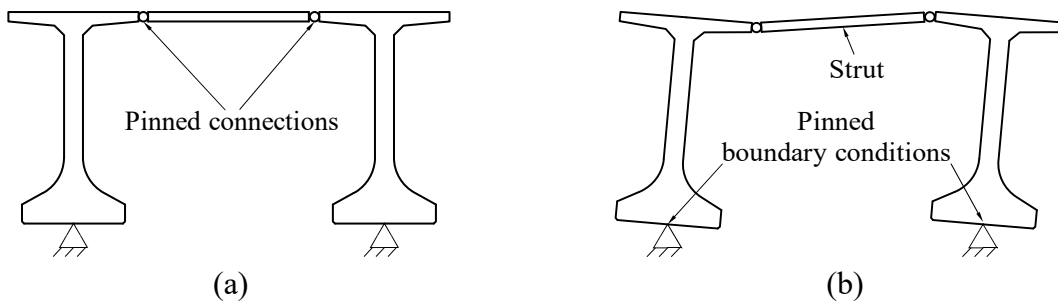
Figure 5.2 Collapse mechanism possible with strut bracing:
(a) Undeformed configuration; (b) Collapse mechanism

5.2.3 Moment-resisting braces

X-braces and K-braces (Figure 5.3) are both examples of moment-resisting braces, which are capable of resisting girder overturning. Unlike struts, the system capacity provided by different moment-resisting brace designs varies significantly, and capacity can be increased by the installation of braces at interior brace points. Systems with moment-resisting braces become more stable as additional girders are added; hence a two-girder system is nearly always the most unstable bridge cross-section possible. In the presence of moment-resisting bracing, the additional roll stiffness and stability provided by anchors is typically negligible.
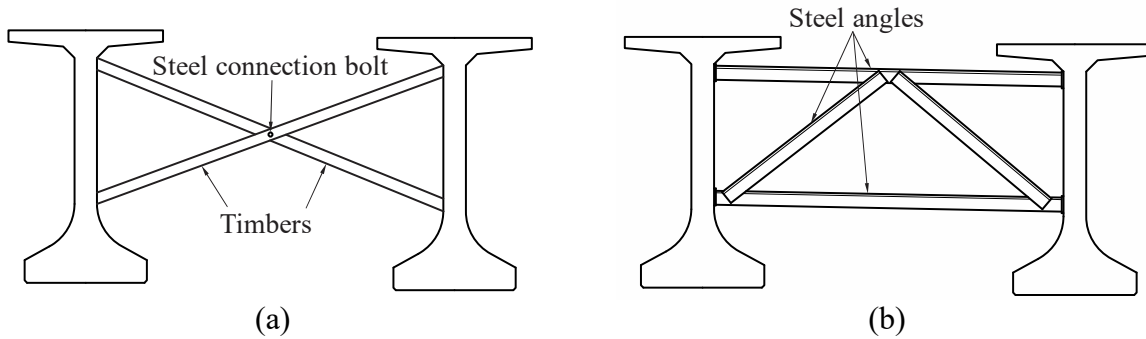
Figure 5.3 Examples of moment-resisting braces: (a) X-brace; (b) K-brace

5.2.4 Modeling of braces

Because the design of bracing has historically been left to the discretion of the contractor, a wide variety of bracing configurations are used in practice. Consequently, in BDK75-977-33, it was not possible for every potential brace configuration to be represented in the parametric studies. After conducting a survey of bracing designs used in the construction of bridges throughout Florida, four (4) representative brace configurations were identified:

- Top strut (Figure 5.4a): a horizontal timber compression strut situated between the edges of the top flanges. The top strut is typically nailed to the underside of a slightly longer timber member, creating 'lips' that rest on the top of the flanges.

- Parallel strut (Figure 5.4b): Two (or more) horizontal timber compression struts wedged in place between the girder webs.

- X-brace (Figure 5.4c): Two diagonal timber members wedged between the webs that cross in the middle to form an 'X' shape. A steel bolt typically passes through both members at the crossing point to create a hinge.

- K-brace (Figure 5.4d): Steel members (typically steel angles) welded together into a 'K'-shaped frame and welded or bolted to steel plates cast into the webs.

The majority of brace designs that were encountered were variations of one of these four basic configurations.

For analysis purposes, braces were modeled primarily with beam elements, with each brace member represented by a single element. At the girder connection points, rigid links were used to connect the braces to the girder elements (i.e., warping beams located at the girder centroids). It was assumed that the brace-girder connections were ideal pins, which was conservative with regard to girder stability. Pins and hinges were modeled with beam end-releases and nodal constraints, respectively.

In BDK75-977-33, during the survey of bracing designs, the vast majority of timber braces that were encountered were composed of 4x4 Southern Pine sawn lumber. According to the *National Design Specification for Wood Construction* (AF&PA, 2005), 4x4 Southern Pine has a 3.5″ x 3.5″ square cross-section and an elastic modulus of E = 495 ksi (based on an E_{min} of 550 ksi for 4-inch-wide "Construction-grade" lumber and a Wet Service Factor of 0.9). These properties were used to model all timber brace members including the top strut, parallel strut, and X-brace. Based on a typical bridge bracing design that was acquired during the survey,

K-brace members were modeled as 4″ x 4″ x ⅜″ steel angles, with an elastic modulus of E = 29000 ksi.
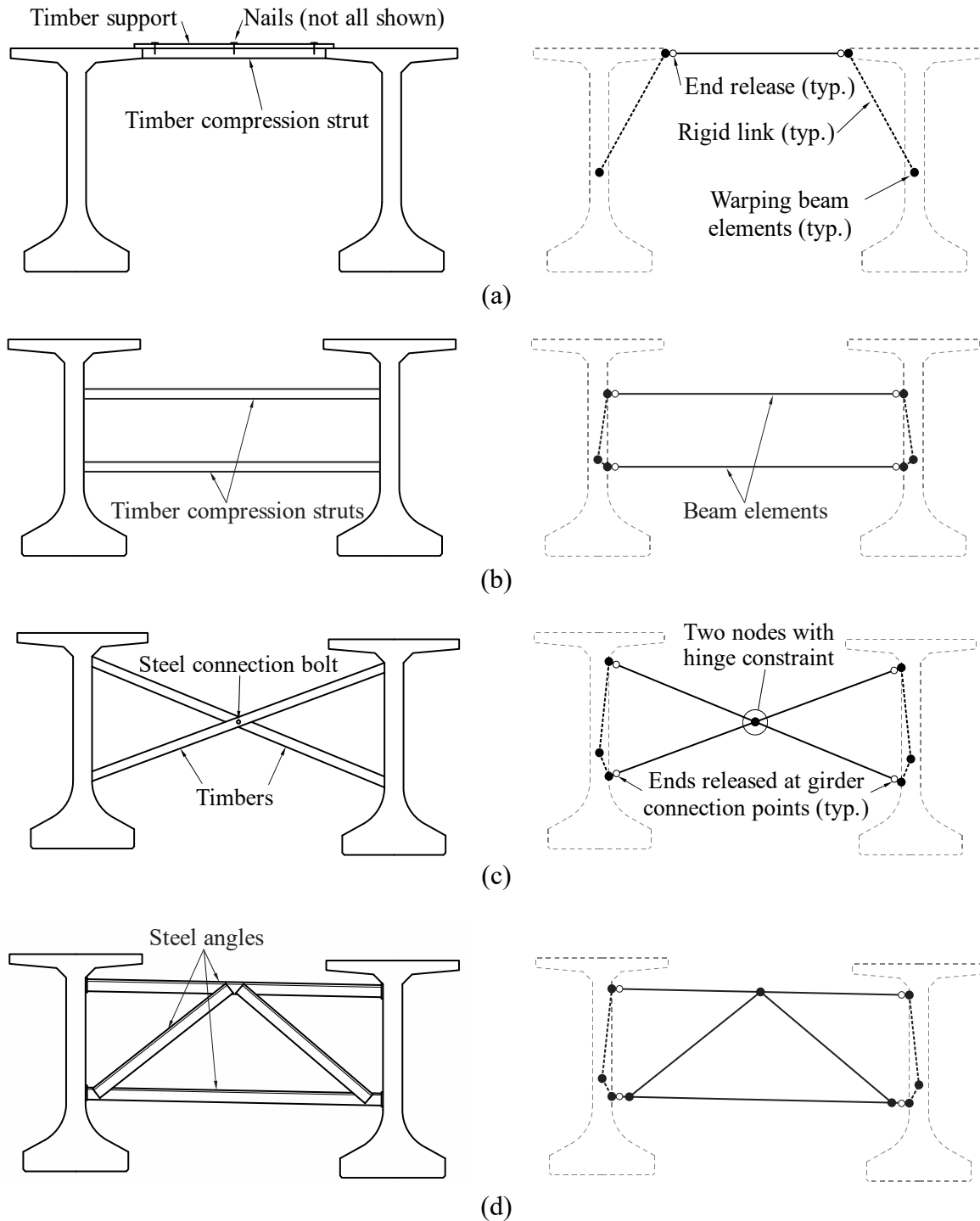
Figure 5.4 Representation of brace configurations in FIB system models:
(a) Top strut brace; (b) Parallel strut brace; (c) X-brace; (d) K-brace

5.2.5 Modeling of bridge skew and wind load

In BDK75-977-33, the final proposed design wind loads (Figure 5.5) were based on a basic 'reduction-and-recovery' trend that was observed in all tested configurations (Consolazio et al., 2013). An initial pressure coefficient (C_P) (i.e., $C_{D,eff}$) was assigned to G1 based on the type of girder section: 2.0 for FIBs. Girder G2 was assigned a C_P of 0 (i.e., no load) while G3 and all subsequent girders were assigned a C_P equal to half of the load on the windward girder.

Pressure coefficients at each girder position:
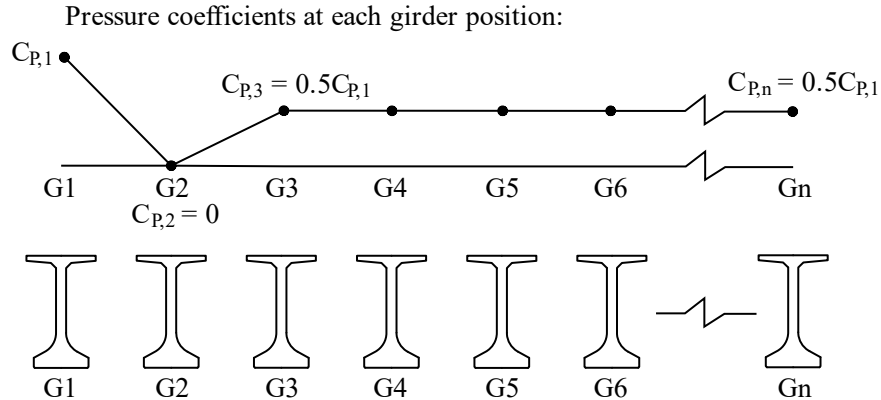
Figure 5.5 Proposed wind load shielding model for stability evaluation from BDK75-977-33

In a braced system of girders, the introduction of bridge skew causes the girders to become staggered longitudinally. This affects system capacity in two ways (Figure 5.6):

- Brace placement: Because girders are installed perpendicular to the girder axes (per *Design Standard No. 20005: Prestressed I-Beam Temporary Bracing*, FDOT, 2014a), the region within which braces can be placed is smaller (shorter) than the span length of the girders. As a result, girder stability can increase due to the reduced distance between brace points.

- Incomplete shielding: In a skewed system, none of the girders are completely shielded with respect to wind load. Rather, an end portion of each girder is exposed to full (unshielded) wind pressure. In BDK75-977-33, the aerodynamic properties of the exposed end region were not measured in a wind tunnel, so specific 'edge effects' that may result from the presence of upwind girders are unknown.

The magnitude of both of these effects is a function of the girder offset length (L_{offset}, Figure 5.6) which is dependent on both skew angle and girder spacing.
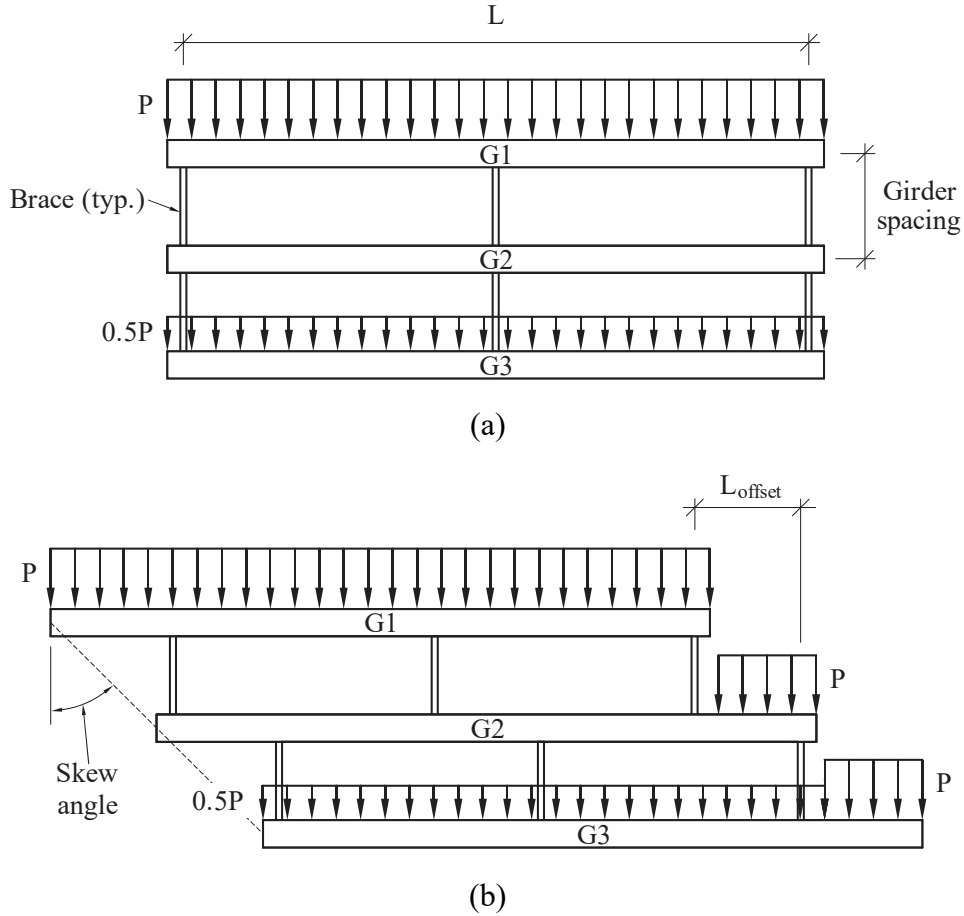
Figure 5.6 Effect of bridge skew on wind loading of braced 3-girder system (plan view):
(a) Unskewed system; (b) Skewed system

Conducting wind tunnel testing to experimentally quantify the effects of skew on girder-end shielding was outside the scope of BDK75-977-33. Consequently, the non-uniform wind pressure distribution shown for leeward girders in Figure 5.6b was an approximation based on engineering judgment. Lacking wind tunnel confirmation of this approximation, it was deemed unwarranted to model this distribution in detail. Instead, a simplified, but statically similar, representation was used in which the wind load on each girder was modeled as a single, weighted-average uniform pressure along the entire length of the girder. The uniform wind load applied to each partially-shielded girder (P) [reported as Eqn. (9.1) in Consolazio et al., 2013] was computed as a weighted average of the shielded and unshielded wind loads, as follows:

$$P = P_U \frac{L_{offset}}{L} + P_S \frac{L - L_{offset}}{L}$$ (5.1)

where P_U is the unshielded wind load (on the windward girder), P_S is the shielded wind load, L is the girder length, and L_{offset} is the length of girder offset produced by skew.

5.3 Parametric study of system capacity of unanchored two-girder system in zero wind

Using the updated sweep Eqn. (3.6), a parametric study was performed using ADINA (2016) to analyze finite element models of strut-braced systems, consisting of two (2) Florida-I Beams (FIBs) without anchors and without wind load, over a range of span lengths. Each stability analysis in the parametric study was performed for the purpose of quantifying the *system capacity* in units of g (the acceleration due to gravity), representing the total gravity load that can be applied before the system becomes unstable (collapses). For each model, gravity load was incrementally increased, iterating until the vertical capacity was reached (i.e., until a system instability occurred).

5.3.1 Parameters

Girder parameters that were varied in the 'unanchored two-girder zero wind' study were the FIB cross-section depth (in.) and span length (ft). All eight (8) standard FIB cross-sections were included, with depths ranging from 36 in. to 96 in. Material properties assumed for the prestressed concrete FIBs were $f_c' = 8.5$ ksi, unit weight = 150 pcf, and Poisson's ratio = 0.2. Using these values and equations provided in PCI (2010), the concrete elastic modulus was computed to be E = 5589 ksi. As noted in Section 4.3, in BDK75-977-33 (Consolazio et al., 2013), the concrete strength was assumed to be $f_c' = 6.5$ ksi (with corresponding E = 4887 ksi). In the present study, however, the concrete strength was adjusted to $f_c' = 8.5$ ksi to better represent typical conditions in Florida bridge construction practice.

Span length ranges for each FIB section considered in the unanchored two-girder zero wind parametric study were consistent with those previously discussed in Section 4.3, with maximum span lengths increased by 10 ft, per FDOT request. Additionally, span lengths were incremented at 5-ft intervals over the final chosen ranges (recall Table 4.1), as opposed to the 10-ft increments used in BDK75-977-33 for the unanchored two-girder zero wind study.

5.3.2 Updated system capacity of unanchored two-girder system in zero wind

The relationships between system capacity (in terms of g) and span length, as previously determined in BDK75-977-33 (without inclusion of thermal sweep), and as determined in the present study (with inclusion of thermal sweep) for unanchored two-girder strut-braced systems in zero wind are compared in Figure 5.7. As expected, system capacity decreased due to the increase in lateral sweep. In both sets of data shown in Figure 5.7, system capacity is correlated with span length (L), but the FIB girder depth (D) has essentially negligible effect on capacity.

In BDK75-977-33, the data shown in Figure 5.7a were used to construct the following baseline capacity (C_0) equation of an unanchored strut-braced system of two girders in zero wind, reported as Eqn. (9.2) in Consolazio et al. (2013):

$$C_0 = 39e^{\frac{-L}{48}} + 0.5 \qquad\qquad (5.2)$$

where C_0 is in g and L is the span length in ft (see Figure 5.8a). For the present study, using the updated baseline capacity data shown in Figure 5.7b (with the inclusion of thermal sweep), the

following updated baseline capacity (C_0) equation of an unanchored two-girder strut-braced system in zero wind was constructed:

$$C_0 = 47 e^{\frac{-L}{42}} + 0.5 \tag{5.3}$$

where C_0 is in g and L is the span length in ft. Forming Eqn. (5.3) involved establishing the curve that fit the data in Figure 5.7b with the minimum root mean square (RMS) error, then rounding and adjusting the fitting coefficients for 1) convenience of use and, 2) to minimize excess conservatism for span lengths exceeding approximately 140 ft (Figure 5.8b).
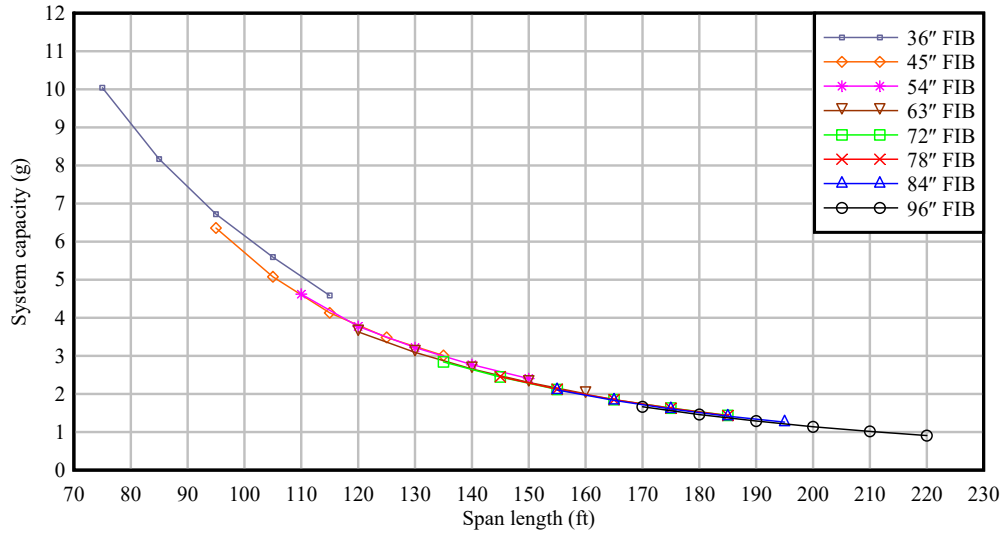
(a)
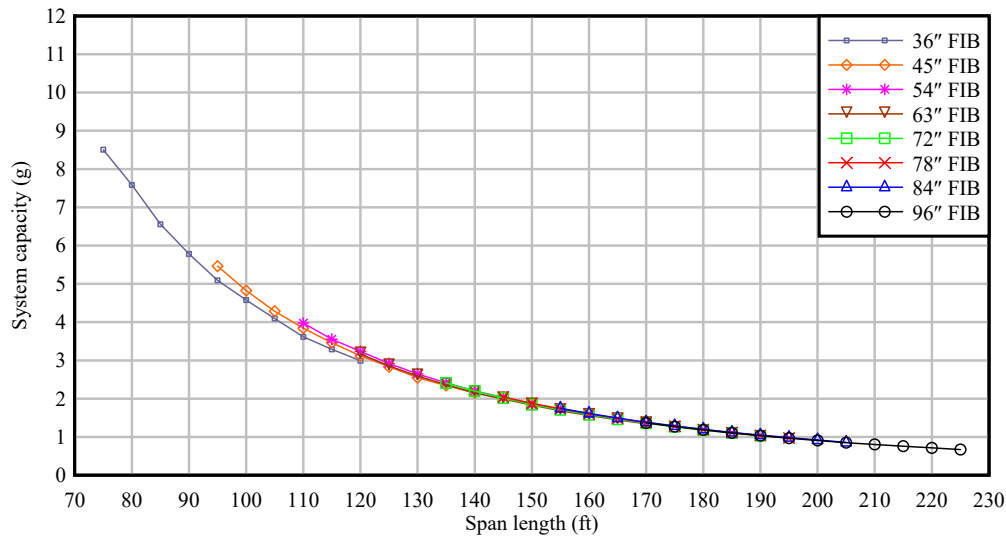
(b)

Figure 5.7 System capacities of unanchored two-girder strut-braced FIB systems in zero wind:
(a) Data from BDK75-977-33 (without inclusion of thermal sweep);
(b) Data from present study (with inclusion of thermal sweep)
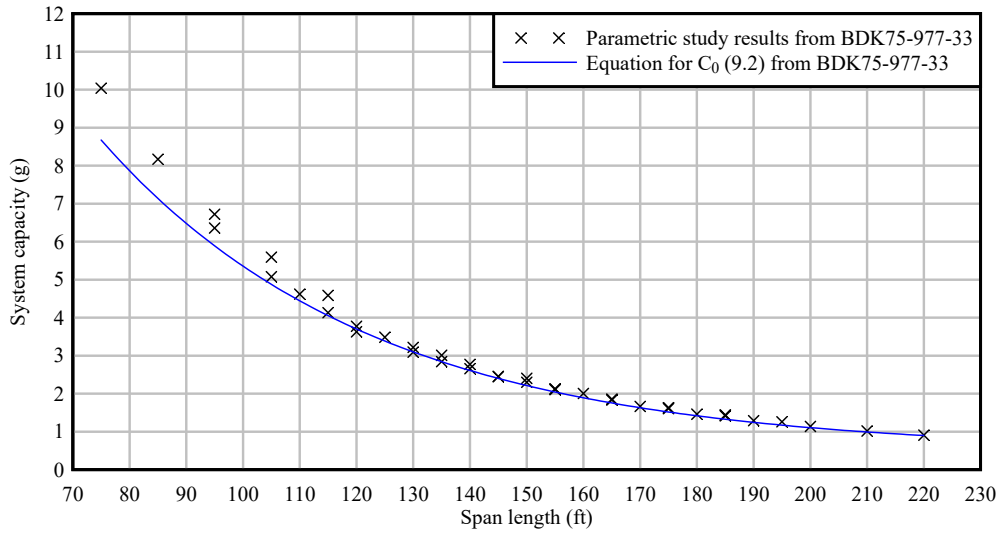
(a)
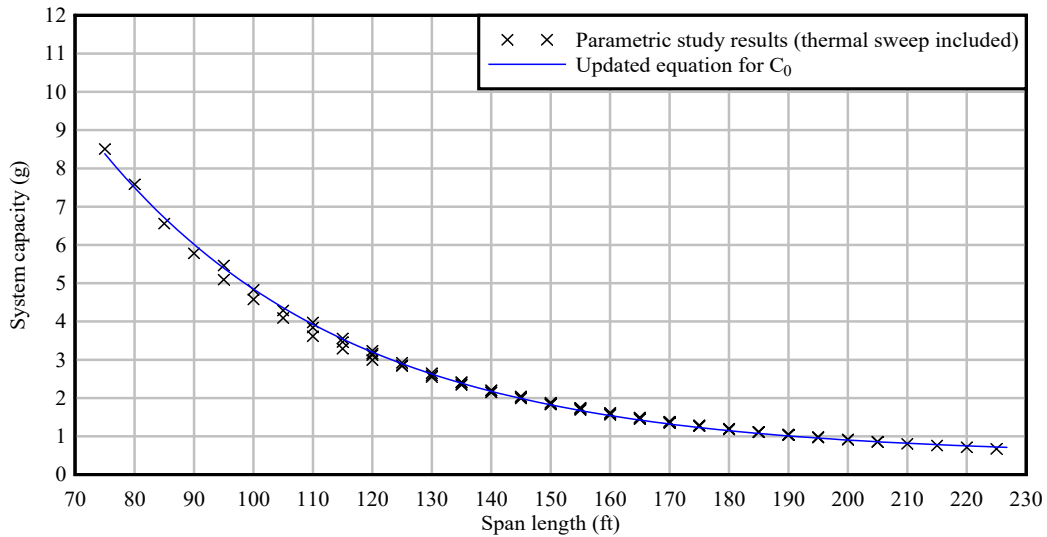
(b)

Figure 5.8 System capacity of an unanchored strut-braced two-girder FIB system
in zero wind as predicted by C_0 Equation:
(a) Data from Figure 5.7a and Eqn. (9.2) from BDK75-977-33;
(b) Data from Figure 5.7b and Eqn. (5.3) developed in present study

5.4 Moment-resisting brace: limited scope parametric study

In BDK75-977-33, the baseline capacity (C_0) equation for an unanchored strut-braced two-girder system in zero wind was used to develop a set of final system capacity (C) equations, reported as Eqn. (9.22) and Eqn. (9.23) in Consolazio et al. (2013), for strut-braced and moment-braced systems, respectively. Development of the final capacity equation was achieved by applying correction factors (developed from parametric studies) to the baseline (C_0) equation.

The final system capacity equation for moment-resisting-braced systems, reported as Eqn. (9.23) in Consolazio et al. (2013) is repeated here for convenience of reference:

$$C = C_0 + \omega \frac{620 k_{brace} e^{\frac{-L}{30}}}{k_{brace} + 1,000,000} - \frac{\sqrt{\overline{P}}}{1,000,000} \left(8L^2 + 0.004 L k_{brace} - 5100L - k_{brace} + 900,000 \right) - \frac{D}{48} \frac{P_U}{w_{sw}}$$

(5.4)

where C is the system capacity in g, L is the span length in ft, D is the FIB cross-section depth in in., P_U is the unshielded wind load in psf, $\overline{P}$ is the average wind load per girder in psf, k_{brace} is the effective brace stiffness in kip-ft/rad, ω is determined from Table 5.1, w_{sw} is the girder self-weight in lbf/ft (Table 5.2), and C_0 [which has been updated in the present study as Eqn. (5.3)] is in g.

Table 5.1 Empirically-determined values of ω for different numbers of interior braces

n_i	Brace locations	ω
0	End bracing	1.0
1	Midpoint bracing	1.4
2	Third-point bracing	1.6
3	Quarter-point bracing	1.7

Table 5.2 Self-weight (w_{sw}) of each FIB cross-sectional shape (from FDOT, 2012b)

Cross-section	w_{sw} (lbf/ft)
36″ FIB	840
48″ FIB	906
54″ FIB	971
63″ FIB	1037
72″ FIB	1103
78″ FIB	1146
84″ FIB	1190
96″ FIB	1278

To account for the effects of wind pressure on system capacity, an average wind pressure per girder, $\overline{P}$ [reported as Eqn. (9.7) in Consolazio et al., 2013] was defined:

$$\overline{P} = \frac{\sum P}{n}$$

(5.5)

where n is the number of girders in the bridge and $\sum P$ is the sum of the individual wind pressures on all girders.

Recalibration of the additional correction factors in Eqn. (5.4) to account for an updated definition of sweep (i.e., with inclusion of thermal sweep) was outside the scope of the present study. However, a limited scope parametric study was conducted to compare system capacities

computed using full FEA bridge models to capacities computed using Eqn. (5.4) supplemented with the updated baseline capacity (C_0) equation [i.e., Eqn. (5.3)].

5.4.1 Selection of parameters for limited scope moment-resisting brace parametric study

System parameters varied in the moment-resisting brace parametric studies that were conducted in BDK75-977-33, and in the present study, were as follows:

- FIB cross-section depth (in.)
- Span length (ft)
- Wind pressure (psf)
- Effective brace stiffness (kip-ft/rad)
- Number of interior brace points
- Skew angle (deg.)

In BDK75-977-33, seven (7) of the eight (8) standard FIB cross-sections were considered. (The 36″ FIB was excluded because the cross-section is so shallow that use of moment-resisting braces is unwarranted and unfeasible). For each FIB, capacity analyses were performed for every combination of span length, wind pressure, effective brace stiffnesses, and number of interior brace points sampled from the values listed in Table 5.3. Only two-girder systems were considered because it was determined from the preliminary sensitivity studies that when moment-resisting braces are used, the two-girder system is always the least stable phase of construction.

Table 5.3 Parameter values used in moment-resisting brace
parametric study from BDK75-977-33

Span length, L (ft)						
45″ FIB	**54″ FIB**	**63″ FIB**	**72″ FIB**	**78″ FIB**	**84″ FIB**	**96″ FIB**
95	110	120	135	145	155	170
105	120	130	145	155	165	180
115	130	140	155	165	175	190
125	140	150	165	175	185	200
135	150	160	175	185	195	205
-	-	-	185	-	-	220

Unshielded wind pressure, P_U (psf)	Eff. brace stiffness, k_{brace} (kip-ft/rad)	Int. brace points, n_i	Skew angle
0	15,000	0	0°
40	200,000	1	2°
80	400,000	2	5°
120	600,000	3	10°
160			25°
			50°

Wind pressure loads were applied to the girders using the shielding pattern proposed in BDK75-977-33 (shown in Figure 5.5), and using the wind pressures listed in Table 5.3. Wind pressures specified in the table refer to the unshielded pressure load applied to the windward girder (G1). Hence, in accordance with the wind load model proposed in BDK75-977-33, the first shielded girder (G2) received no wind load and all subsequent girders (G3, G4, etc.), if any, received half of the listed pressure load. The maximum wind pressure of 160 psf was determined using the *Structures Design Guidelines* (FDOT, 2012d) by assuming a pressure coefficient of C_P = 2.0, a basic wind speed of V = 150 mph, a bridge elevation of z = 75 ft, a gust effect factor of G = 0.85 and a load multiplier of γ_{ws} = 1.4 (corresponding to the Strength III limit state).

For the moment-resisting braces, the number of interior brace points varied from 0 (end bracing only) to 3 (end bracing plus quarter-point interior bracing), and girders in each system model were spaced at 6 ft on center. Furthermore, in moment-resisting braces, changes in girder spacing produce changes in the geometric configuration of the brace members, thus changing the effective stiffness of the braces. Such changes can significantly affect system capacity and must be considered. In moment-resisting brace parametric studies, the effects of changing girder spacing were accounted for by varying the effective brace stiffness parameter, even though the physical length of the reference brace remained a constant 6 ft.

In the present project (BDV31-977-46), parameters for a limited scope parametric study were determined by selecting a reduced set of FIB cross-section depths, span lengths, and skew parameters from those used in the previous moment-resisting-brace parametric study (BDK75-977-33). Final parameters selected for the limited scope parametric study are listed in Table 5.4 (and can be compared to the complete list of parameter values used in BDK75-977-33, shown in Table 5.3). To cover a range of upper and lower bounding system capacities, 54" FIB, 78" FIB, and 96" FIB cross-sections were selected. Similarly, for each FIB cross-section depth, minimum span length, intermediate span length, and a maximum span length were selected. Skew angles of 0° and 25° were selected to cover a wide range of common skew angles used in bridge design. Parametric values of the remaining parameters (i.e., unshielded wind pressure, effective brace stiffness, and number of interior brace points) were the same as used in BDK75-977-33. In total, 1,440 models were analyzed.

Table 5.4 Selected parameter values used in the present moment-resisting brace parametric study

Span length, L (ft)		
54″ FIB	78″ FIB	96″ FIB
110	145	170
130	165	190
150	185	220

Unshielded wind pressure, P_U (psf)	Eff. brace stiffness, k_{brace} (kip-ft/rad)	Int. brace points, n_i	Skew angle
0	15,000	0	0°
40	200,000	1	25°
80	400,000	2	
120	600,000	3	
160			

5.4.2 Updated system capacity of moment-resisting brace

Results from the limited scope parametric study and corresponding predicted capacities (C) determined using Eqn. (5.3) and Eqn. (5.4) [i.e., Eqn. (9.23) from BDK75-977-33] are displayed in Figure 5.9. Results are sorted by descending capacity—and separated by FIB girder type and skew angle—to visualize the level of conservatism in predicted capacities. Results from BDK75-977-33 corresponding to the parameters selected for the present study (i.e., parameters listed in Table 5.4) are shown in Figure 5.9a, and compared with predicted system capacity (C) quantities using Eqn. (9.23) and Eqn. (9.2) from BDK75-977-33. Results from the present study are compared with predicted system capacities (C) calculated using Eqn. (5.3) and Eqn. (5.4) in Figure 5.9b.

The level of conservatism in the final moment-resisting-braced system capacity (C) equation with an updated baseline (C_0) equation is displayed in the form of a histogram in Figure 5.10. In BDK75-977-33, systems with capacities exceeding 10 g (i.e., extremely stable systems) were excluded from consideration in the development of the final moment-resisting-braced system capacity prediction equation. Under the same criteria, predicted capacities for essentially all systems (99%) considered in the present limited scope parametric study (with an updated definition of sweep) were conservative.
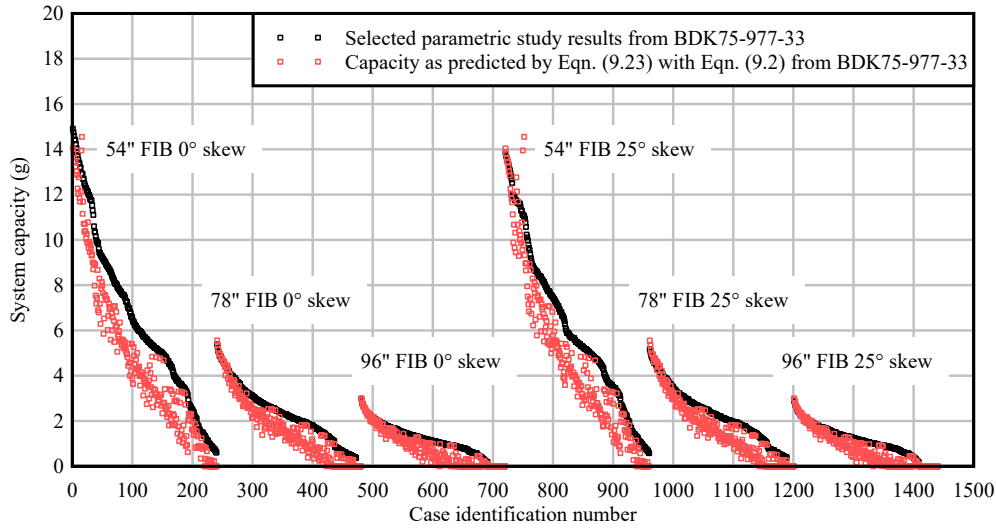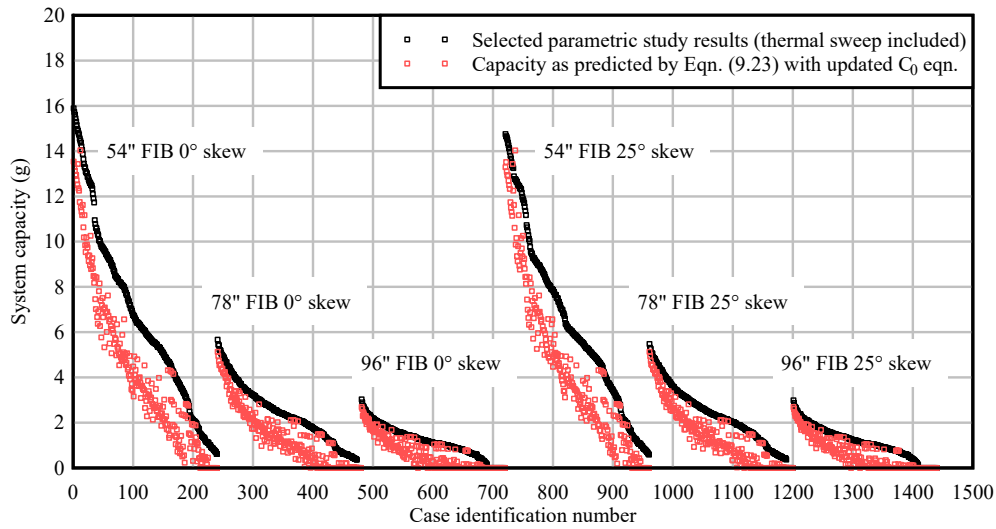
Figure 5.9 System capacity of moment-resisting two-girder FIB system:
(a) Partial data from BDK75-977-33 and predicted capacity from Eqn. (9.23) from BDK75-977-33; (b) Updated FEA data developed in present study, and predicted capacity from Eqn. (5.3) (present study) and Eqn. (5.4)

The moderate increase in conservatism evident in Figure 5.9b (i.e., a larger gap between parametric capacities and predicted capacities), compared with Figure 5.9a, is the result of two influences. First, the reduced capacities predicted by the baseline capacity (C_0) Eqn. (5.3) (accounting for thermal sweep) propagate through Eqn. (5.4) to yield lower system capacity (C) values. This downward influence of C_0 on computed C values is illustrated in Figure 5.11. Second, the parametric finite element data shown in Figure 5.9b are obtained from models that employ a concrete strength of $f_c' = 8.5$ ksi, rather than the $f_c' = 6.5$ ksi that was assumed in

BDK75-977-33. Due to the increase in concrete strength f_c', and corresponding increase in concrete modulus E_c, the capacities computed by finite element analysis increase (Figures 5.12 and 5.13). Thus the combined effects of reduced C_0 and increased E_c moderately increase the gap between empirically predicted capacity and finite element computed capacity.
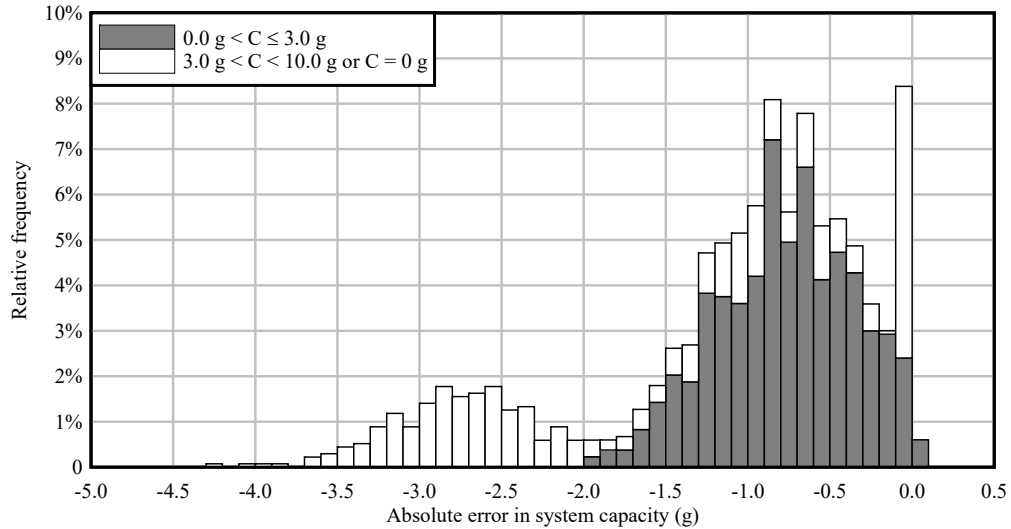
Figure 5.10 Absolute error of system capacity quantities predicted
by Eqn. (5.4) from BDK75-977-33 with updated C_0 equation [Eqn. (5.3)]
(Note: negative absolute error indicates conservative prediction of capacity)
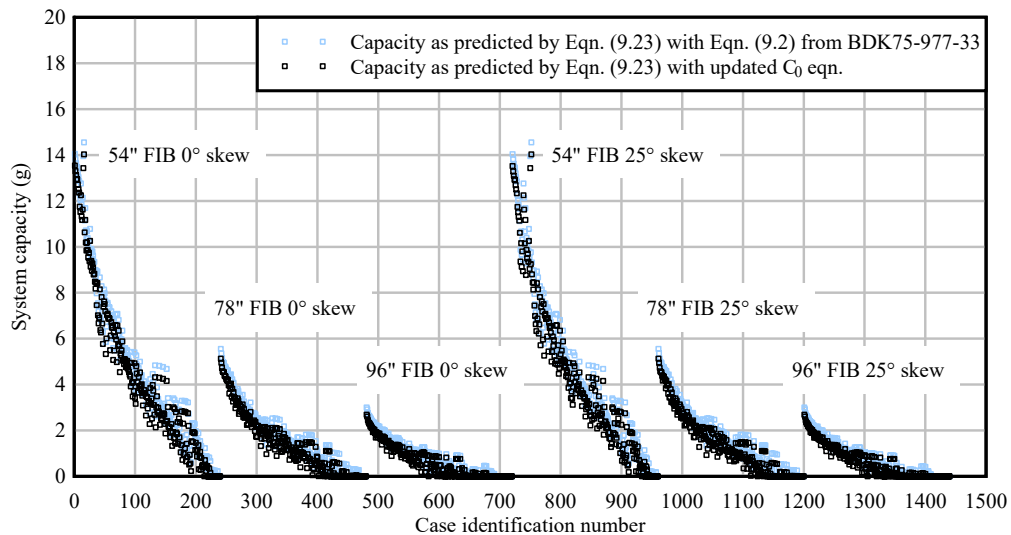
Figure 5.11 Comparison of predicted capacities
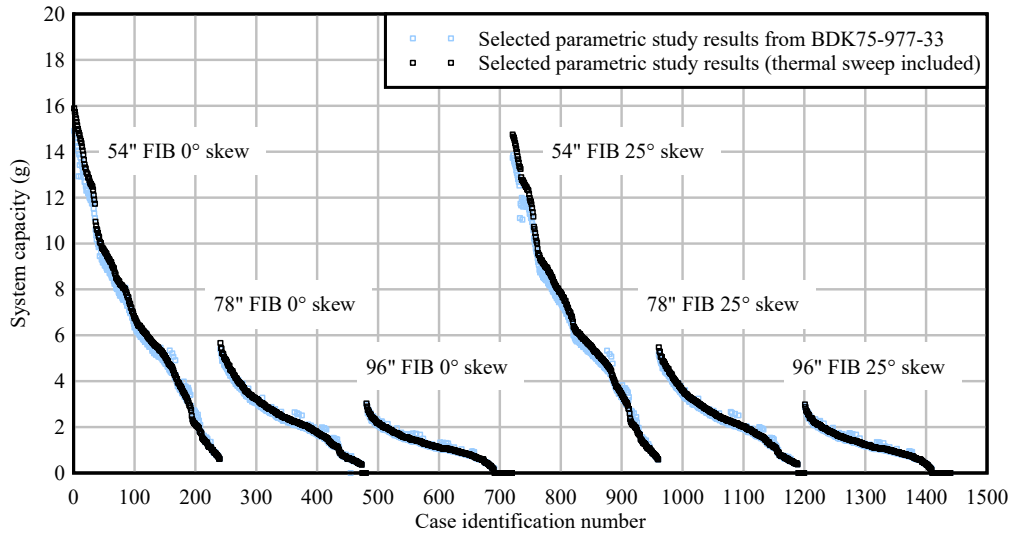
Figure 5.12 Comparison of selected parametric study data from BDK75-977-33 with updated parametric study data (thermal sweep included)
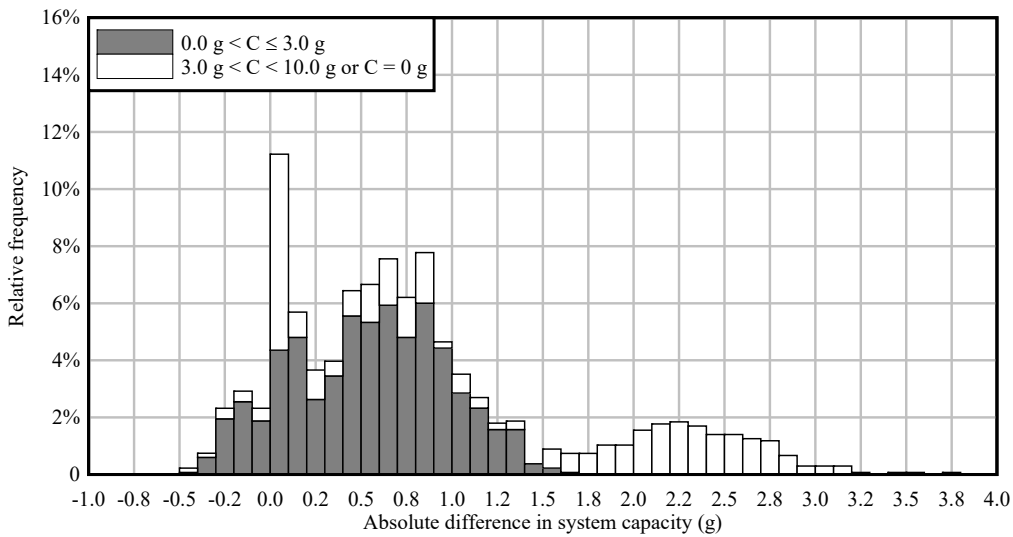
Figure 5.13 Absolute difference of current to previous parametric study system capacity quantities (Note: positive absolute difference indicates increased system capacity from previous study)

CHAPTER 6
PROCEDURES DEVELOPMENT FOR CONSTRUCTION LOAD
DISTRIBUTION FACTOR EQUATIONS

6.1 Introduction

In the development of distribution factors for girder end shears and moments that are induced by bridge construction loads, the deck placement (concrete application and finishing) was the construction stage and process considered. Components of the bridge construction loads considered were as follows:

- Concrete deck: Throughout the deck placement and finishing process, the wet (plastic) concrete has *negligible stiffness*. Consequently, a non-composite girder system must support these construction loads. However, in the final bridge condition, the bridge deck works together with the girders as a composite system to resist and distribute loads to the supporting girders. Since the wet (non-structural) concrete load is incrementally applied to bridges in the longitudinal direction, this load is treated as a variable length load in the finite element analyses. Partial application of concrete deck loads to the girder system will be further explained later in this report.

- Stay-in-place formwork: Stay-in-place (SIP) formwork systems support intra-girder loads (wet concrete) that span transversely between girder top flanges (Figure 6.1). Stay-in-place forms consist of corrugated metal panels that are attached to the tips of the top flange of adjacent girders. The connection between the SIP forms and the girder flange is considered to be incapable of transmitting moments, therefore the SIP forms are essentially treated as being 'simply supported' on the girder flange tips.
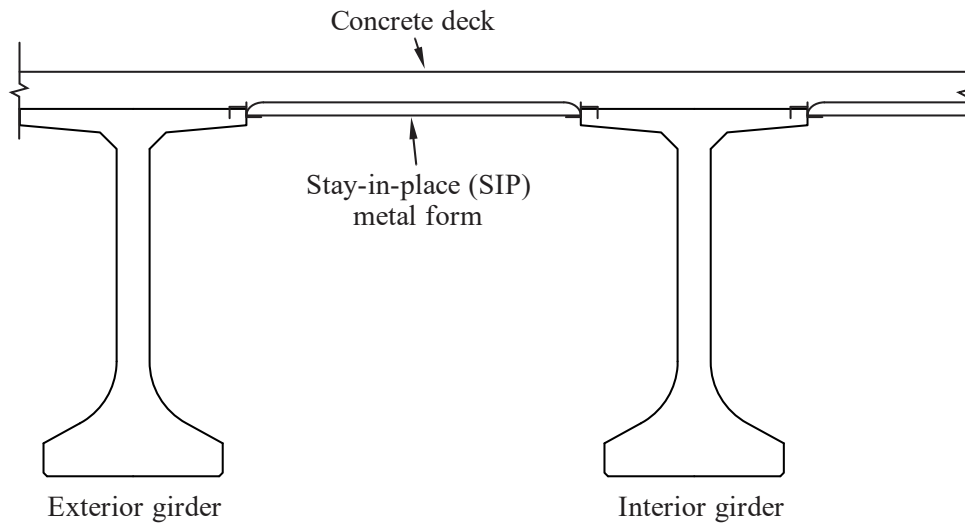
Figure 6.1 Stay-in-place formwork (section view)

- Overhang formwork: It is typical for the deck of a bridge to extend past the exterior (fascia) girders, thereby producing cantilevered overhangs (Figure 6.2). During construction, *overhang brackets* (Figure 6.3) are used to temporarily support the cantilever portion of the wet deck slab that extends beyond exterior girders. These temporary structural bracket

systems support the overhang formwork, wet concrete, construction walkway, workers and concrete finishing machine. In BDK75-977-70, a survey of representative literature from overhang bracket manufacturers was conducted to quantify representative cross-sectional properties and longitudinal spacing requirements. Most commercially available formwork systems consist of timber joists and sheathing supported on steel bridge overhang brackets (Figure 6.4). It is important to note that all of the gravity loads supported by the overhang brackets are eccentric relative to the exterior girders, and as such apply torque loads to the exterior girders in the overall cross-sectional system.

Overhang supported by overhang brackets
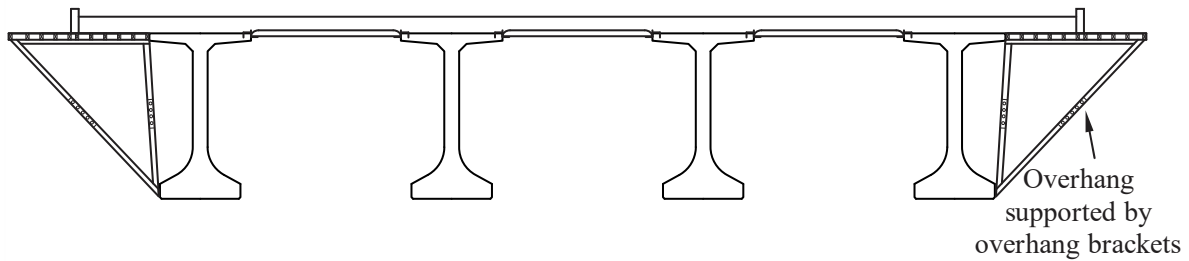
Figure 6.2 Temporary support brackets used to support deck overhangs during construction

Figure 6.3 Cantilever overhang supported by overhang brackets
(Photo credit: Clifton and Bayrak, 2008)
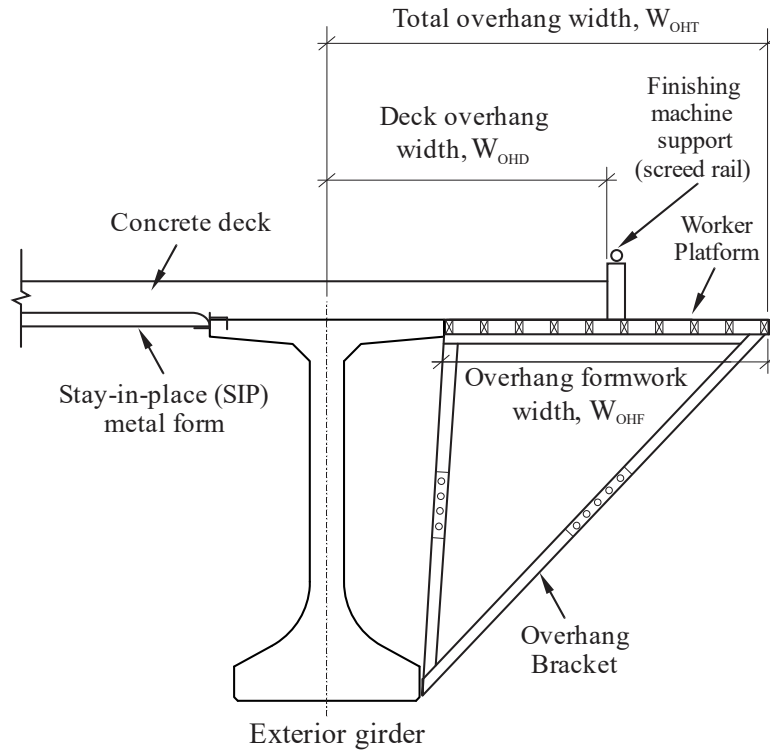
Figure 6.4 Details of overhang formwork support brackets and loads

- Finishing machine: Bridge deck finishing machines (Figure 6.5) spread, compact, and finish the freshly placed wet concrete deck surface. The finishing machine is an open steel frame that is supported at the extremities of the bridge width on the overhang brackets described above. Drive wheels (commonly referred to as bogies) move the paver longitudinally along the length of the bridge and are eccentrically supported by screed rails (Figure 6.4) on each side of the bridge. A suspended paving carriage with augers, drums, and floats finishes the concrete surface as it moves transversely from side to side across the width of the bridge (perpendicular to the longitudinal movement of the finishing machine along the length of the bridge). Concrete is typically placed just ahead of the travelling finishing machine using separate equipment, such as a pump.

- Live loads: Live loads that are present during the deck finishing process consist of workers, temporary materials, and supplementary construction equipment. For modeling purposes, these loads are treated as either uniform pressure loads, or as line loads, as will be discussed in greater detail later.

Figure 6.5 Typical bridge deck finishing machine in operation
(Photo credit: Gomaco)

6.2 Modeling multi-girder bridge systems during construction

Numerical modeling and analysis techniques developed in FDOT study BDK75-977-70 (Consolazio and Edwards, 2014), were extended in the present study for purposes of quantifying girder forces induced by construction loads. Each numerical finite element model was suitable for analyzing construction loads acting on systems of precast concrete girders (Florida-I Beams) braced together (including the influence of brace configuration, bearing pad stiffness, etc.). The modeling techniques allow for consideration of different Florida-I Beam cross-sections, span lengths, girder spacings, deck overhang widths, skew angles, number of girders, number of braces, and bracing configurations (K-brace and X-brace). Additionally, partial coverage of wet (non-structural) concrete load and variable positioning of deck finishing machine loads were considered. In all cases, structural element forces were determined using large-displacement (i.e., geometrically nonlinear) analyses, in which static loads were applied to the models in incremental steps, taking into account the deformed state of the structure at each step.

Construction loads applied beyond the lateral extents of an exterior girder are structurally supported during construction by *overhang brackets*. Specifically, the finishing machine, formwork, overhang wet concrete, and construction worker live loads are typical loads supported by overhangs. To define the lateral eccentricity of the overhang construction loads, two offset parameters were established (in BDK75-977-70). To be consistent with the *FDOT Instructions for Design Standard No. 20010: Prestressed Florida-I Beams* (FDOT, 2014b), the concrete finishing machine was offset 2.5 in. from the overhang edge (Figure 6.6). In the *FDOT Concrete I-girder Beam Stability Program*, in addition to providing calculations for determining bracing adequacy and girder stability, several recommended values for the overhang geometry are specified, including a 2-ft worker platform width. Therefore, for all the numerical studies conducted herein, the worker platform was assumed to extend 2 ft beyond the finishing machine supports (Figure 6.6).

In the finite element bridge models, components of the overhang brackets were modeled with beam elements, using representative cross-sectional properties obtained from a survey of overhang bracket manufacturers. To represent the offset eccentricities between the girder centroid and bracket connection points, the deformable overhang bracket elements were connected to girder warping beam elements using rigid links (Figure 6.7). To model interaction between the overhang bracket and the girder bottom flange, two co-located—but separate—nodes were used: one at the bottom vertex of the metal overhang bracket, and a second at the end of the rigid link representing the surface of the girder bottom flange. At this location, the overhang bracket bears against (i.e., is in compressive contact with) the girder bottom flange. To model this behavior structurally, a constraint condition was defined such that the lateral (X-direction) translations of the two co-located nodes were constrained to match, while permitting independent movements (relative slip) in the vertical direction.

Overhang bracket nodes were positioned (Figure 6.7) to define: the three corners of the triangular system; and all locations of load discontinuities (i.e., deck overhang edge) and load application points (i.e., finishing machine and worker line load application points). The worker line load was conservatively applied to the center of the worker platform width. Thus, the load application of the worker line load was laterally offset in the X-direction 12 in. from the assumed finishing machine application point and 14.5 in. from the deck overhang edge (Figure 6.7).
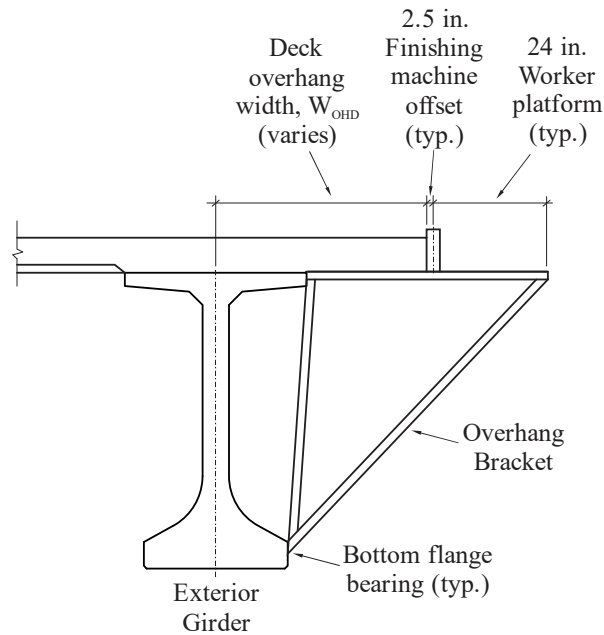
Figure 6.6 Overhang bracket components and geometry
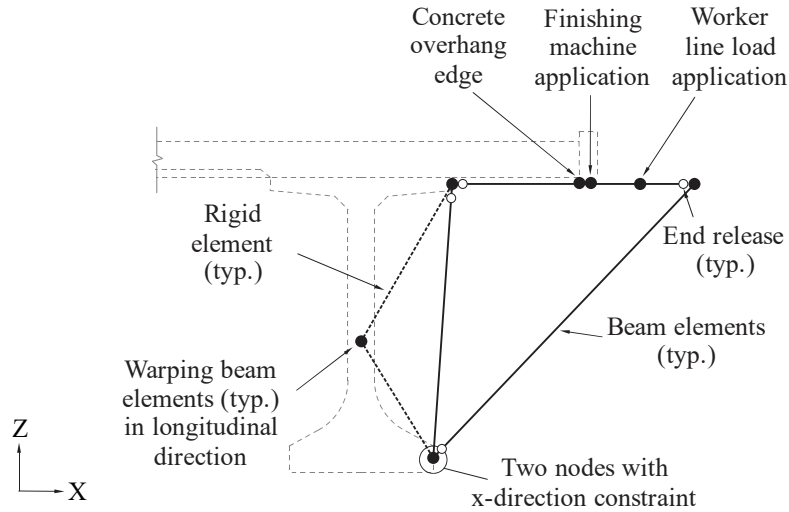
Figure 6.7 Details of overhang bracket model

Combining each of the previously mentioned modeling components, an overall illustration of a typical FIB system model is presented in Figure 6.8. Based on a review of literature obtained from typical overhang bracket manufacturers, brackets were commonly found to be spaced at between 4 ft and 6 ft on-center longitudinally along the span length of a bridge. Therefore, an average longitudinal spacing of 5 ft was used for all brackets (Figure 6.9).

Shown in Figure 6.8 and Figure 6.9 are rigid vertical elements (links)—extending from girder centroid to girder top surface—which were included in the model for application of construction loads on each girder. These rigid elements account for the vertical eccentricity between the girder centroid and the girder top surface (where loads were applied). It was determined that brace forces induced by construction loads were not sensitive to changes in the longitudinal spacing of the rigid vertical elements, consequently the rigid links were given an arbitrary longitudinal spacing of 1 ft in the span direction.
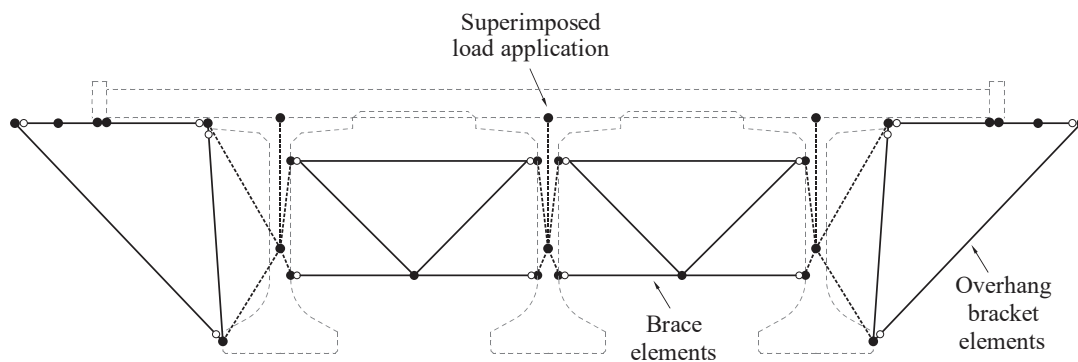
Figure 6.8 Cross-sectional view of overall braced girder system model
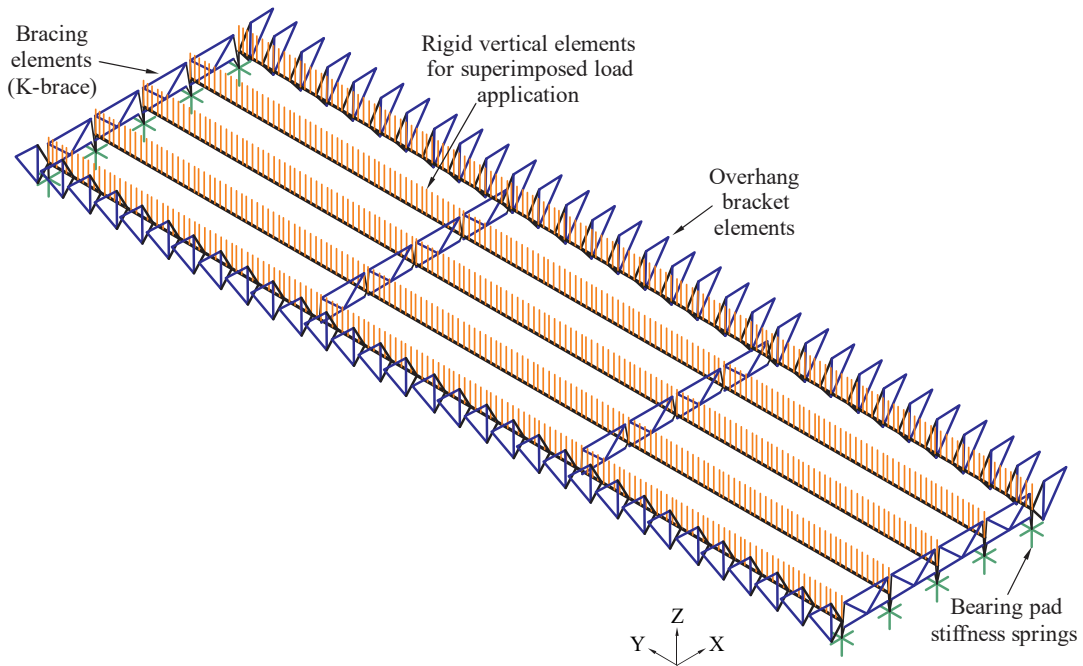
Figure 6.9 Isometric view of braced girder system model

6.3 Application of construction loads

During bridge construction, self-weight (i.e., gravity) loads from girders, braces, formwork, and overhang brackets act in combination with a variety of superimposed loads. A key load among the superimposed loads is the application of concrete finishing machine weight. Finishing machines are supported near the extremities of the bridge width by several wheels. The common Terex Bid-Well 4800 machine has a total wheel base of approximately 8 ft in the longitudinal (bridge span) direction. Since this wheel base is small relative to the typical span lengths of prestressed girder bridges, the finishing machine wheel reaction forces were idealized as single concentrated loads (one load on each side of the bridge, equal to half the total machine weight). Construction loading conditions specified in the *Structures Design Guidelines* (FDOT, 2016) stipulate that, in the absence of manufacturer's specifications, the finishing machine weight shall vary as a function of bridge width, as indicated in Table 6.1. For the present study, the FDOT minimum bridge width specification was reduced from 26 ft to 0 ft, to enable inclusion of bridge configurations narrower than 26 ft, and 'bridge width' was defined to be the completed (finished) bridge deck width (i.e., from edge to edge of the deck, excluding temporary overhang formwork).

Table 6.1 Varying finishing machine load
(based on FDOT *Structures Design Guidelines*, 2016)

Bridge Width, W (ft)	Total Weight of finishing machine (kips)
$0 < W \leq 32$	7
$32 < W \leq 56$	11
$56 < W \leq 80$	13
$80 < W \leq 120$	16

46

As concrete placement and finishing of the bridge deck progresses, concentrated live loads (e.g., workers standing on the overhang platforms) will be applied at the lateral extremities of a bridge. To account for such loads, the *AASHTO Guide Design Specifications for Bridge Temporary Works* (2008) recommends that a 'worker line load' of 75 lb/ft (un-factored) be applied along the outside edge of each deck overhang. The line load is stipulated to be applied as a moving load (i.e., co-located with the finishing machine position) but with a fixed longitudinal length of 20 ft, so as to not introduce excessive conservatism. For numerical modeling purposes, when the finishing machine was either at the start or the end of a bridge, the worker line load was applied over the first or last 20 ft of the structure, respectively. For all other cases, where the finishing machine was positioned at an interior brace point, the 20-ft worker line load was longitudinally extended 10 ft ahead of and behind the finishing machine.

Additionally, in accordance with AASHTO design specifications, an un-factored 20-psf construction live load was also applied to each numerical bridge model analyzed. To be consistent with FDOT guidelines, the 20-psf live load was extended over the entire bridge width, and was extended 50 ft in longitudinal direction, but centered on the finishing machine location (*Structures Design Guidelines*, FDOT, 2016). For load cases where the finishing machine was located at either the start or the end of a bridge (i.e., within 25 ft of either end), the construction live load was applied over the first or last 50 ft of the bridge length.

In physical bridge construction, wet concrete pressure load is applied to a bridge (by way of stay-in-place forms) over incrementally increasing lengths, as deck placement progresses. The wet concrete is typically placed just ahead of the moving finishing machine using a pump, therefore, in a vast majority of paving situations, the location of the finishing machine and the end of the concrete coverage will coincide. For purposes of numerical modeling, the loading conditions considered in this study included placement of concrete deck loading over the *full length* of bridge as well as *partial lengths* of bridge. For partial coverage cases, the position of the finishing machine was taken to coincide with the location of the furthest placed concrete.

6.3.1 Construction load groups considered

Construction loads were separated into two groups (Table 6.2) so that distribution factors could be computed *separately* for each group. The key distinction between the two load groups was that loads included in Load Group 1 were considered to be *live loads*, whereas loads in Load Group 2 were considered to be *dead loads*. To ensure that maximum (i.e., controlling) distribution factors were quantified in the construction load parametric study, multiple load cases for each load group were analyzed. Construction Load Group 1 load cases are shown in Figures 6.11-6.14. Similarly, Construction Load Group 2 loads were analyzed with multiple load cases where the wet concrete deck location was incrementally advanced in the longitudinal span direction (stopping at each brace point), as illustrated in Figures 6.16-6.19.

Table 6.2 Summary of construction load groups in parametric studies

Construction Load Group 1	Load type	Load	Reference
Live load	Temporary	20 psf (for 50 ft, longitudinally)	I
Worker line load	Temporary	75 lb/ft (for 20 ft, longitudinally)	I
Finishing machine	Temporary	Varies with bridge width (Table 6.1)	I

I: per FDOT Structures Design Guidelines (2016)

Construction Load Group 2	Load type	Load	Reference
Wet concrete deck	Permanent	106.25 psf (8.5" thick, 150 pcf)	I
Wet concrete build-up	Permanent	50 lb/ft	I
Stay-in-place forms	Permanent	20 psf	I
Overhang formwork	Temporary	10 psf	II
Overhang brackets	Temporary	Self-weight	

I: per FDOT Structures Design Guidelines (2016)
II: per FDOT recommendations
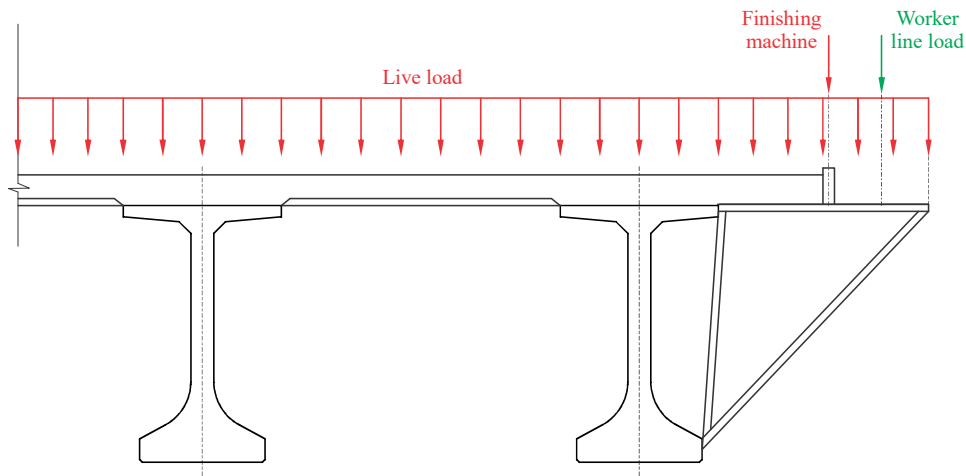
Figure 6.10 Cross-sectional summary of construction *Load Group 1* (*LG1*) loads
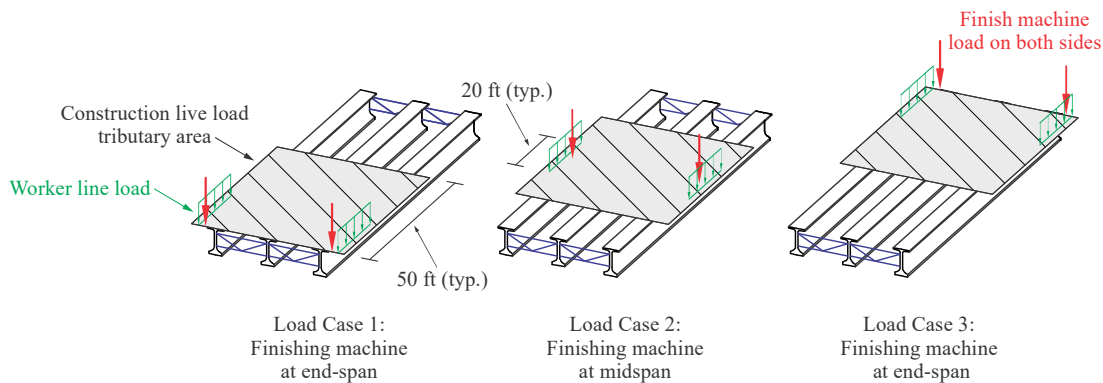
Figure 6.11 Construction *Load Group 1* as a function of finishing machine location
(Bridge with only end-span braces; no interior braces)

Load Case 1:
Finishing machine
at end-span

Load Case 2:
Finishing machine
at midspan

Load Case 3:
Finishing machine
at end-span
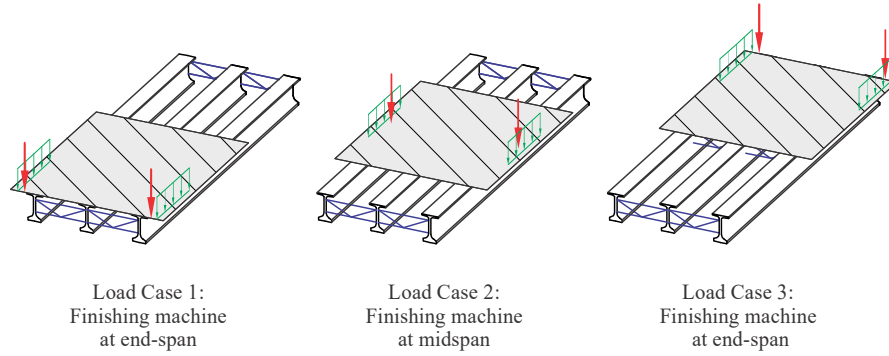
Figure 6.12 Construction *Load Group 1* as a function of finishing machine location
(Bridge with end-span and midspan bracing)

Load Case 1:
Finishing machine
at end-span

Load Case 2:
Finishing machine
at 1/3-span

Load Case 3:
Finishing machine
at midspan

Load Case 4:
Finishing machine
at 2/3-span

Load Case 5:
Finishing machine
at end-span
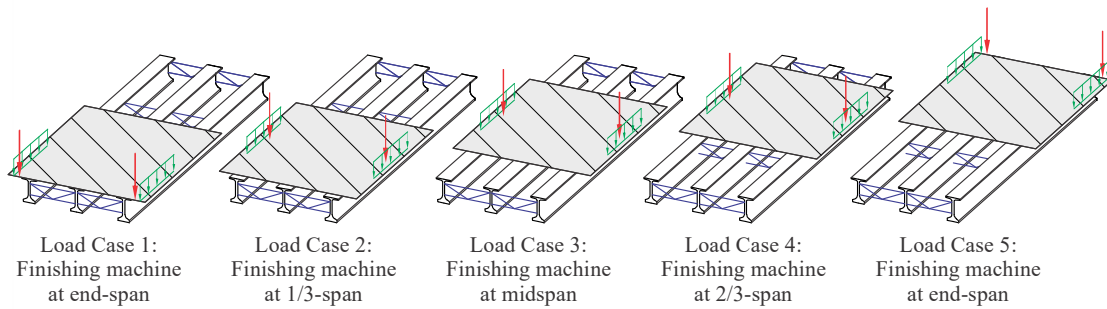
Figure 6.13 Construction *Load Group 1* as a function of finishing machine location
(Bridges with third-point bracing)

Load Case 1:
Finishing machine
at end-span

Load Case 2:
Finishing machine
at 1/4-span

Load Case 3:
Finishing machine
at midspan

Load Case 4:
Finishing machine
at 3/4-span

Load Case 5:
Finishing machine
at end-span
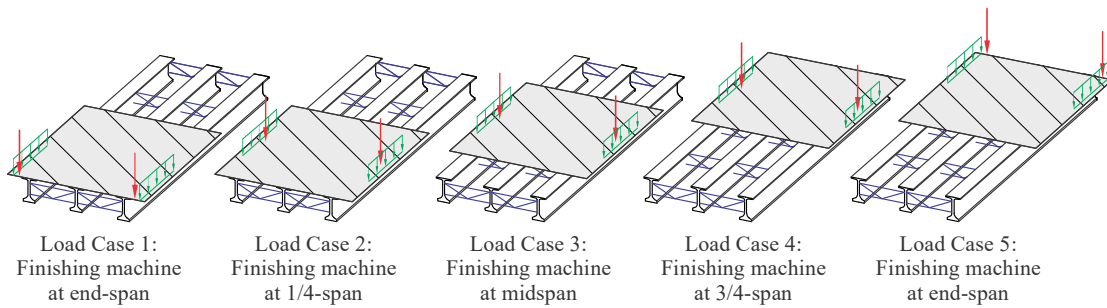
Figure 6.14 Construction *Load Group 1* as a function of finishing machine location
(Bridges with quarter-point bracing)
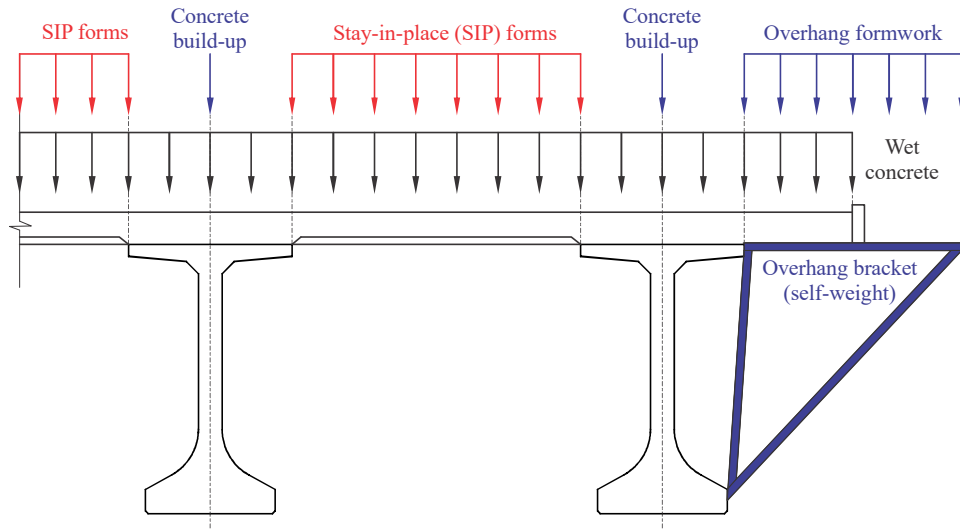
Figure 6.15 Cross-sectional summary of construction *Load Group 2* (*LG2*) loads
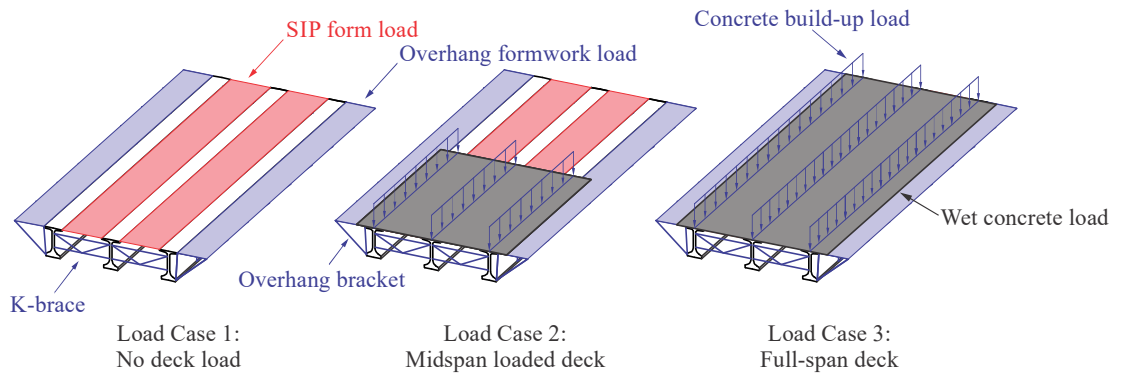
Figure 6.16 Construction *Load Group 2* with incremental deck load
(Bridge with only end-span braces; no interior braces)
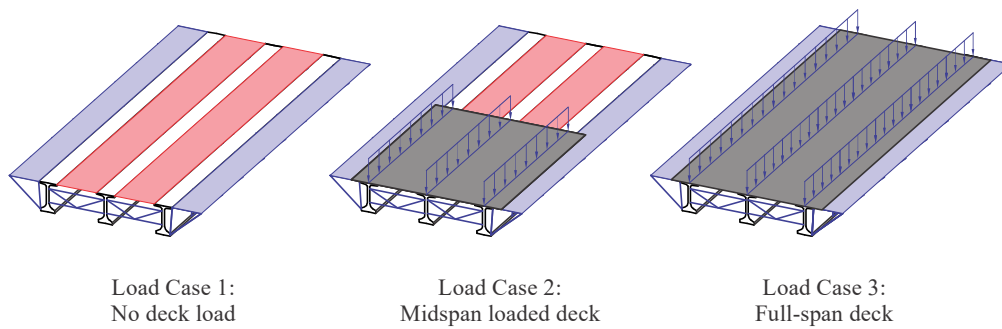
Figure 6.17 Construction *Load Group 2* with incremental deck load
(Bridge with end-span and midspan bracing)

Load Case 1:   Load Case 2:   Load Case 3:   Load Case 4:
No deck load   1/3-span deck   2/3-span deck   Full-span deck
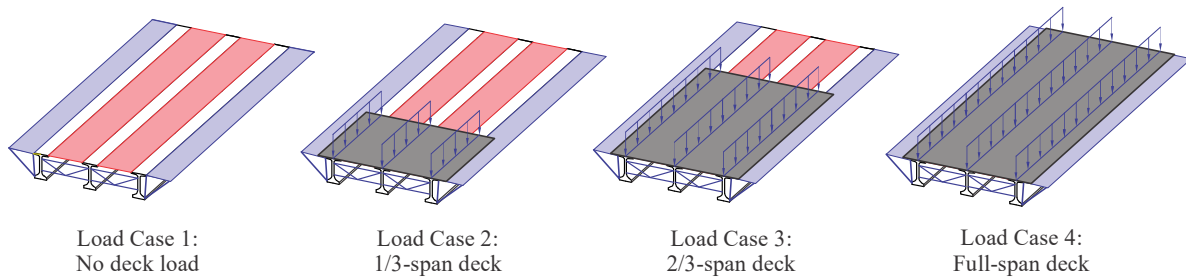
Figure 6.18 Construction *Load Group 2* with incremental deck load
(Bridges with third-point bracing)

Load Case 1:   Load Case 2:   Load Case 3:   Load Case 4:   Load Case 5:
No deck load   1/4-span deck   1/2-span deck   3/4-span deck   Full-span deck
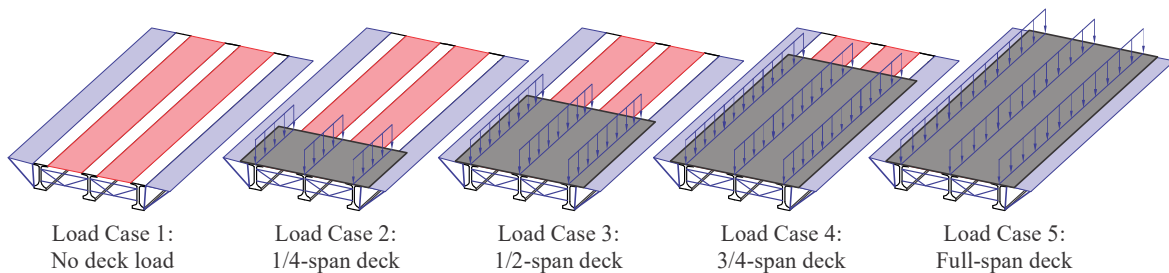
Figure 6.19 Construction *Load Group 2* with incremental deck load
(Bridges with quarter-point bracing)

6.3.2 Application of construction loads

Construction loads that are applied between adjacent girders (e.g., on the stay-in-place forms) produce vertical reaction forces that act on the tips of the girder top flanges. Since all Florida-I Beams have a top flange width of 48 in., the lateral eccentricity between the girder centroid and the formwork reaction force (Figure 6.20) is 24 inches (half of the girder top flange width). For numerical modeling and analysis purposes, each eccentric reaction force of this type was converted into statically equivalent forces and moments (Figure 6.20) which were then applied along the centerlines of the girders.

Consequently, all intra-girder distributed pressure loads that were applied over the width of the stay-in-place formwork were converted into equivalent nodal forces and moments. Other types of construction loads, such as the overhang loads (overhang formwork, worker line load, etc.), were applied directly to nodes in the structural model based on the appropriate tributary areas (Figure 6.21).

51
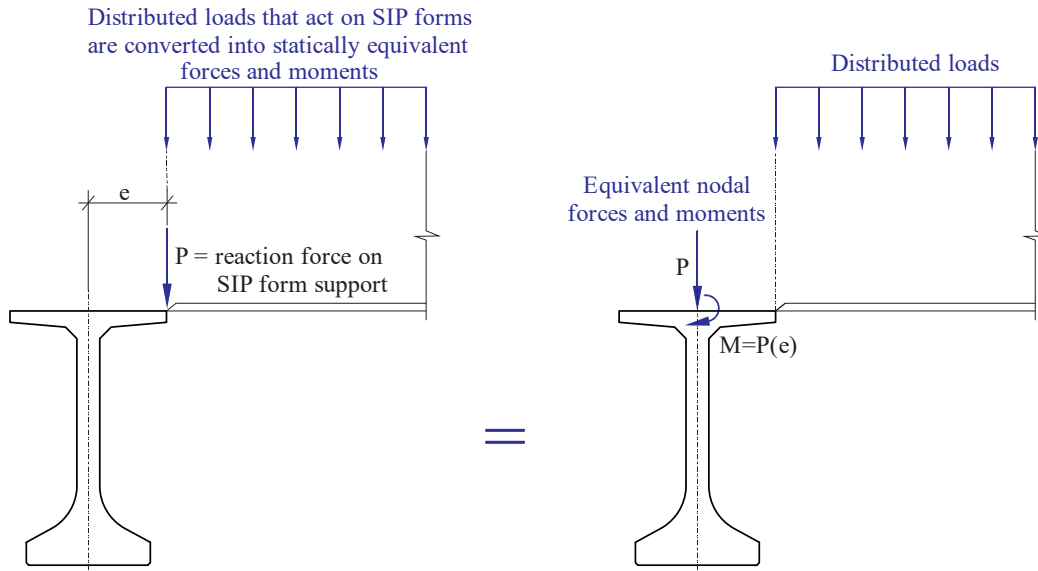
Figure 6.20 Eccentric reaction forces from loads applied to SIP forms, and statically equivalent nodal force and moment applied to top of girder
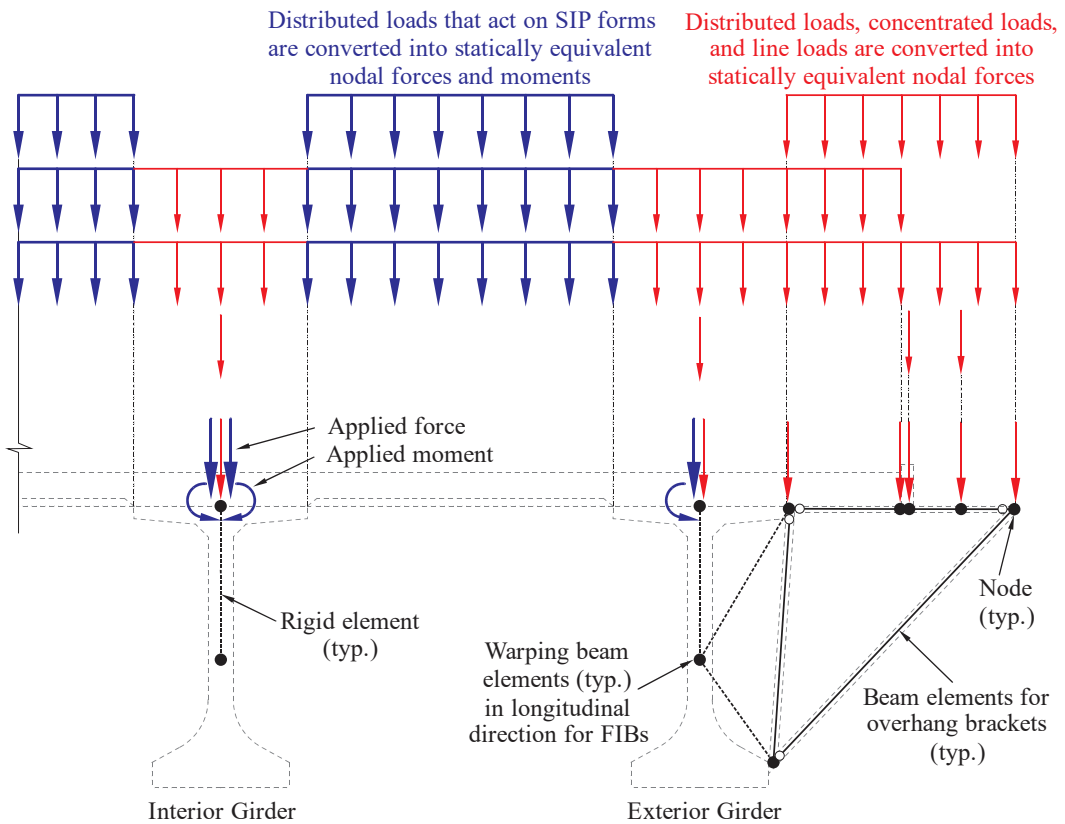
Figure 6.21 All construction loads (LG1 and LG2) converted to equivalent nodal loads

CHAPTER 7
DEVELOPMENT OF CONSTRUCTION LOAD DISTRIBUTION FACTOR EQUATIONS

7.1 Construction load distribution factor parametric study

7.1.1 Scope

To develop empirical construction load distribution factor (*DF*) equations, a large-scale construction load distribution factor parametric study was conducted. Three-dimensional (3-D) structural analyses were conducted (using automation scripts) to generate and analyze structural analysis models using the ADINA (2016) finite element code. The parametric study was conducted to quantify girder end shear forces and maximum girder moments. Since several geometric parameters influence the magnitude and distribution of maximum girder moments and girder end shear forces caused by construction loads, it was necessary to conduct a parametric study covering a wide range of possible parameters:

- Construction Load Group (*LG1* or *LG2*)
- FIB cross-section depth (in.)
- Span length (ft)
- Skew angle (deg.)
- Number of brace points (end-span only, 1/2 point, 1/3 point, 1/4 point)
- Brace type (K-brace or X-brace)
- X-brace material type (steel or timber)
- Deck overhang width (in.)
- Girder spacing (ft)
- Number of girders
- Finishing machine location or non-structural deck dead load location

Specific parameter values that were included in the parametric study—which involved 290,304 separate analyses—are listed in Table 7.1.

Span lengths were chosen to represent a shorter-than-typical length, a practical minimum, an intermediate length, and a practical maximum length (per design FDOT aids cited in Consolazio and Edwards, 2014). Additional geometric parameters, such as skew angle, deck overhang width, and girder spacing, were selected to cover a range of typical bridge configurations, as determined in Consolazio and Edwards (2014) based on a survey of typical Florida bridges and FDOT design recommendations.

Table 7.1 Parameter values used in the distribution factor parametric study

Span length, *L* (ft)						
45″ FIB	**54″ FIB**	**63″ FIB**	**72″ FIB**	**78″ FIB**	**84″ FIB**	**96″ FIB**
40	50	60	60	70	80	80
90	110	120	130	140	160	170
110	130	140	150	160	180	190
130	150	160	170	180	200	210

Skew angle	Intermediate-span brace points, n_i	Deck overhang width, (in.)	Girder spacing, (ft)	Girders, n_g
0°	0	25	6	3
15°	1	48	9	5
30°	2	72	12	9
45°	3			

In regard to the choice of cross-brace (X-brace) construction material—i.e., timber or steel—that was implemented in the numerical bridge models, the original intent was to identify whichever material produced the more conservative results, and then include only that material in the final parametric study. However, after conducting a preliminary sensitivity study, it was determined that timber X-braces produced larger exterior girder end shear forces and moments in some cases, while steel X-braces produced larger interior girder end shear forces and moments. Consequently, separate analyses of both timber X-brace configurations and steel X-brace configurations were modeled for each bridge included in the parametric study.

7.1.2 Special cases

As a consequence of including timber X-braces in the parametric study, some Load Group 2 (LG2) models were found—through analysis—to be unstable. However, all such cases were found to correspond to long span bridges with *end-span-only* timber X-bracing. Using timber X-bracing *only* at the ends of a bridge is not typical practice and does not meet standard bracing design requirements. Consequently, each model that was determined to be unstable in this manner was removed from the distribution factor parametric study.

7.2 Definition of distribution factors

After analyzing all parametric models using ADINA (2016), girder end shear forces and maximum girder moments were quantified and processed into distribution factors, which were defined as:

$$DF_V = \frac{V_{GIRDER}}{\sum V_{GIRDER}} \tag{7.1}$$

$$DF_M = \frac{M_{GIRDER}}{\sum M_{GIRDER}} \tag{7.2}$$

where, DF_V is the girder end shear force distribution factor, V_{GIRDER} is the girder end shear force, $\sum V_{GIRDER}$ is the sum of the girder end shear forces *at the same end* of the bridge system, DF_M is the maximum girder moment distribution factor, M_{GIRDER} is the maximum girder moment (along the span length), and $\sum M_{GIRDER}$ is the sum of the maximum girder moments *in the entire system*. Note that based on this definition, two (2) girder end shear forces (and subsequent end shear force distribution factors) and one (1) maximum girder moment (and subsequent maximum girder moment distribution factor) were quantified for every girder in every bridge model analyzed in the parametric study.

Due to the eccentric nature of most construction loads—where loads such as the finishing machine load are applied to overhang formwork and are therefore applied *indirectly* to exterior girders—distribution factors were further separated into exterior girder factors and interior girder factors. In total, the following eight (8) distribution factors for Load Groups 1 and 2 were defined:

$$DF_{V\ EXT\ LG1} = \frac{V_{EXT\ LG1}}{\sum V_{GIRDER\ LG1}} \tag{7.3}$$

$$DF_{V\ INT\ LG1} = \frac{V_{INT\ LG1}}{\sum V_{GIRDER\ LG1}} \tag{7.4}$$

$$DF_{M\ EXT\ LG1} = \frac{M_{EXT\ LG1}}{\sum M_{GIRDER\ LG1}} \tag{7.5}$$

$$DF_{M\ INT\ LG1} = \frac{M_{INT\ LG1}}{\sum M_{GIRDER\ LG1}} \tag{7.6}$$

$$DF_{V\ EXT\ LG2} = \frac{V_{EXT\ LG2}}{\sum V_{GIRDER\ LG2}} \tag{7.7}$$

$$DF_{V\ INT\ LG2} = \frac{V_{INT\ LG2}}{\sum V_{GIRDER\ LG2}} \tag{7.8}$$

$$DF_{M\ EXT\ LG2} = \frac{M_{EXT\ LG2}}{\sum M_{GIRDER\ LG2}} \tag{7.9}$$

$$DF_{M\ INT\ LG2} = \frac{M_{INT\ LG2}}{\sum M_{GIRDER\ LG2}} \tag{7.10}$$

where, $DF_{V\ EXT\ LG1}$ is the end shear force distribution factor for an exterior girder with construction *Load Group 1* loads applied, $V_{EXT\ LG1}$ is the end shear force for an exterior girder with *LG1* loads applied, and $\sum V_{GIRDER\ LG1}$ is the sum of the girder end shear forces *at the same*

end of the bridge system. Similarly, for the remaining distribution factors, the subscripts $_{EXT}$ and $_{INT}$ are used to distinguish between exterior and interior girders, respectively, while subscripts $_{LG1}$ and $_{LG2}$ are used to distinguish between the application of Load Group 1 and Load Group 2 loads, respectively.

Distribution factors were computed only for *superimposed* construction loads, not self-weight. To quantify distribution factors due only to *superimposed* construction loads, moments and end shear forces produced only by gravity (i.e., moments and end shear forces due to girder self-weight and brace self-weight alone) were subtracted from moments and end shear forces produced by the *combined* effects of gravity and *superimposed* construction loads.

7.2.1 Distribution factor sensitivities

Due to the large number of parameters considered in the parametric study (11 in total), supplementary limited-scope sensitivity studies were conducted prior to the development of empirical distribution factor equations. These additional studies were used to quantify the sensitivity of computed distribution factors to variations of a single parameter (while all remaining parameters were kept constant). Additionally, the sensitivity studies were used to determine if any of the 11 parameters could be omitted from the final empirical distribution factor development process.

7.2.2 Illustrative examples

After conducting several limited-scope sensitivity studies, it was determined that distribution factors were most sensitive to geometric parameters that influence the overall bridge geometry. For example, an increase in the number of girders was found to decrease certain distribution factor quantities, as shown in Figure 7.1. However, other parameters were found to have little or no influence on distribution factors. For example, girder depth was determined to be minimally influential, as shown in Figure 7.2.
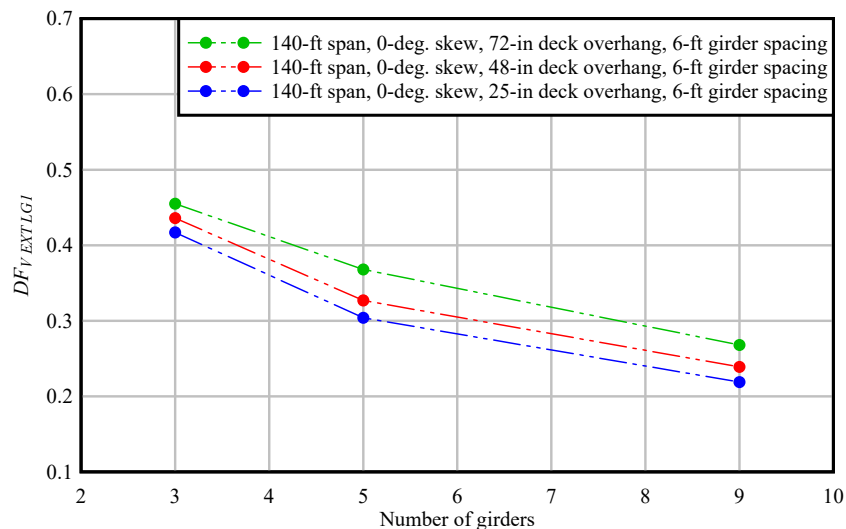
Figure 7.1 *DF* sensitivity to number of girders
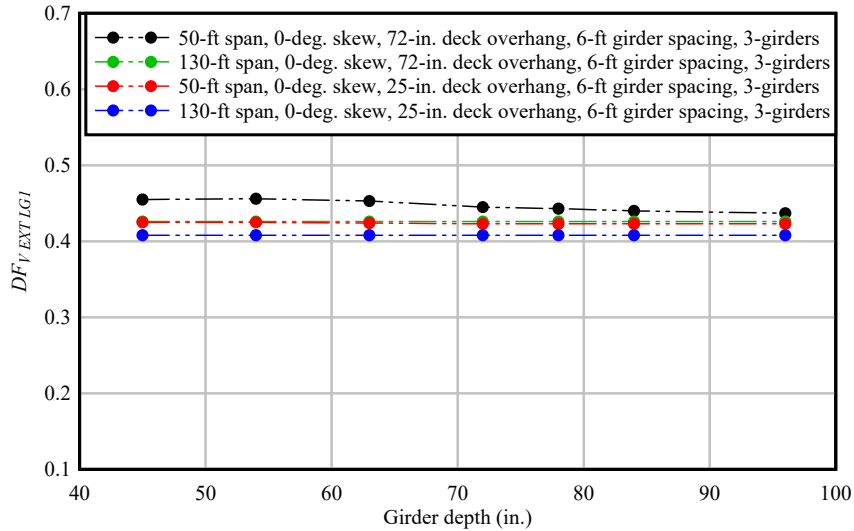
Figure 7.2 *DF* sensitivity to girder depth

7.2.3 Selection of culled data

As previously noted, two (2) separate girder end shear forces (and subsequent end shear force distribution factors) and one (1) maximum girder moment (and subsequent maximum girder moment distribution factor) were quantified for every girder in every model analyzed in the parametric study. However, considering the intended purpose of the parametric study—to provide the designing engineer with a method for quantifying *maximum* interior and exterior girder end shear forces and moments in a construction-stage structural system for both loading conditions—some distribution factors quantified in the parametric study were non-critical. In conducting the parametric study, multiple models were analyzed with all parameters being identical except for the finishing machine location or deck placement location (as multiple models were used to investigate girder end shear forces and moments for different stages of the entire construction-phase of the bridge). Therefore, it was not of interest to use distribution factors associated with non-critical construction stages in the development of empirical distribution factor equations.

For example, for cases where *LG1* loads (including the finishing machine) were applied near one end of the bridge system, the girder end shear forces at the other (far) end of the bridge were relatively low, compared to girder end shear forces near the applied load. Therefore, including distribution factors associated with low (non-critical) girder end shear forces in the development of empirical distribution factor equations would not produce desired distribution factor prediction equations (or subsequent *maximum* girder end shear force predictions). As a result, only distribution factor quantities *associated with maximum* interior and exterior girder end shear forces and moments were used to develop empirical *DF* equations, thus culling cases from the complete large-scale parametric-study data to produce a 'selected' or 'reduced volume' data set.

7.2.4 Key parameters exhibiting sensitivity

Based on results from the sensitivity studies, it was determined that empirical *DF* equations, for both *LG1* and *LG2*, would be developed considering the following parameters:

- Number of girders
- Span length (ft)
- Deck overhang width (ft)
- Girder spacing (ft)
- Skew angle (deg.)

Furthermore, from the perspective of static equilibrium, deck overhang width and girder spacing have approximately inverse influences on distribution factors. For this reason, these two parameters were combined into a single *dimensionless* ratio (ft/ft), reducing the total number of independent parameters considered in the empirical fitting process to four (4).

Based on the reduction of parameters considered in the empirical fitting process (from 11 to 4), distribution factor data were correspondingly culled. Specifically, distribution factor data were reduced in volume by *grouping* together all models that had matching values of: number of girders, span length, deck overhang width, girder spacing, and skew angle. For each such *group* of analyzed models, the values $DF_{V\ EXT}$, $DF_{V\ INT}$, $DF_{M\ EXT}$, and $DF_{M\ INT}$ were quantified. These four distribution factors were defined as the distribution factors associated with the largest (i.e., most critical) interior or exterior girder end shear force or maximum moment *for that group of analyzed models*. This grouping process further culled the distribution factor data such that there were 1,836 data values for each distribution factor and for each *Load Group* (3 girder number configurations $\times$ 17 span lengths $\times$ 3 deck overhang widths $\times$ 3 girder spacing dimensions $\times$ 4 skew angles = 1836).

7.3 Formation of baseline empirical distribution factor equations

From the culled distribution factor data, empirical fits for *LG1* and *LG2* were developed, using a root mean square (RMS) error minimization scheme, where the generalized functional form of all eight (8) distribution factor (*DF*) equations was defined as:

$$DF = \underbrace{a_1 + \left(a_2 N\right)^{a_3} \left(a_4 L\right)^{a_5} \left(a_6 \frac{OH}{S}\right)^{a_7}}_{ALL\ DF\ EQNS} + \underbrace{a_8 \left(\theta\right)^{a_9}}_{OPTIONAL} \tag{7.11}$$

where *DF* is the distribution factor, *N* is the number of girders, *L* is the span length in ft, *OH* is the deck overhang width in ft, *S* is the girder center-to-center spacing in ft, θ is the skew angle in deg., and a_1 through a_9 are fitting constants. Eqn. (7.11) is the most general form used to generate empirical *DF* fits. However, based on sensitivity study results, the optional skew angle term was later removed from a majority (but not all) of the *DF* prediction equations. For conditions where *DF* was found to be *insensitive* to skew, the number of critical distribution factor data points used in the fitting process was further culled to 459.

In order to compute values of the best fit parameters a_1 through a_9 in an optimal manner, an error function minimization process was used. The root mean square (RMS) error function was defined as the square root of the sum of the squares of the distribution factor prediction errors—differences between reduced distribution factor data and empirical distribution factor

predictions—accumulated across the entire reduced data set and divided by the number of cases considered. Minimizing the RMS error function with respect to the fitting parameters a_1 through a_9 produced preliminary empirical distribution factor prediction equations.

7.4 Modifications to achieve desired level of prediction error

As a consequence of developing fits with an RMS error minimization scheme, the empirically predicted distribution factors were conservative in 50% of cases when compared to distribution factors computed from corresponding finite element analyses. Moreover, the empirically predicted *DF* values themselves are less important than the values of shear (V) and moment (M) that are produced by *application* of the *DF* equations in design. The distribution factors developed here were intended to be used in conjunction with static analyses (i.e., a simple one-dimensional beam models) to predict interior and exterior girder end shear forces and moments. Therefore, an automation script was developed to conduct a static (beam) analysis for every case (geometric configuration) analyzed in the parametric study. Using the empirically-fit distribution factor equations, interior and exterior girder end *shear* force predictions and maximum interior and exterior girder *moment* predictions were compared to the corresponding finite element results to determine the level of conservatism produced by *application* of the predicted *DF* quantities. A normalized prediction error was defined as:

$$E_N = \frac{DF \cdot [V|M]_{STATIC}}{[V|M]_{FEA}} \qquad (7.12)$$

$$E_N = \frac{[V|M]_{PREDICTION}}{[V|M]_{FEA}} \qquad (7.13)$$

where E_N is the normalized error, *DF* is the empirically predicted distribution factor, *[V|M]* indicates shear (V) or moment (M), *[V|M]STATIC* is the maximum end shear force or moment quantified using a static (beam) analysis, and *[V|M]FEA* is the girder end shear force or maximum girder moment quantified from finite element analysis. Using the empirically developed *DF* equation in conjunction with a static analysis, a final interior or exterior girder end shear force or maximum moment prediction, *[V|M]PREDICTION*, was quantified and compared with the end shear force or moment quantified using a finite element analysis. Per this definition, normalized error values greater than or equal to 1.0 indicate a conservative prediction of *[V|M]*, and values less than 1.0 indicate an unconservative prediction of *[V|M]*.

When girder end shear forces and moments computed using empirically predicted *DF* values and simplified beam analysis were compared to shears and moments computed from three-dimensional FEA, it was found that final girder *[V|M]PREDICTION* values exhibited conservatism in excess of the 50% conservatism that was built into the empirical *DF* equations. An illustration of this additional conservatism in the prediction of exterior girder end shear forces with *LG1* loads applied is shown in Figure 7.3. The level of excess conservatism varied between each of the remaining seven (7) *DF* equations, when used in conjunction with a static beam analysis. A supplementary 'exceedance factor' was thus introduced in the final distribution factor equation to permit desired levels of exceedance (i.e., a desired level of conservatism) to be achieved. The exceedance parameter was introduced by applying a shift to the normalized error in the following manner:

$$E_N = \frac{DF \cdot [V|M]_{STATIC}}{[V|M]_{FEA}} + C \tag{7.14}$$

$$E_N = \frac{DF \cdot [V|M]_{STATIC}}{[V|M]_{FEA}} + \overbrace{\frac{\beta \left(DF \cdot [V|M]_{STATIC} \right)}{[V|M]_{FEA}}}^{C} \tag{7.15}$$

$$E_N = \frac{(1+\beta) \cdot DF \cdot [V|M]_{STATIC}}{[V|M]_{FEA}} \tag{7.16}$$

where C is a constant used to shift the normalized error to a desired exceedance level, and β is the defined exceedance factor. As shown above, β was used to relate the desired shift of the normalized error to the final form of the DF equation. Additionally, the exceedance factor provided the ability to achieve specific levels of conservatism, without necessitating adjustments to any of the empirically fit constants, a_1 through a_9, in the DF equations.

To provide future flexibility in the implementation of the equations developed from this study, β values were quantified at four (4) different levels of exceedance for each distribution factor DF expression. Each β value was quantified in an iterative manner to achieve a desired exceedance level of predicted girder end shear force or maximum girder moment. Exceedance levels of 50% (mean $[V|M]$ prediction error of zero), 84%, 95%, and 98% were identified as being of future value to the FDOT. In the 95% case, $[V|M]$ predictions computed using the empirically predicted DF values and simplified beam analysis would be conservative (relative to FEA prediction) in 95% of cases. The levels of 84% and 98% corresponded to exceedance thresholds at 1-standard deviation above 'zero mean error' (i.e., 50% exceedance), and 2-standard deviations above zero mean error, respectively. To illustrate the influence of establishing β at different levels of exceedance, normalized errors for exterior girder end shear force predictions with $LG1$ loads applied are shown in Figure 7.4 – Figure 7.7.

Figure 7.3 Shear (V) prediction error for the culled data set using $DF_{V\,EXT\,LG1}$ in conjunction with a static beam analysis, without introduction of β (Note: an exceedance of 57% indicates a moderate level of implicit conservatism relative to the 'zero mean error' condition, i.e., 50% exceedance)

Figure 7.4 Shear (V) prediction error for the culled data set using $DF_{V\,EXT\,LG1}$ in conjunction with a static beam analysis, shifted with β to a 50% exceedance level

Figure 7.5 Shear (V) prediction error for the culled data set using $DF_{V\,EXT\,LG1}$ in conjunction with a static beam analysis, shifted with β to an 84% exceedance level

Figure 7.6 Shear (V) prediction error for the culled data set using $DF_{V\,EXT\,LGI}$ in conjunction with a static beam analysis, shifted with β to a 95% exceedance level
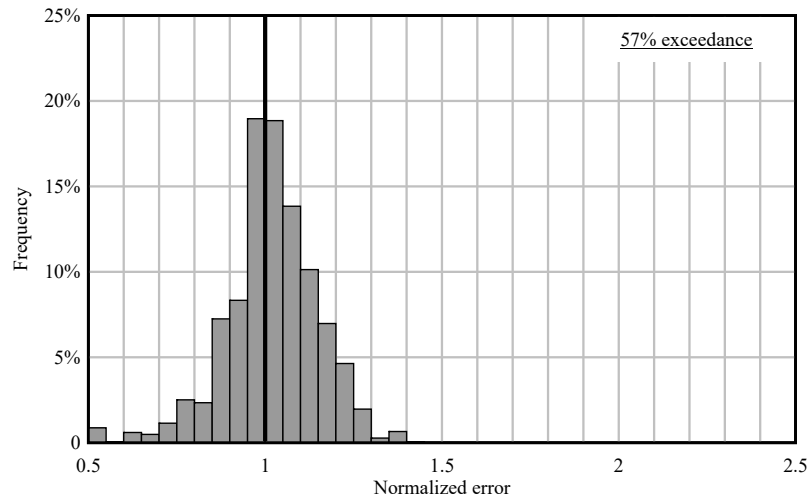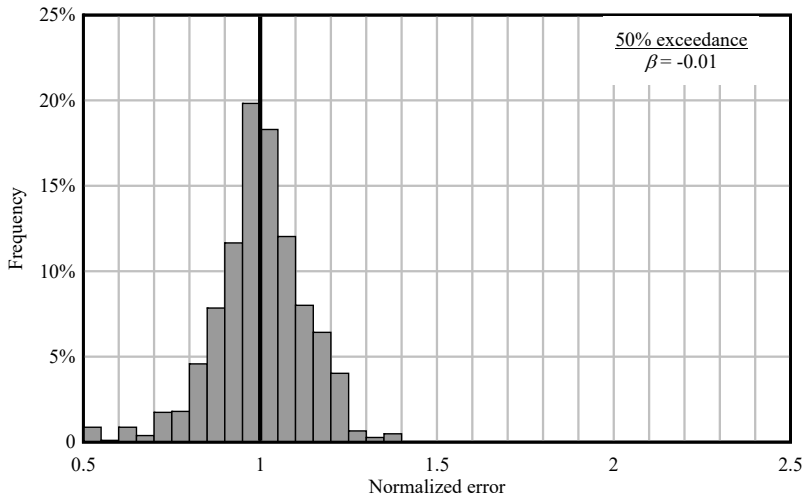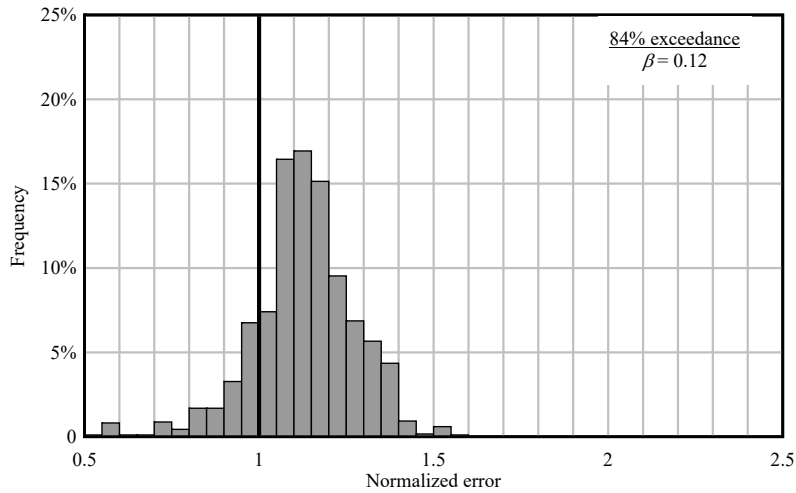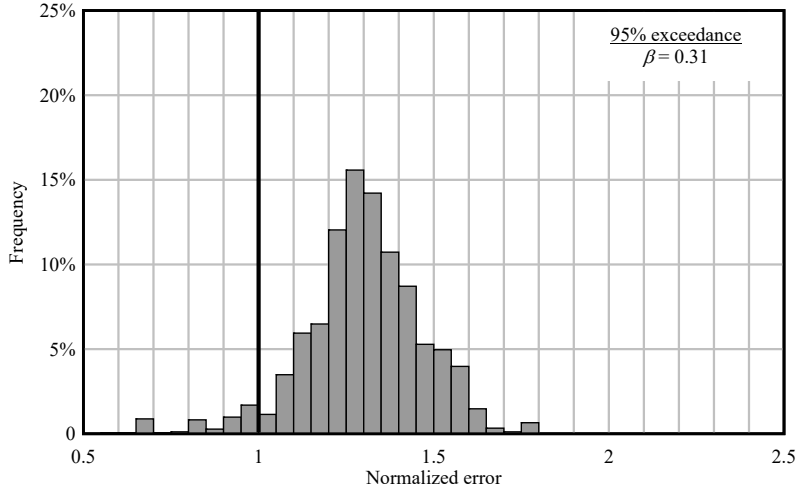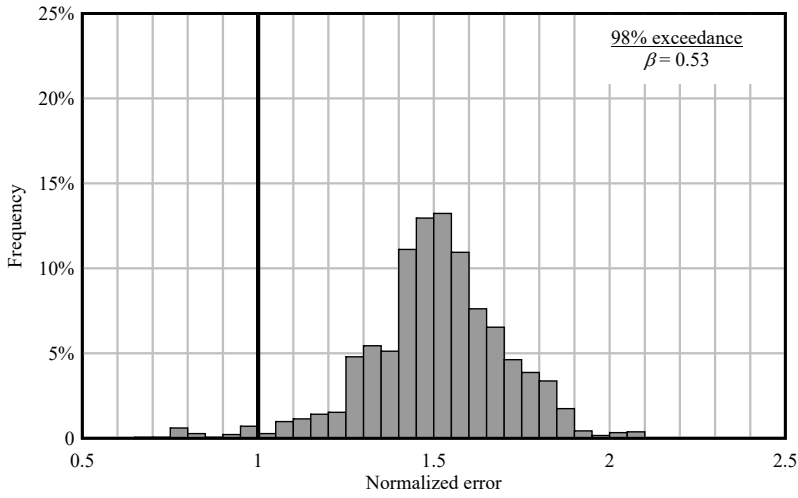

Figure 7.7 Shear (V) prediction error for the culled data set using $DF_{V\,EXT\,LGI}$ in conjunction with a static beam analysis, shifted with β to a 98% exceedance level

7.5 Final distribution factor equations for design

The final (general) form of the empirically developed distribution factor equations was defined as:

$$DF = \left(1+\beta\right)\left[a_1 + \left(a_2 N\right)^{a_3}\left(a_4 L\right)^{a_5}\left(a_6\frac{OH}{S}\right)^{a_7} + a_8\left(\theta\right)^{a_9}\right] \tag{7.17}$$

where DF is the predicted distribution factor, N is the number of girders in the bridge cross-section, L is the span length in ft, OH is the deck overhang width in ft, S is the girder center-to-center spacing in ft, θ is the skew angle in deg., a_1 through a_9 are empirical fit constants listed in Table 7.2, and β is exceedance factor selected to achieve a desired level of exceedance (i.e., conservatism) listed in Table 7.3. (Detailed summaries and illustrations of normalized error for each β value are provided in Appendix D for all cases: interior and exterior girder end shear forces and moments).

Table 7.2 Constants for distribution factors (DF) calculation

DF equation	a_1	a_2	a_3	a_4	a_5	a_6	a_7	a_8	a_9
$DF_{V\,EXT\,LG1}$	-0.26	0.60	-0.41	0.03	-0.03	1.76	0.27	0.10	0.02
$DF_{V\,INT\,LG1}$	-0.90	0.13	-0.11	0.01	0.02	4.80	0.02	0.03	0.01
$DF_{M\,EXT\,LG1}$	-0.23	0.47	-0.33	2.51	-0.09	27.00	0.09	0	0
$DF_{M\,INT\,LG1}$	0.06	1.94	-1.22	0.53	0.17	8.63	-0.03	0	0
$DF_{V\,EXT\,LG2}$	-0.01	0.78	-0.93	0.91	0.06	0.81	0.36	0	0
$DF_{V\,INT\,LG2}$	0.03	0.89	-1.08	1.04	0.04	10.16	-0.16	0	0
$DF_{M\,EXT\,LG2}$	-0.06	1.66	-0.77	2.29	-0.01	24.58	0.17	0	0
$DF_{M\,INT\,LG2}$	0.01	0.72	-1.09	18.19	0.01	14.01	-0.16	0	0

Table 7.3 Distribution factor (DF) exceedance values

β constant	50% exceedance	84% exceedance	95% exceedance	98% exceedance
$DF_{V\,EXT\,LG1}$	-0.01	0.12	0.31	0.53
$DF_{V\,INT\,LG1}$	-0.04	0.14	0.29	0.42
$DF_{M\,EXT\,LG1}$	-0.04	0.01	0.08	0.14
$DF_{M\,INT\,LG1}$	-0.03	0.06	0.12	0.20
$DF_{V\,EXT\,LG2}$	-0.09	0.03	0.12	0.15
$DF_{V\,INT\,LG2}$	-0.05	0.05	0.17	0.27
$DF_{M\,EXT\,LG2}$	-0.01	0.06	0.15	0.17
$DF_{M\,INT\,LG2}$	-0.01	0.06	0.11	0.15

7.5.1 Application of proposed method

To illustrate the application of the proposed method for quantifying interior and exterior girder end shear forces and moments, an example involving the calculation of exterior girder end shear, for construction load group *LG1*, is presented. After collapsing all construction loads (point, line, and pressure) into an equivalent one-dimensional beam loading diagram (Figure 7.8), a simple static beam analysis is performed to compute the maximum girder end shear. The exterior girder end shear force for construction load group *LG1* is then determined as:

$$V_{EXT\ LG1} = V_{STATIC\ LG1} \cdot DF_{V\ EXT\ LG1} \tag{7.18}$$

where $V_{EXT\ LG1}$ is the empirically predicted exterior girder end shear force, $V_{STATIC\ LG1}$ is the maximum end shear force quantified from the static beam analysis, and $DF_{V\ EXT\ LG1}$ is the *LG1* exterior girder end shear force distribution factor computed using Eqn. (7.17), Table 7.2, and Table 7.3. (As noted previously, comprehensive illustrations of the approach, for interior and exterior girder end shear forces and moments, are shown in Appendix D).
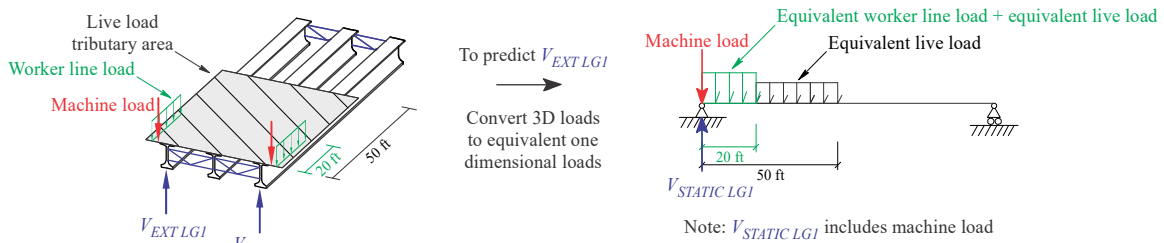

Figure 7.8 Computation of exterior girder end shear force
for construction load group *LG1*

7.5.2 Prediction error for full (unculled) parametric data set

In Figure 7.9, the level of conservatism incorporated into the empirical prediction of exterior girder end shear force is compared for two different data sets. In Figure 7.9a, normalized errors (50% exceedance; Table 7.3; β=-0.01) are illustrated for the 'culled' data set that was used in the formation of the empirical *DF* equation. The 459 cases included in this data set include *only* critical loading conditions and critical structural configurations (i.e., those producing maximum girder forces). In Figure 7.9b, normalized errors (again computed using β=-0.01) are plotted for critical loading conditions, but for *all* structural configurations (36,288 cases rather than 459). Evident in Figure 7.9b is the fact that the use of the proposed empirical prediction method produces a 70% exceedance (rather than 50%) when applied to all structural configurations. Thus, application of the proposed method to a much larger and more generalized set of structures (than was used in the fitting process) is found to be conservative, but not overly so. In Figure 7.10, an analogous example is presented but for a different exceedance level. In Figure 7.10a, normalized errors are plotted *only* for critical loading conditions and critical structural configurations (459 cases; 95% exceedance; Table 7.3; β=+0.31). In Figure 7.10b, normalized errors (again computed using β=+0.31) are plotted for critical loading conditions, but for *all* structural configurations (36,288 cases). In Figure 7.10b, use of the proposed empirical prediction method produces a 96% exceedance (rather than 95%) when applied to all structural configurations considered in the study. Thus, once again, application of the proposed method to a larger and more generalized set of structures is found to be conservative, but not overly so.
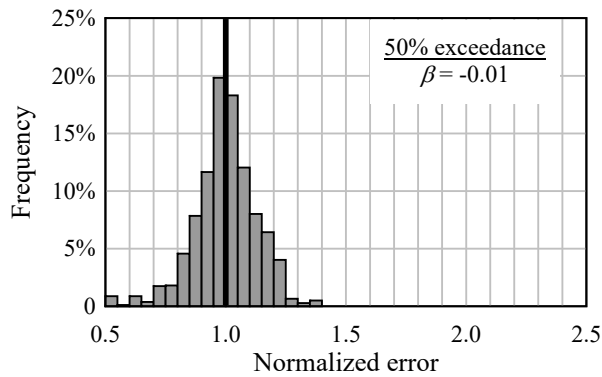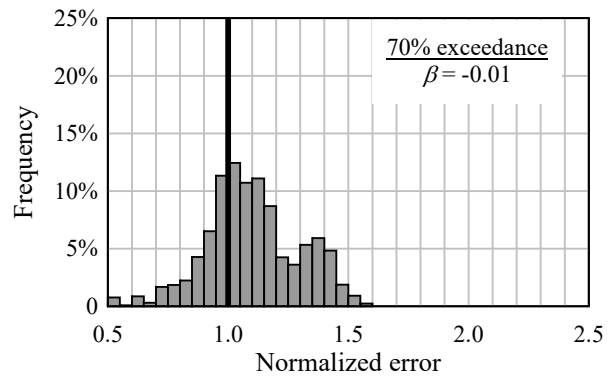
Figure 7.9 Prediction error for $V_{EXT\,LGI}$ using Eqn. (7.17) and a 50% exceedance level:
(a) For the reduced data set; (b) For the complete large-scale parametric study
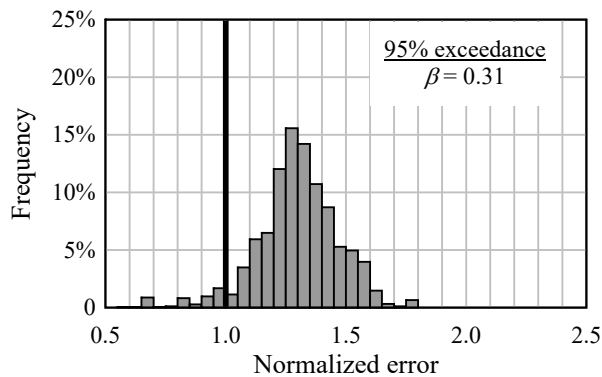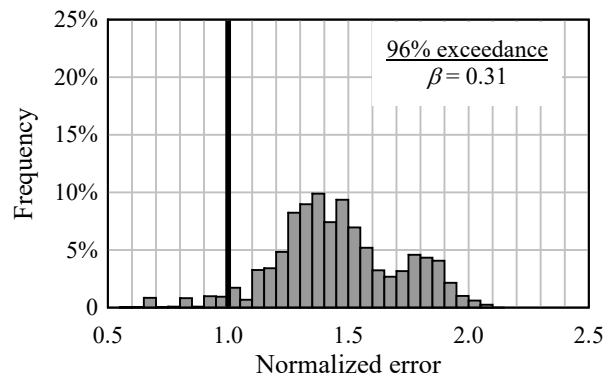
Figure 7.10 Prediction error for $V_{EXT\,LGI}$ using Eqn. (7.17) and a 95% exceedance level:
(a) For the reduced data set; (b) For the complete large-scale parametric study

7.5.3 Proposed method compared to traditional tributary area method for Load Group 2

In structural design for construction *Load Group 2* loads, it is conventional practice to compute girder end shear forces and moments by assuming that the distribution of load shall be based on using a tributary area for each girder in the bridge system. Therefore, it was desirable to compare interior and exterior girder end shear force and maximum moment predictions from the tributary area design method to girder end shear force and maximum moment values computed using the proposed *DF* equation approach of the present study. In Figure 7.11 – Figure 7.14, values computed using the proposed *DF* method [using Eqn. (7.17), a 95% exceedance level, and a static analysis] are compared to values computed using the conventional tributary area method. In each case, the shear values have been normalized by FEA results from the culled data set (459 cases). The culled data set was selected as opposed to the full data set for comparison, due to

65

redundant predictions that arise when using the tributary area method for specific bridge parameters. For example, two cases with different skew angles (and all remaining parameters the same) will produce equal predictions for both cases, using the tributary area method. Similarly, parameters such as the number of braces and girder depth will not influence quantities computed using the tributary area method. As a result, only the culled data set was considered.

As shown in Figure 7.11 – Figure 7.14, predictions using the traditional tributary area method relative to the corresponding FEA results were less conservative compared to the proposed *DF* equation approach. This observation can be attributed to the assumed simplification in the transfer (distribution) of load using the tributary area method. Finite element analysis, from which the proposed *DF* expressions were derived, more accurately model the distribution of load, as compared to the simplified tributary area method.

Figure 7.11 Prediction error for $V_{EXT\,LG2}$ using: (a) Eqn. (7.17) and a 95% exceedance level; (b) Traditional tributary area method

Figure 7.12 Prediction error for $V_{INT\,LG2}$ using: (a) Eqn. (7.17) and a 95% exceedance level; (b) Traditional tributary area method
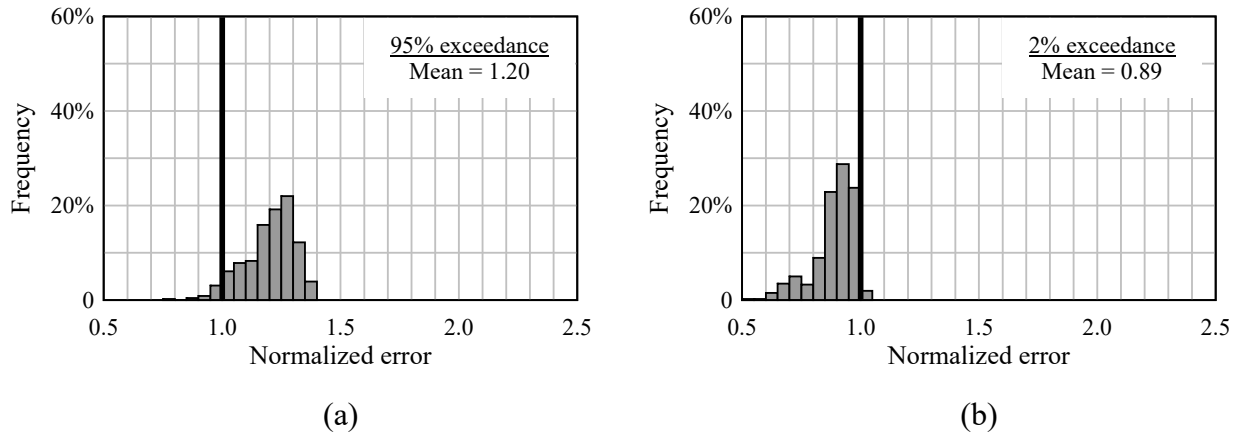
66

Figure 7.13 Prediction error for $M_{EXT\,LG2}$ using: (a) Eqn. (7.17) and a 95% exceedance level; (b) Traditional tributary area method
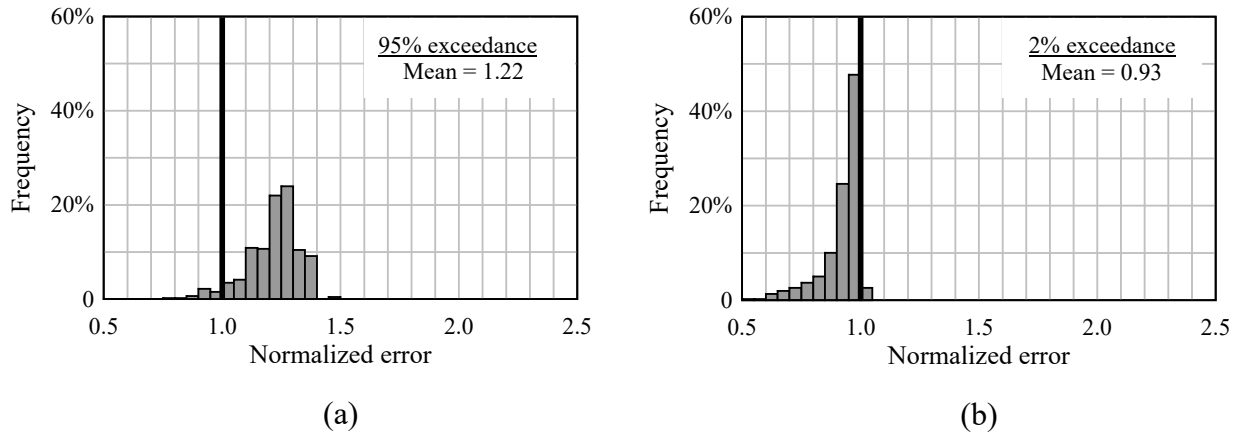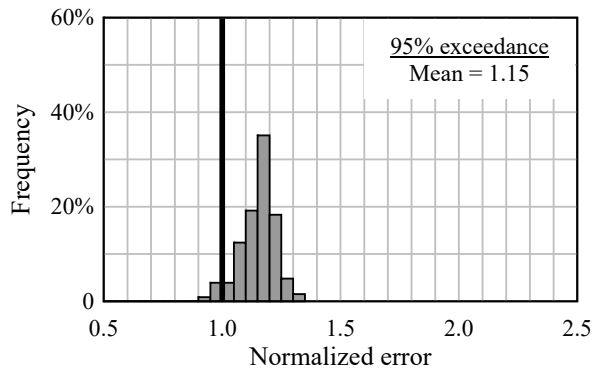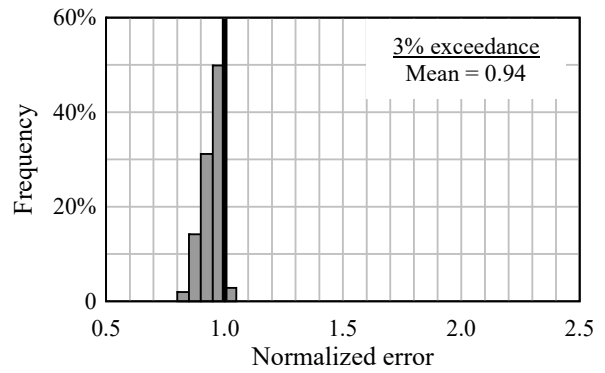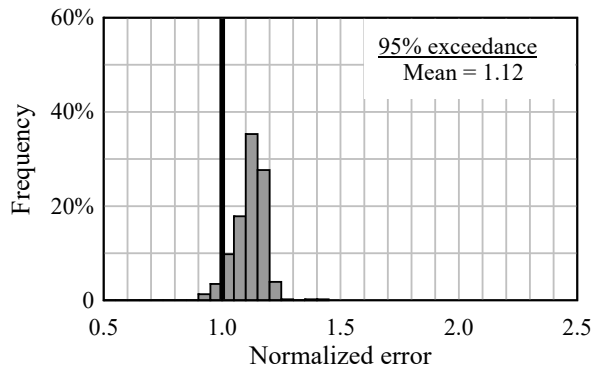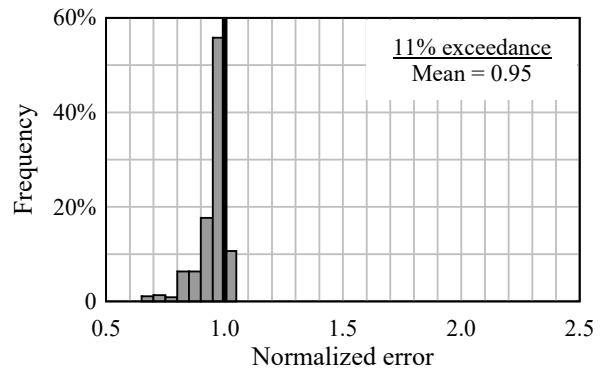

Figure 7.14 Prediction error for $M_{INT\,LG2}$ using: (a) Eqn. (7.17) and a 95% exceedance level; (b) Traditional tributary area method

CHAPTER 8
SUMMARY, CONCLUSIONS, AND RECOMMENDATIONS

8.1 Summary and Conclusions

In the first phase of this study, finite element models of Florida-I Beams were developed and analyzed for the purpose of updating previously developed capacity equations for wind load and gravity load. Using data available in published engineering literature, an approximate representation of thermally induced girder sweep was developed for bridges that are located in Florida. Importantly, thermal sweep values were found to be on the same order of magnitude as those corresponding to allowable fabrication (i.e., construction) sweep tolerances. Finite element analyses of numerical models that included the effects of thermal sweep, revealed—as expected—that girder capacities were diminished by inclusion of thermal sweep. Consequently, updated capacity equations—Eqn. (4.5) and Eqn. (5.3)—that account for thermal sweep were developed to replace design capacity equations previously developed in FDOT study BDK75-977-33 (Consolazio et al., 2013). Additionally, a limited-scope parametric study indicated that the updated baseline gravity load capacity Eqn. (5.3) can be used in conjunction with Eqn. (9.23) from Consolazio et al. (2013) to account for a number of additional system characteristics (brace stiffness, number of braces, etc.).

In the second phase of this study, finite element analyses of partially constructed bridge systems—consisting of multiple Florida-I Beam (FIBs) with construction loads—were used to quantify distribution factors (*DF*) for interior and exterior girder end shear forces and maximum girder moments. A large-scale parametric study was conducted, with consideration of different Florida-I Beam cross-sections, span lengths, girder spacing, deck overhang widths, skew angles, number of girders, number of braces, and bracing configurations (K-brace and X-brace), to quantify shear and moment distribution factor data. These data were quantified separately for two different construction load groups and subsequently used to develop empirical distribution factor equations for use in bridge design. The proposed *DF* equations incorporate the use of an exceedance factor that can be selected to achieve various desired levels of conservatism. The proposed empirical *DF* equations, when used in conjunction with simple static beam analyses, provide an efficient and accurate means of conservatively computing girder end shear forces and maximum girder moments during the construction-phase, without the need for detailed finite element analysis.

8.2 Recommendations

Based on the analytical data generated during this study, the following recommendations are suggested:

- The newly developed unanchored girder wind capacity ($P_{max,0}$) Eqn. (4.5), which incorporates the influence of estimated thermal sweep (reproduced below), should be used as a replacement for the corresponding equation previously developed in FDOT study BDK75-977-33 [see Eqn. (8.2) in Consolazio et al., (2013) which has been reproduced herein as Eqn. (4.4)]:

$$P_{max,0} = 63e^{\frac{-L}{55}}\left(\frac{1}{3} + 15e^{\frac{-D}{79}}\right) - 34e^{\frac{-D}{72}} - \frac{1}{8} \tag{4.5}$$

where $P_{max,0}$ is the wind capacity in psf, L is the span length in ft, and D is the FIB cross-section depth in inches.

- The newly developed baseline buckling capacity (C_0) equation for an unanchored two-girder strut-braced system in zero wind, Eqn. (5.3), which incorporates the influence of estimated thermal sweep (and is reproduced below), should be used as a replacement for the corresponding equation previously developed in FDOT study BDK75-977-33 [see Eqn. (9.2) in Consolazio et al., (2013) which has been reproduced herein as Eqn. (5.2)]. Additionally, the newly developed C_0 Eqn. (5.3) can be used in conjunction with Eqn. (9.23) from FDOT study BDK75-977-33 (Consolazio et al. 2013), which has been reproduced herein as Eqn. (5.4):

$$C_0 = 47e^{\frac{-L}{42}} + 0.5 \tag{5.3}$$

where C_0 is in g and L is the span length in ft.

- It is recommended that the distribution factors (DF) expressions developed in this study—Eqn. (7.17), Table 7.2, and Table 7.3 (reproduced below)—be used in the calculation of girder end shear forces and moments that are caused by the application of construction loads. It has been demonstrated that the use of these distribution factor expressions—coupled with simple beam analyses—produces more accurate shear and moment data than does the traditional tributary width analysis approach:

$$DF = (1+\beta)\left[a_1 + (a_2 N)^{a_3} (a_4 L)^{a_5} \left(a_6 \frac{OH}{S}\right)^{a_7} + a_8 (\theta)^{a_9}\right] \tag{7.17}$$

where DF is the predicted distribution factor, N is the number of girders in the bridge cross-section, L is the span length in ft, OH is the deck overhang width in ft, S is the girder center-to-center spacing in ft, θ is the skew angle in deg., a_1 through a_9 are empirical fit constants listed in Table 7.2, and β is exceedance factor selected to achieve a desired level of exceedance (i.e., conservatism) listed in Table 7.3.

Table 7.2 Constants for distribution factors (*DF*) calculation

DF equation	a_1	a_2	a_3	a_4	a_5	a_6	a_7	a_8	a_9
$DF_{V\ EXT\ LG1}$	-0.26	0.60	-0.41	0.03	-0.03	1.76	0.27	0.10	0.02
$DF_{V\ INT\ LG1}$	-0.90	0.13	-0.11	0.01	0.02	4.80	0.02	0.03	0.01
$DF_{M\ EXT\ LG1}$	-0.23	0.47	-0.33	2.51	-0.09	27.00	0.09	0	0
$DF_{M\ INT\ LG1}$	0.06	1.94	-1.22	0.53	0.17	8.63	-0.03	0	0
$DF_{V\ EXT\ LG2}$	-0.01	0.78	-0.93	0.91	0.06	0.81	0.36	0	0
$DF_{V\ INT\ LG2}$	0.03	0.89	-1.08	1.04	0.04	10.16	-0.16	0	0
$DF_{M\ EXT\ LG2}$	-0.06	1.66	-0.77	2.29	-0.01	24.58	0.17	0	0
$DF_{M\ INT\ LG2}$	0.01	0.72	-1.09	18.19	0.01	14.01	-0.16	0	0

NOTE: *DF* equations were developed specifically for construction loads specified by FDOT SDG (2016)

Table 7.3 Distribution factor (*DF*) exceedance values

β constant	*50% exceedance*	*84% exceedance*	*95% exceedance*	*98% exceedance*
$DF_{V\ EXT\ LG1}$	-0.01	0.12	0.31	0.53
$DF_{V\ INT\ LG1}$	-0.04	0.14	0.29	0.42
$DF_{M\ EXT\ LG1}$	-0.04	0.01	0.08	0.14
$DF_{M\ INT\ LG1}$	-0.03	0.06	0.12	0.20
$DF_{V\ EXT\ LG2}$	-0.09	0.03	0.12	0.15
$DF_{V\ INT\ LG2}$	-0.05	0.05	0.17	0.27
$DF_{M\ EXT\ LG2}$	-0.01	0.06	0.15	0.17
$DF_{M\ INT\ LG2}$	-0.01	0.06	0.11	0.15

REFERENCES

AASHTO (American Association of State Highway and Transportation Officials) (2008). *Guide Design Specification for Bridge Temporary Works*, AASHTO, Washington, D.C.

AASHTO (American Association of State Highway and Transportation Officials) (2010). *LRFD Bridge Design Specifications: 5th Edition*, AASHTO, Washington, D.C.

ADINA (2016). *Theory and Modeling Guide, Volume 1: ADINA Solids & Structures*, ADINA R&D, Inc, Watertown, MA.

AF&PA (American Forest & Paper Association) (2005). *National Design Specification for Wood Construction and Supplement*, AF&PA, Washington, D.C.

Clifton, S. and Bayrak, O. (2008). *Bridge Deck Overhang Construction,* Technical Report IAC: 88-5DD1A003-2, University of Texas, Austin, TX.

Consolazio, G., Gurley, K., and Harper, Z. (2013). *Bridge Girder Drag Coefficients and Wind-Related Bracing Recommendations*, Structures Research Report No. 2013/87322, University of Florida, Gainesville, FL.

Consolazio, G. and Edwards, S. (2014). *Determination of Brace Forces Caused by Construction Loads and Wind Loads During Bridge Construction*, Structures Research Report No. 2014/101350-102056, University of Florida, Gainesville, FL.

CTL Group (2007). *Investigation of Red Mountain Freeway Bridge Girder Collapse*, Arizona Department of Transportation Bridge Group, CTL Group Project No. 262291, Skokie, IL.

FDOT (Florida Department of Transportation) (2012a). *Design Standard No. 20510: Composite Elastomeric Bearing Pads – Prestressed Florida-I Beams*, FDOT, Tallahassee, FL.

FDOT (Florida Department of Transportation) (2012b). *Instructions for Design Standard No. 20010: Prestressed Florida-I Beams*, FDOT, Tallahassee, FL.

FDOT (Florida Department of Transportation) (2012c). *Instructions for Design Standard No. 20510: Composite Elastomeric Bearing Pads – Prestressed Florida-I Beams*, FDOT, Tallahassee, FL.

FDOT (Florida Department of Transportation) (2012d). *Structures Manual Volume I: Structures Design Guidelines*, FDOT, Tallahassee, FL.

FDOT (Florida Department of Transportation) (2014a). *Design Standard No. 20005: Prestressed I-Beam Temporary Bracing*, FDOT, Tallahassee, FL.

FDOT (Florida Department of Transportation) (2014b). *Instructions for Design Standard No. 20010: Prestressed Florida-I Beams*, FDOT, Tallahassee, FL.

FDOT (Florida Department of Transportation) (2016). *Structures Manual Volume I: Structures Design Guidelines*, FDOT, Tallahassee, FL.

Hurff, Jonathan B. (2010). *Stability of Precast Prestressed Concrete Bridge Girders Considering Imperfections and Thermal Effects*. Doctoral dissertation, School of Civil and Environmental Engineering, Georgia Institute of Technology, Atlanta.

Lee, Jong-Han (2010). *Experimental and Analytical Investigation of the Thermal Behavior of Prestressed Concrete Bridge Girders Including Imperfections*. Doctoral dissertation, School of Civil and Environmental Engineering, Georgia Institute of Technology, Atlanta.

Lee, Jong-Han (2012). "Investigation of extreme environmental conditions and design thermal gradients during construction for prestressed concrete bridge girders". *ASCE Journal of Bridge Engineering*, Vol. 17, No. 3, pp. 547-556.

PCI (2010). PCI Design Handbook: 7th Edition, Precast/Prestressed Concrete Institute, Chicago, IL.

PCI (2011). PCI Bridge Design Manual, 3rd Edition, Precast/Prestressed Concrete Institute, Chicago, IL.

APPENDIX A
CROSS-SECTIONAL PROPERTIES OF FLORIDA-I BEAMS

In this study, finite element models were analyzed to evaluate girder shear forces and moments in Florida-I Beams (FIBs). In each model, the FIBs were modeled using *warping beams*, specialized beam elements available in the ADINA finite element code, which require the calculation of a comprehensive set of cross-sectional properties. This appendix provides mathematical definitions of all such properties and corresponding numeric values that were calculated for each FIB cross-sectional shape.

Mathematical definitions of cross-sectional properties that are required to use the warping beam element in ADINA are listed in Table A.1. Each property requires the evaluation of an integral over the area of the cross-section, in which the integrands are written in terms of coordinates x and y, referenced to the geometric centroid of the section (Figure A.1). Some properties also require knowledge of the warping function, $\psi(x,y)$, which represents the torsionally-induced out-of-plane warping displacements per rate of twist at every point on the cross-section. (The units of ψ are therefore in/(rad/in) or in^2.)

Table A.1 Definitions of cross-sectional properties required for use of a warping beam element

| Property	Integral form	Units	Description
A	$\int_A dA$	in^2	Cross-sectional area
I_{xx}	$\int_A y^2 dA$	in^4	Strong-axis moment of inertia
I_{yy}	$\int_A x^2 dA$	in^4	Weak-axis moment of inertia
I_{xy}	$\int_A xy\, dA$	in^4	Product of inertia
x_s	$-\dfrac{1}{I_{xx}}\int_A \left(y\psi_c\right)dA$	in	X-coordinate of shear center
y_s	$\dfrac{1}{I_{yy}}\int_A \left(x\psi_c\right)dA$	in	Y-coordinate of shear center
J	$\int_A \left(x^2 + y^2 + x\dfrac{d\psi}{dy} - y\dfrac{d\psi}{dx}\right)dA$	in^4	St. Venant torsional constant
C_ω	$\int_A \psi^2 dA$	in^6	Warping constant
I_{xr}	$\int_A x\left(x^2 + y^2\right)dA$	in^5	Twist/weak-axis bending coupling term
I_{yr}	$\int_A y\left(x^2 + y^2\right)dA$	in^5	Twist/strong-axis bending coupling term
$I_{\omega r}$	$\int_A \psi\left(x^2 + y^2\right)dA$	in^6	Twist/warping coupling term
I_{rr}	$\int_A \left(x^2 + y^2\right)^2 dA$	in^6	Wagner constant
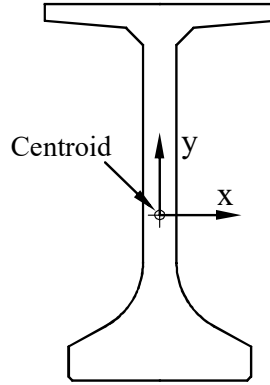
Figure A.1 Coordinate system used in the calculation of cross-sectional properties

For general cross-sectional shapes (e.g., an FIB), analytical (closed-form) solutions for $\psi(x,y)$ do not exist; instead the warping field $\psi(x,y)$ must be solved numerically. In this study, the calculation of $\psi(x,y)$ for each FIB shape was accomplished by discretizing the cross-sectional shape into a high-resolution mesh of thousands of two-dimensional triangular elements, and then employing a finite element approach to solve the governing differential equation.

In general, solutions for $\psi(x,y)$ change depending on the assumed location of the center of twist. In the literature, the term 'warping function' typically refers to a particular solution (ψ in Table A.1) corresponding to a state of *pure torsion*, i.e., torsion about the shear center. As a result, prior knowledge of the location of the shear center is required to compute several of the warping beam properties. However, it is possible to calculate the coordinates of the shear center, x_s and y_s (Table A.1), using an alternative solution to the warping function (ψ_c), where the center of twist is assumed to be located at the centroid of the section. Therefore, two different warping functions were computed for each FIB section: first the section centroid was used to compute ψ_c and then the location of the shear center, obtained from ψ_c, was used to compute ψ as well as the remaining cross-sectional properties.

Because all FIB cross-sections are symmetric about the y-axis, I_{xy}, x_s, I_{xr}, and $I_{\omega r}$ have a value of zero (0) by definition. The remaining (non-zero) cross-sectional properties calculated for each FIB shape are summarized in Table A.2.

Table A.2 Cross-sectional properties of Florida-I Beams

Section	A (in²)	I_{xx} (in⁴)	I_{yy} (in⁴)	y_s (in)	J (in⁴)	C_ω (in⁶)	I_{yr} (in⁵)	I_{rr} (in⁶)
36″ FIB	807	127,700	81,283	3.00	30,864	11,577,000	703,250	86,224,000
45″ FIB	870	226,810	81,540	3.46	31,885	21,835,000	1,521,200	167,760,000
54″ FIB	933	360,270	81,798	3.81	32,939	35,370,000	2,760,500	315,370,000
63″ FIB	996	530,790	82,055	4.07	33,973	52,203,000	4,471,300	562,480,000
72″ FIB	1059	741,060	82,314	4.27	35,041	72,337,000	6,693,800	951,390,000
78″ FIB	1101	904,610	82,484	4.38	35,693	87,610,000	8,473,400	1,314,600,000
84″ FIB	1143	1,087,800	82,657	4.46	36,421	104,350,000	10,504,000	1,781,400,000
96″ FIB	1227	1,516,200	83,002	4.56	37,859	142,280,000	15,336,000	3,107,900,000

APPENDIX B
EXAMPLE CALCULATIONS:
78" FIB THERMAL SWEEP

Presented in this appendix is a calculation worksheet that was prepared to determine thermal sweep for a Florida-I Beam, at an arbitrary span length. Furthermore, thermal sweep quantities (and subsequent thermal sweep ratios) were computed using transverse temperature gradients proposed in the present study, based on a literature review conducted in the present study (Lee, 2010).

Thermal sweep for a 78" Florida-I Beam

END VIEW
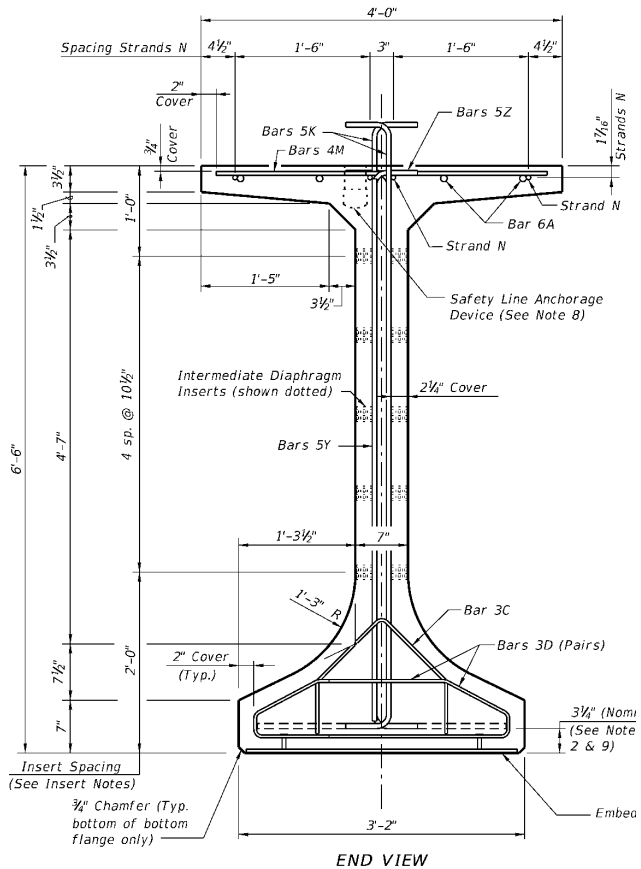
FIB dimensions from FDOT website
(Design Standards eBook 2014, http://www.dot.state.fl.us/rddesign/DS/14/STDs.shtm)

Concrete material properties ...

$Ec := 5589$ ... (ksi) Modulus of elasticity (based on fc' = 8.5 ksi)

$\alpha := 12 \cdot 10^{-6}$ ... (1/ºC) Coefficient of thermal expansion

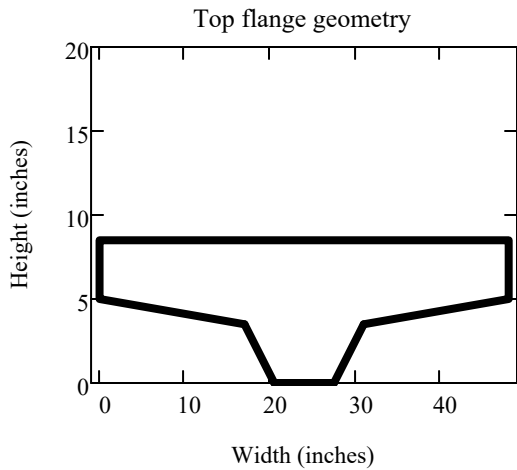Thermal sweep calculations using WINTER temperature gradients ...

76

▶ Vectors for plotting top flange

$$\text{TopFlangeWidthDim} := \begin{pmatrix} 0 \\ 17 \\ 20.5 \\ 27.5 \\ 31 \\ 48 \end{pmatrix}$$

... (in.) Top flange width transition points (used in function below)

$$\text{TopFlangeHeightDim} := \begin{pmatrix} 3.5 \\ 5 \\ 8.5 \\ 8.5 \\ 5 \\ 3.5 \end{pmatrix}$$

... (in.) Top flange height at each transition point (used in function below)

Top flange geometry

$$\text{TopFlangeHeight}(x) := \text{linterp}(\text{TopFlangeWidthDim}, \text{TopFlangeHeightDim}, x)$$

... (in.) Top flange height as a function of x (width)

77

<u>Top flange temperature gradient (adapted from Lee 2010) ...</u>

TopFlangeWidth := 48   ... (in.) Total top flange width

B_{top} := TopFlangeWidth ÷ 4 = 12   ... (in.) Dimension specified in top flange temperature gradient

x := 0, TopFlangeWidth·0.01 .. TopFlangeWidth   ... (in.) Range variable for top flange temperature gradient

T1 := 19   ... (°C) Maximum top flange temperature (T1) for Atlanta, GA in winter (Lee 2012)

T2 := T1 ÷ 4 = 4.8   ... (°C) Temperature at first B_{top} dimension

T3 := 0   ... (°C) Temperature at second B_{top} dimension

λ := 5 ÷ 19.6 = 0.26   ... Dimensionless ratio proposed for current project to add ascending branch

T4 := λ·T1 = 4.8   ... (°C) Temperature at right end (additional ascending branch)

$$\text{TopFlangeTemperatures} := \begin{pmatrix} T1 \\ T2 \\ T3 \\ T4 \end{pmatrix} = \begin{pmatrix} 19.0 \\ 4.8 \\ 0.0 \\ 4.8 \end{pmatrix}$$ ... (°C) Top flange temperatures for top flange temperature gradient

$$\text{BtopDim} := \begin{pmatrix} 0 \\ B_{top} \\ 2 \cdot B_{top} \\ \text{TopFlangeWidth} \end{pmatrix} = \begin{pmatrix} 0 \\ 12 \\ 24 \\ 48 \end{pmatrix}$$ ... (in.) Top flange width dimension at each temperature value

$$\text{TopFlangeTemp(x)} := \begin{vmatrix} e \leftarrow \text{linterp(BtopDim, TopFlangeTemperatures, x)} & \text{if } x \geq 0 \wedge x \leq \text{TopFlangeWidth} \\ e \leftarrow 0 & \text{otherwise} \\ \text{return } e \end{vmatrix}$$

... (°C) Top flange temperature as a function of x (width)

78
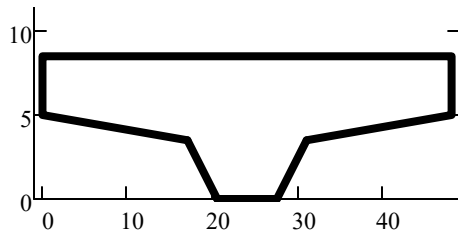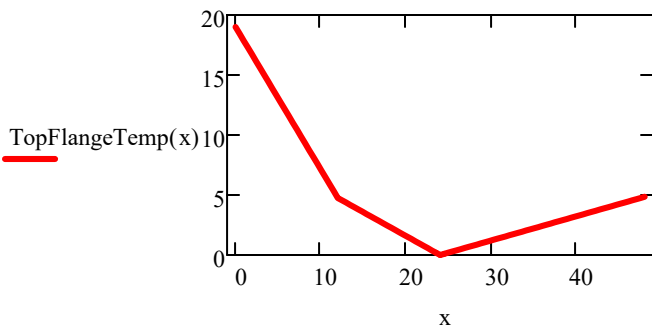
Top flange moment calculation ...

$$\text{TopFlangeMoment} := \int_0^{\text{TopFlangeWidth}} Ec \cdot \alpha \cdot \text{TopFlangeTemp}(x) \cdot \text{TopFlangeHeight}(x) \cdot \left(\frac{\text{TopFlangeWidth}}{2} - x \right) dx = 535.5$$
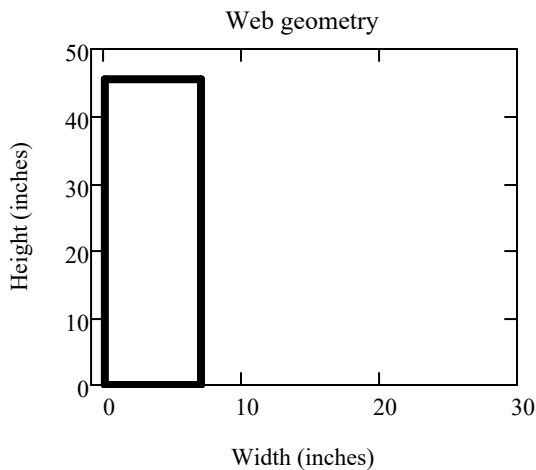
$\text{TopFlangeMoment} \div 12 = 44.6$ ... (kip-ft) Top flange moment due to applied top flange temperature gradient

Web dimensions ...

▶ Vectors for plotting web

$\text{WebWidthDim} := \begin{pmatrix} 0 \\ 7 \end{pmatrix}$ ... (in.) Web width transition points (used in function below)

$\text{WebHeightDim} := \begin{pmatrix} 45.5 \\ 45.5 \end{pmatrix}$ ... (in.) Web height at each transition point (used in function below)

Web geometry

$\text{WebHeight}(x) := \text{linterp}(\text{WebWidthDim}, \text{WebHeightDim}, x)$

... (in.) Web height as a function of x (width)

<u>Web temperature gradient (adapted from Lee 2010) ...</u>

WebWidth := 7 ... (in.) Total web width

B_{web} := WebWidth ÷ 2 = 3.5 ... (in.) Dimension specified in web temperature gradient

x := 0, WebWidth·0.01 .. WebWidth ... (in.) Range variable for web temperature gradient

T1 := 15 ... (ºC) Maximum web temperature (T1) for Atlanta, GA in winter (Lee 2012)

T2 := T1 ÷ 4 = 3.8 ... (ºC) Temperature at first B_{web} dimension

T3 := 0 ... (ºC) Temperature at second B_{web} dimension

$$\text{WebTemperatures} := \begin{pmatrix} T1 \\ T2 \\ T3 \end{pmatrix} = \begin{pmatrix} 15.0 \\ 3.8 \\ 0.0 \end{pmatrix}$$ ... (ºC) Web temperatures for web temperature gradient

$$\text{BwebDim} := \begin{pmatrix} 0 \\ B_{web} \\ \text{WebWidth} \end{pmatrix} = \begin{pmatrix} 0 \\ 3.5 \\ 7 \end{pmatrix}$$ ... (in.) Web width dimensions at each temperature point

$$\text{WebTemp(x)} := \begin{vmatrix} e \leftarrow \text{linterp(BwebDim, WebTemperatures, x)} & \text{if } x \geq 0 \wedge x \leq \text{WebWidth} \\ e \leftarrow 0 & \text{otherwise} \\ \text{return } e \end{vmatrix}$$

... (ºC) Web temperature as a function of x (width)

80
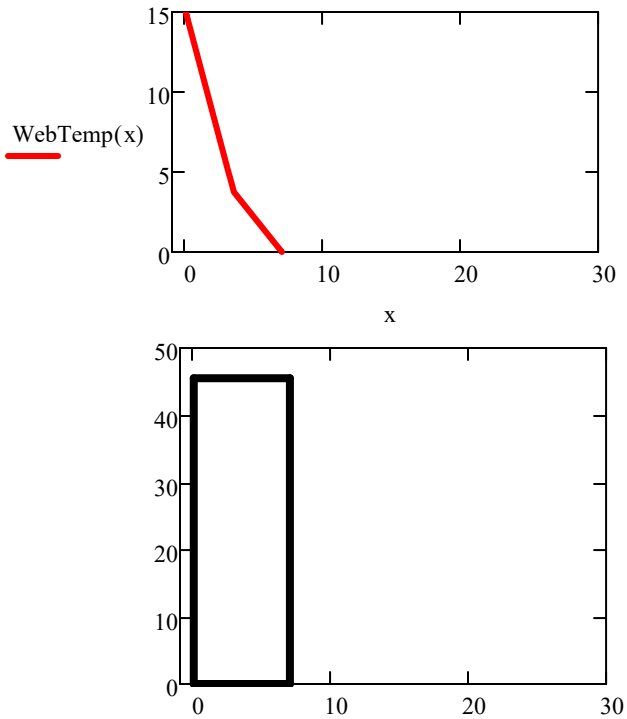
Web moment calculation ...

$$\text{WebMoment} := \int_0^{\text{WebWidth}} \text{Ec} \cdot \alpha \cdot \text{WebTemp(x)} \cdot \text{WebHeight(x)} \cdot \left(\frac{\text{WebWidth}}{2} - x \right) dx = 186.9$$

$\text{WebMoment} \div 12 = 15.6$ ... (kip-ft) Top flange moment due to applied top flange temperature gradient
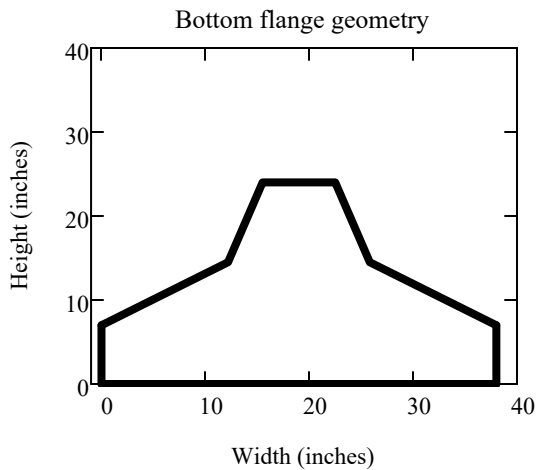
Bottom flange dimensions ...

▶ Vectors for plotting bottom flange

$$\text{BottomFlangeWidthDim} := \begin{pmatrix} 0 \\ 12.185 \\ 15.5 \\ 22.5 \\ 25.815 \\ 38 \end{pmatrix}$$ ... (in.) Bottom flange width transition points (used in function below)

$$\text{BottomFlangeHeightDim} := \begin{pmatrix} 7 \\ 14.5 \\ 24 \\ 24 \\ 14.5 \\ 7 \end{pmatrix}$$ ... (in.) Bottom flange height at each transition point (used in function below)

Bottom flange geometry

$\text{BottomFlangeHeight(x)} := \text{linterp(BottomFlangeWidthDim, BottomFlangeHeightDim, x)}$

... (in.) Bottom flange height as a function of x (width)

81

<u>Bottom flange temperature gradient (adapted from Lee 2010) ...</u>

$\text{BottomFlangeWidth} := 38$ ... (in.) Total bottom flange width

$B_{bot} := \text{BottomFlangeWidth} \div 4 = 9.5$ ... (in.) Dimension specified in bottom flange temperature gradient

$x := 0, \text{BottomFlangeWidth} \cdot 0.01 \,.. \text{BottomFlangeWidth}$ ... (in.) Range variable for top flange temperature gradient

$T1 := 25$ ... (°C) Maximum bottom flange temperature (T1) for Atlanta, GA in winter (Lee 2012)

$T2 := \dfrac{4}{9} T1 = 11.1$ ... (°C) Temperature at first B_{bot} dimension

$T3 := \dfrac{1}{9} T1 = 2.8$ ... (°C) Temperature at second B_{bot} dimension

$T4 := 0$ ... (°C) Temperature at third B_{bot} dimension

$\lambda := 4 \div 25.6 = 0.16$ ... Dimensionless ratio proposed for current project to add ascending branch

$T5 := \lambda \cdot T1 = 3.9$ ... (°C) Temperature at right end (additional ascending branch)

$$\text{BottomFlangeTemperatures} := \begin{pmatrix} T1 \\ T2 \\ T3 \\ T4 \\ T5 \end{pmatrix} = \begin{pmatrix} 25.0 \\ 11.1 \\ 2.8 \\ 0.0 \\ 3.9 \end{pmatrix}$$ ... (°C) Bottom flange temperatures for top flange temperature gradient

$$\text{BbotDim} := \begin{pmatrix} 0 \\ B_{bot} \\ 2 \cdot B_{bot} \\ 3 \cdot B_{bot} \\ \text{BottomFlangeWidth} \end{pmatrix} = \begin{pmatrix} 0 \\ 9.5 \\ 19 \\ 28.5 \\ 38 \end{pmatrix}$$ ... (in.) Bottom flange width dimensions at each temperature point

$\text{BottomFlangeTemp(x)} := \begin{array}{|l} e \leftarrow \text{linterp(BbotDim, BottomFlangeTemperatures, x)} \quad \text{if } x \geq 0 \wedge x \leq \text{BottomFlangeWidth} \\ e \leftarrow 0 \quad \text{otherwise} \\ \text{return } e \end{array}$

       ... (°C) Bottom flange temperature as a function of x (width)
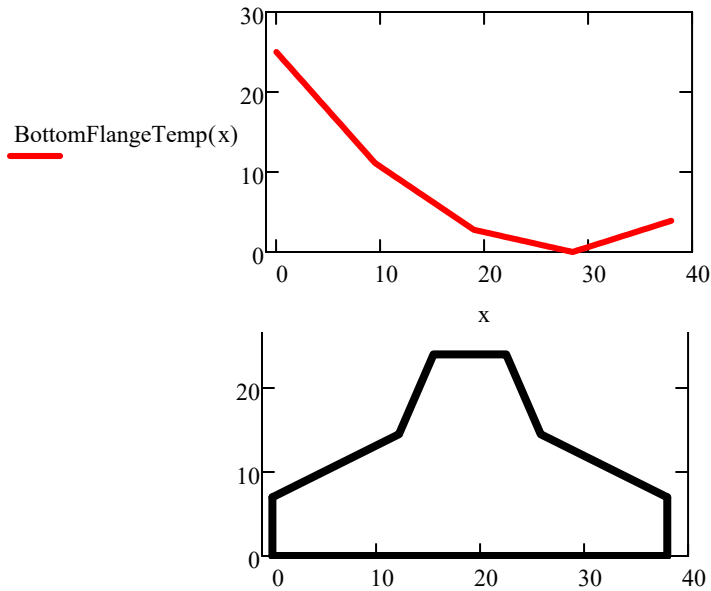
Bottom flange moment calculation ...

$$\text{BottomFlangeMoment} := \int_0^{\text{BottomFlangeWidth}} \text{Ec}\cdot\alpha\cdot\text{BottomFlangeTemp(x)}\cdot\text{BottomFlangeHeight(x)}\cdot\left(\frac{\text{BottomFlangeWidth}}{2} - x\right) dx$$

$\text{BottomFlangeMoment} \div 12 = 146.6$ ... (kip-ft) Bottom flange moment due to applied top flange temperature gradient

Thermal sweep and sweep ratio calculations ...

$$L := \begin{pmatrix} 145\cdot12 \\ 170\cdot12 \\ 195\cdot12 \end{pmatrix} = \begin{pmatrix} 1740 \\ 2040 \\ 2340 \end{pmatrix}$$ ... (in.) Minimum, intermediate, and maximum span length for a 78" FIB

$I_y := 82484$ ... (in.^{4}) Weak-axis moment of inertia for a 78" FIB (Appendix A)

$\text{TotalMoment} := \text{TopFlangeMoment} + \text{WebMoment} + \text{BottomFlangeMoment}$

$\text{TotalMoment} \div 12 = 206.8$ ... (kip-ft) Total moment due to winter transverse temperature gradients

$$\text{WinterThermalSweep} := \frac{\text{TotalMoment}\cdot L^2}{8\cdot \text{Ec}\cdot I_y} = \begin{pmatrix} 2.04 \\ 2.80 \\ 3.68 \end{pmatrix}$$ ... (in.) thermal sweep for a 78" FIB due to winter transverse gradients for the three span lengths considered

$$\text{FabricationSweep} := \frac{1}{8}\cdot\frac{L}{(10\cdot12)} = \begin{pmatrix} 1.81 \\ 2.13 \\ 2.44 \end{pmatrix}$$ ... (in.) Largest allowable sweep due to fabrication errors (PCI, 1/8" for every 10 ft of span length)

$$\text{WinterSweepRatio} := \frac{\text{WinterThermalSweep}}{\text{FabricationSweep}} = \begin{pmatrix} 1.12 \\ 1.32 \\ 1.51 \end{pmatrix}$$ ... Winter sweep ratios for a 78" FIB considering the minimum, intermediate, and maximum span lengths

APPENDIX C
EXAMPLE CALCULATIONS:
TEMPORARY BRACING ASSESSMENT FOR AN FIB BRIDGE

Presented in this appendix is an updated version of a calculation worksheet that was previously presented in the final report for FDOT study BDK75-977-33 (Consolazio et al., 2013). Example calculations demonstrating the assessment of temporary bracing requirements for a typical FIB bridge are illustrated. The updated calculation worksheet shown in this appendix utilizes equations from Consolazio et al. (2013) together with Eqn. (4.5) and Eqn. (5.3) from the present study.

Design of temporary bracing for an FIB bridge

Plan view

- 2% cross-slope

Section view
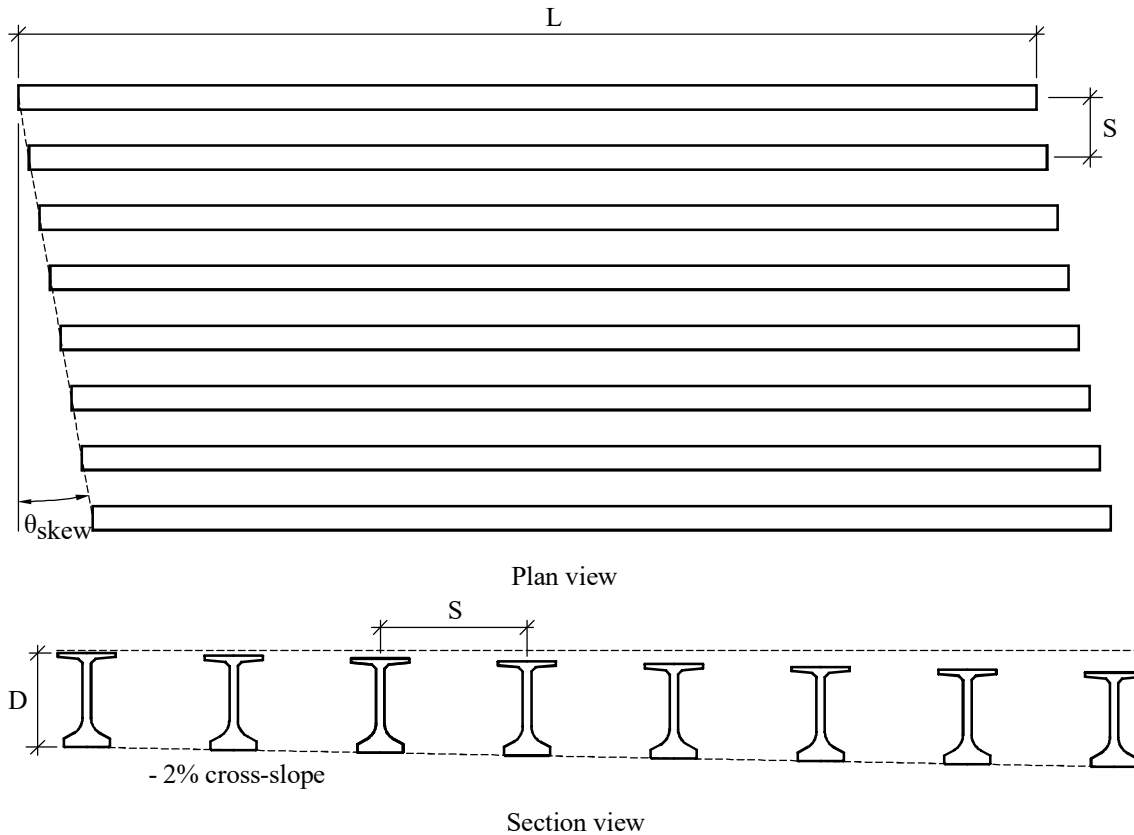
System parameters...

FIB78   ... Girder type

$D := 78$ ... (in) Section depth

$w_{sw} := 1146$ ... (lbf/ft) Girder self-weight

$L := 170$ ... (ft) Span length

$n := 8$ ... Number of girders

$S := 10$ ... (ft) Girder spacing

$\theta_{skew} := 10$ ... (deg) Skew angle

$\theta_{skew} := \theta_{skew} \cdot \dfrac{\pi}{180} = 0.175$ ... Convert from deg to rad

Wind loads...
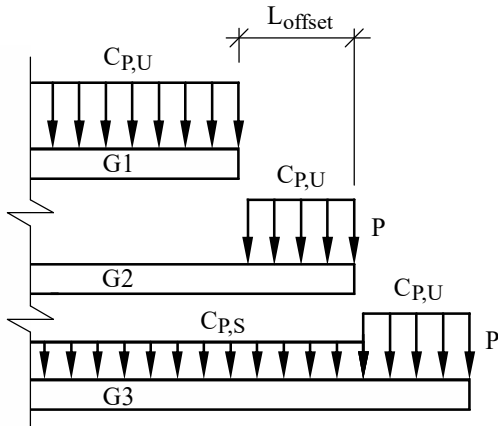
$$V := 110 \qquad \text{... (mph) Basic wind speed}$$

$$G := 0.85 \qquad \text{... Gust effect factor (SDG §2.4.1E)}$$

$$z := 20 \qquad \text{... (ft) Elevation of bridge girders}$$

$$K_z := 2.01 \cdot \left(\frac{z}{900}\right)^{0.2105} = 0.902 \qquad \text{... Velocity pressure exposure coefficient (SDG §2.4.1D)}$$

$$C_{P,U} := 2.0 \qquad \text{... Pressure coefficient for \underline{unshielded} FIB (Girder G1) (Figure 5.17 in BDK75-977-33)}$$

$$C_{P,S} := 1.0 \qquad \text{... Pressure coefficient for \underline{shielded} FIB (girders G3, G4, etc) (Figure 5.17 in BDK75-977-33)}$$

$$P_U := 0.6\left(2.56 \cdot 10^{-6} \cdot K_z \cdot V^2 \cdot G \cdot C_{P,U}\right) = 0.028 \qquad \text{... (ksf) Design wind pressure for unshielded FIB (SDG §2.4.1D)}$$

$$P_U := P_U \cdot 1000 = 28.5 \qquad \text{... Convert from ksf to psf}$$

$$P_S := 0.6\left(2.56 \cdot 10^{-6} \cdot K_z \cdot V^2 \cdot G \cdot C_{P,S}\right) = 0.014 \qquad \text{... (ksf) Design wind pressure for shielded FIB (SDG §2.4.1D)}$$

$$P_S := P_S \cdot 1000 = 14.2 \qquad \text{... Convert from ksf to psf}$$

$$L_{offset} := S \cdot \tan\left(\theta_{skew}\right) = 1.8 \qquad \text{... (ft) Skew offset length (see figure above)}$$

$$L_{shielded} := L - L_{offset} \qquad \text{... (ft) Shielded length}$$
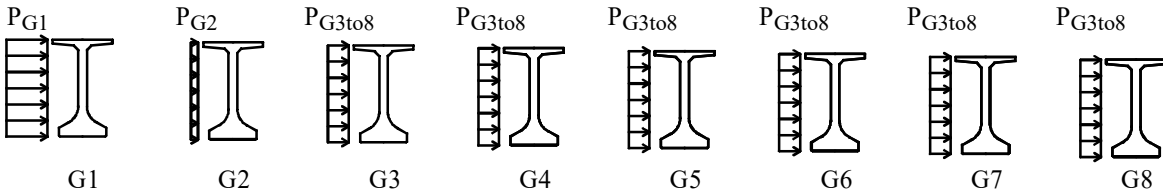
$$P_{G1} := P_U = 28.5 \qquad \text{... (psf) Average wind load on girder G1}$$

$$P_{G2} := \frac{0 \cdot L_{shielded} + P_U \cdot L_{offset}}{L} = 0.3 \qquad \text{... (psf) Average wind load on girder G2}$$

$$P_{G3to8} := \frac{P_S \cdot L_{shielded} + P_U \cdot L_{offset}}{L} = 14.4 \qquad \text{... (psf) Average wind load on girders G3, G4, etc.}$$

$$P_{bar} := \frac{P_{G1} + P_{G2} + P_{G3to8} \cdot (n-2)}{n} = 14.4 \qquad \text{... (psf) Average wind load per girder (Equation 9.7 in BDK75-977-33)}$$

86

Compute anchor roll stiffness...
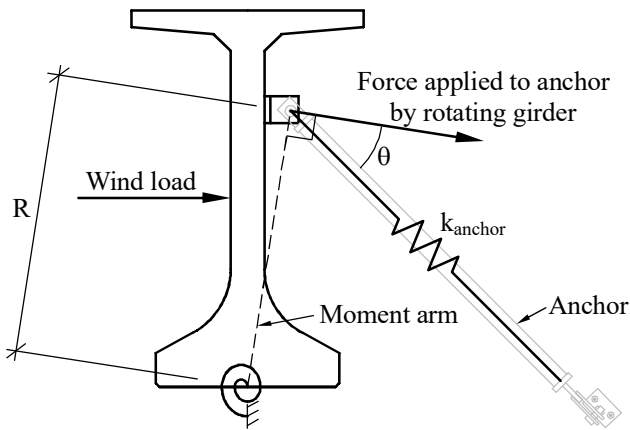
$k_{anchor} := 75$ ... (kip/in) Axial stiffness of anchor (Figure 7.6 in BDK75-977-33)

$R := 55$ ... (in) Anchor moment arm (Figure 7.6 in BDK75-977-33)

$\theta := 45$ ... (deg) Angle between anchor and girder force vector (Figure 7.6 in BDK75-977-33)

$\theta := \theta \cdot \dfrac{\pi}{180}$ ... Convert from deg to rad

$k_{roll,anchor} := k_{anchor} \cdot (\cos(\theta))^2 \cdot R^2 = 113438$ ... (kip-in/rad) Roll stiffness of anchor (Equation 7.4 in BDK75-977-33)

$k_{roll,anchor} := k_{roll,anchor} \div 12 = 9453$ ... Convert from kip-in/rad to kip-ft/rad

Compute wind capacity of individual girder ...

$$P_{max,0} := 63e^{\frac{-L}{55}}\left(\frac{1}{3} + 15e^{\frac{-D}{79}}\right) - 34e^{\frac{-D}{72}} - \frac{1}{8} = 5.327$$

          ... (psf) Updated wind capacity of unanchored girder (Equation 4.5 in BDV31-977-46)

$$P_{max} := P_{max,0} + 11e^{\frac{-L}{22}}\left(k_{roll,anchor}\right) = 51.147$$

          ... (psf) Final wind capacity of anchored girder (Equation 8.6 in BDK75-977-33)

$P_{G1} = 28.498$ $P_{max} > P_{G1}$ ... OK (Wind capacity exceeds design wind load)

Compute capacity of multi-girder system (strut braces)...

$$C_0 := 47 \cdot e^{\frac{-L}{42}} + 0.5 = 1.321$$

          ... (g) Updated baseline system capacity (Equation 5.3 in BDV31-977-46)

Compute effective stiffness of K-brace...
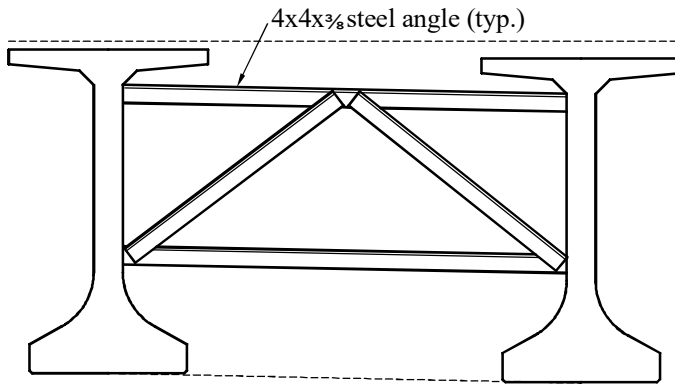
K-Brace design
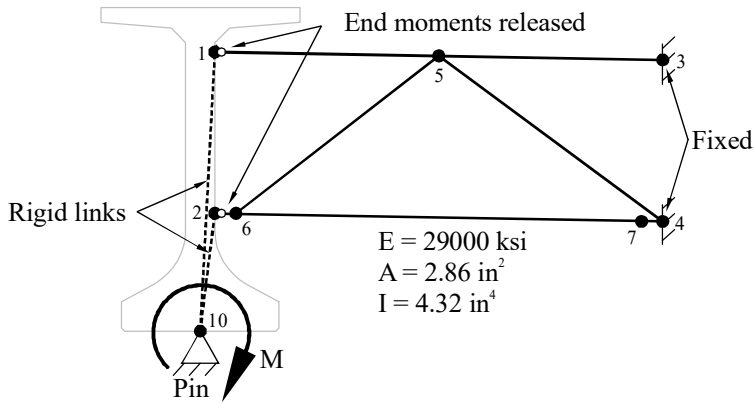
Structural model used for
determination of effective brace stiffness

Node	X-Coordinate	Y-Coordinate
1	3.50	69.50
2	3.50	24.00
3	116.50	67.10
4	116.50	21.60
5	60.00	68.30
6	6.50	23.94
7	113.50	21.66
10	0.00	0.00

$M := 1$ ... (kip-in) Unit moment load applied to structural model

$\theta_{10} := 2.26 \cdot 10^{-7}$ ... (rad) Angular displacement computed from model at node 10

$k_{brace} := \dfrac{M}{\theta_{10}} = 4.425 \times 10^6$ ... (kip-in/rad) Effective brace stiffness

$k_{brace} := k_{brace} \div 12 = 3.687 \times 10^5$ ... Convert from kip-in/rad to kip-ft/rad

88

Compute capacity of multi-girder system (K-braces at girder ends)

<div align="center">Table 9.4</div>

n_i	Brace locations	ω
0	End bracing	1.0
1	Midpoint bracing	1.4
2	Third-point bracing	1.6
3	Quarter-point bracing	1.7

$n_i := 0$ ...Number of interior brace points

$\omega := 1$ ...Interior brace coefficient (Table 9.4 in BDK75-977-33, reproduced above)

$$C := C_0 + \omega \cdot \frac{620 \cdot k_{brace} \cdot e^{\frac{-L}{30}}}{k_{brace} + 1000000} - \frac{\sqrt{P_{bar}}}{1000000}\left(8 \cdot L^2 + 0.004 \cdot L \cdot k_{brace} - 5100 \cdot L - k_{brace} + 900000\right) - \frac{D \cdot P_U}{48 w_{sw}} = 1.303$$

... (g) Final system capacity (Equation 9.23 in BDK75-977-33)

$C > 1$ ... OK

APPENDIX D
DETAILED ILLUSTRATIONS:
QUANTIFYING EXTERIOR AND INTERIOR GIRDER END SHEAR FORCES AND
MAXIMUM MOMENTS WITH CONSTRUCTION LOADS APPLIED

Presented in this appendix are detailed illustrations of the proposed method for quantifying interior and exterior girder end shear forces and maximum moments. In each case, a simply supported static beam analysis is presented in conjunction with the proposed construction load distribution factor (*DF*) equations.

Load Group 1 – Exterior girder end shear force prediction

To predict $V_{EXT\ LG1}$

Convert 3D loads to equivalent one dimensional loads

Live load tributary area
Worker line load
Machine load
$V_{EXT\ LG1}$
$V_{EXT\ LG1}$
20 ft
50 ft

Equivalent worker line load + equivalent live load
Machine load
Equivalent live load
20 ft
50 ft
$V_{STATIC\ LG1}$

Note: $V_{STATIC\ LG1}$ includes machine load
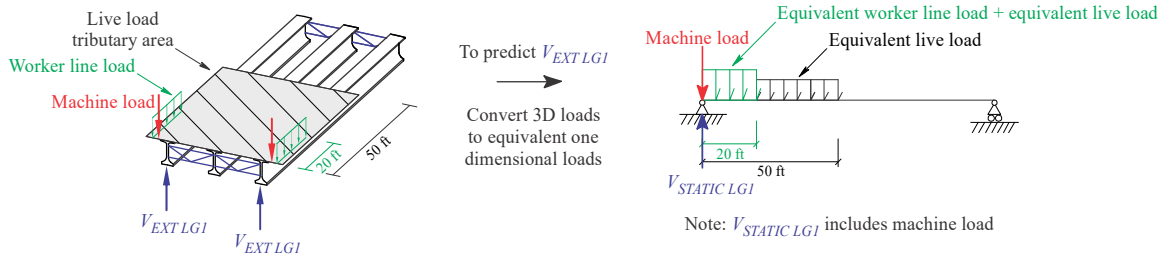
$$V_{EXT\ LG1} = V_{STATIC\ LG1} \times DF_{V\ EXT\ LG1}$$

$$DF_{V\ EXT\ LG1} = \left(1+\beta\right)\left[-0.26 + \left(0.60\,N\right)^{-0.41}\left(0.03\,L\right)^{-0.03}\left(1.76\frac{OH}{S}\right)^{0.27} + 0.10\left(\theta\right)^{0.02}\right]$$

where:
$V_{EXT\ LG1}$	=	Load Group 1 exterior girder end shear force prediction
$V_{STATIC\ LG1}$	=	Maximum Load Group 1 end shear force using a static analysis (as shown above)
$DF_{V\ EXT\ LG1}$	=	Load Group 1 exterior girder end shear force distribution factor
β	=	Exceedance factor (selected from figures below)
N	=	Number of girders
L	=	Span length (ft)
OH	=	Deck overhang width (ft)
S	=	Girder center-to-center spacing (ft)
θ	=	Skew angle (deg.)

50% exceedance
$\beta = -0.01$

84% exceedance
$\beta = 0.12$

95% exceedance
$\beta = 0.31$

98% exceedance
$\beta = 0.53$
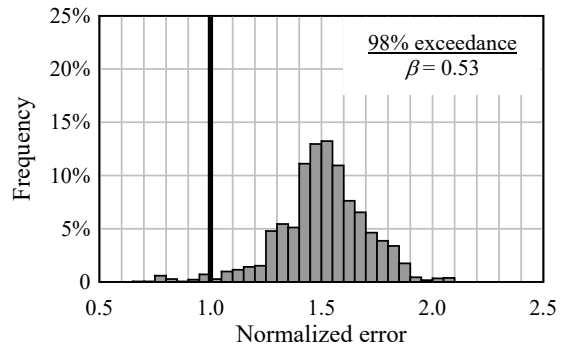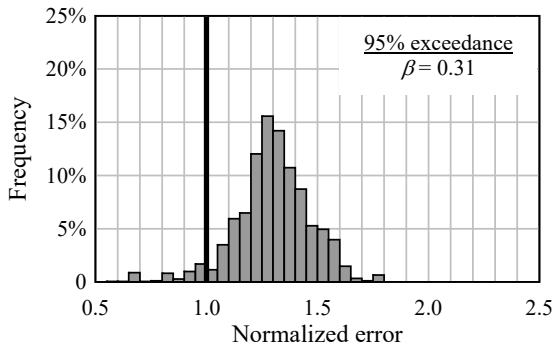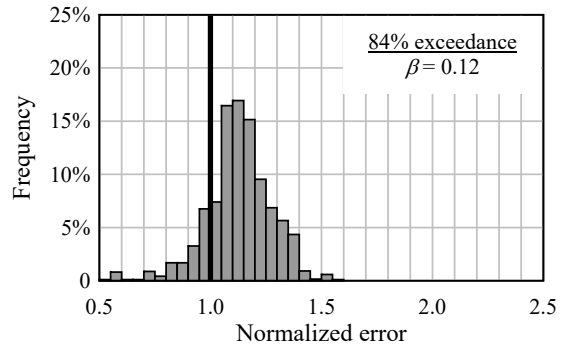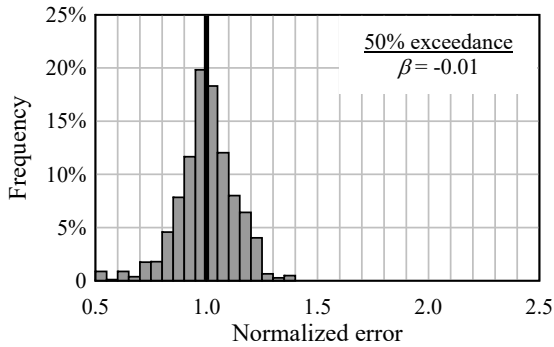
Note: Normalized error defined as $\dfrac{V_{prediction}}{V_{FEA}}$, where normalized error ≥ 1.0 indicates a conservative prediction

Load Group 1 – Interior girder end shear force prediction
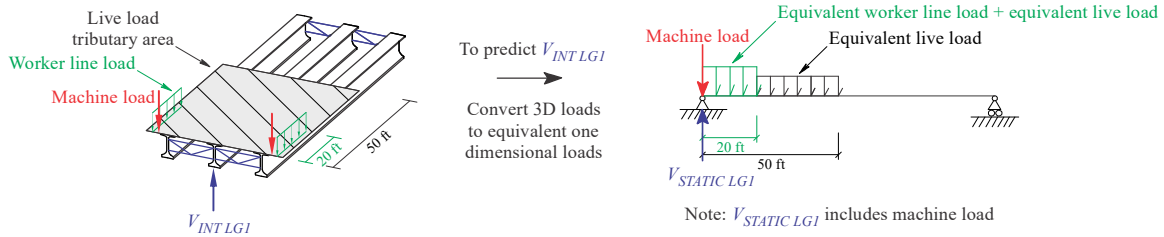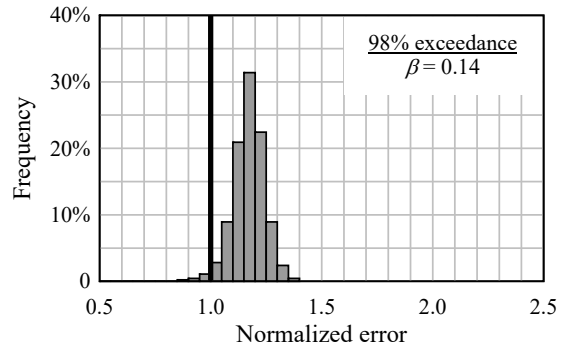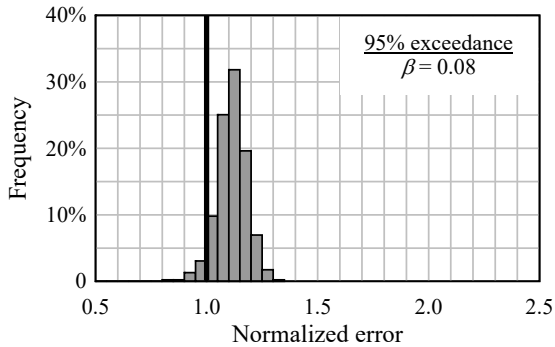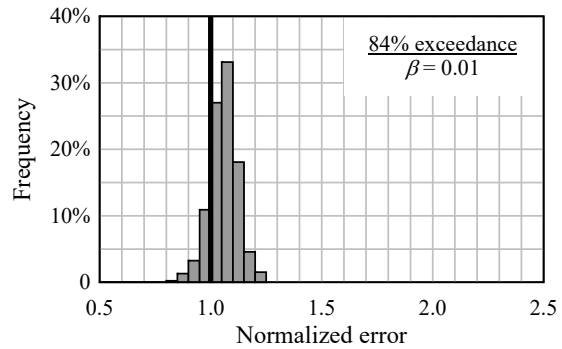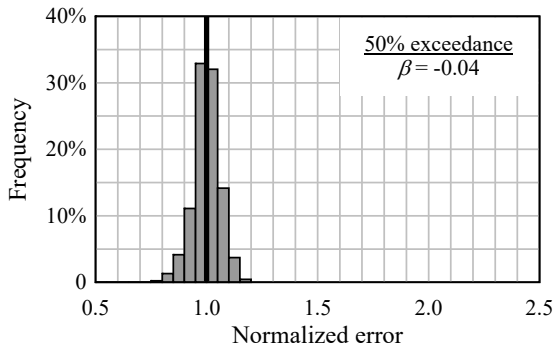

$$V_{INT\;LG1} = V_{STATIC\;LG1} \times DF_{V\;INT\;LG1}$$

$$DF_{V\;INT\;LG1} = (1 + \beta)\left[-0.90 + (0.13N)^{-0.11}(0.01L)^{0.02}\left(4.80\frac{OH}{S}\right)^{0.02} + 0.03(\theta)^{0.01}\right]$$

where:

$V_{INT\;LG1}$	=	Load Group 1 interior girder end shear force prediction
$V_{STATIC\;LG1}$	=	Maximum Load Group 1 end shear force using a static analysis (as shown above)
$DF_{V\;INT\;LG1}$	=	Load Group 1 interior girder end shear force distribution factor
β	=	Exceedance factor (selected from figures below)
N	=	Number of girders
L	=	Span length (ft)
OH	=	Deck overhang width (ft)
S	=	Girder center to center spacing (ft)
θ	=	Skew angle (deg.)

Note: Normalized error defined as $\dfrac{V_{prediction}}{V_{FEA}}$, where normalized error ≥ 1.0 indicates a conservative prediction

92
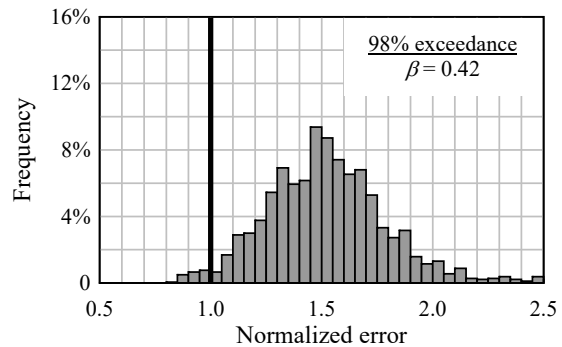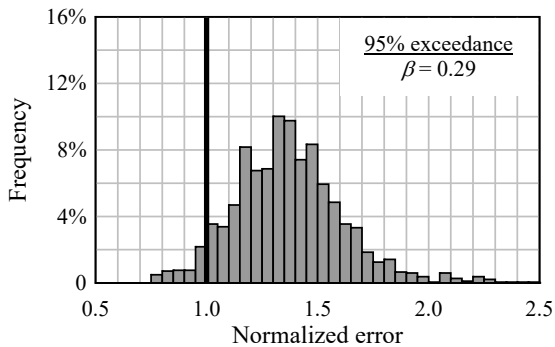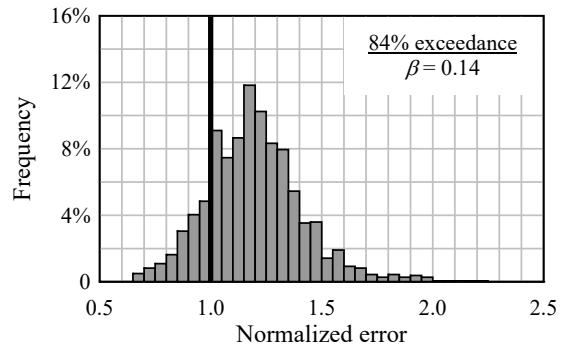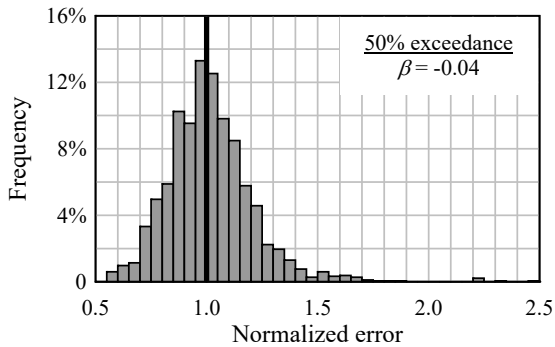
Load Group 1 – Exterior girder maximum moment prediction
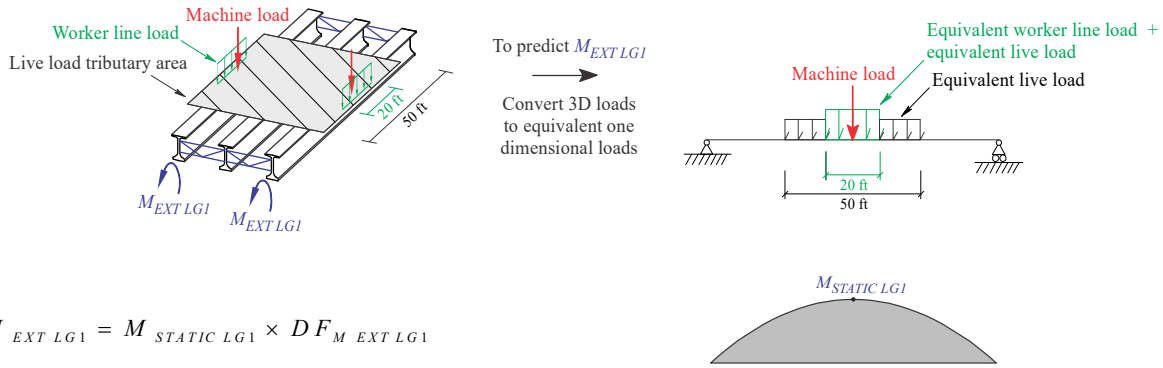
$$M_{EXT\,LG1} = M_{STATIC\,LG1} \times DF_{M\,EXT\,LG1}$$
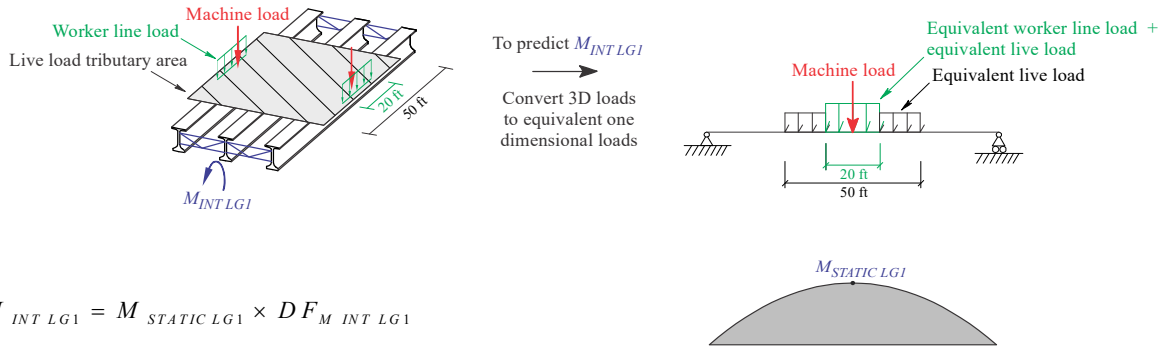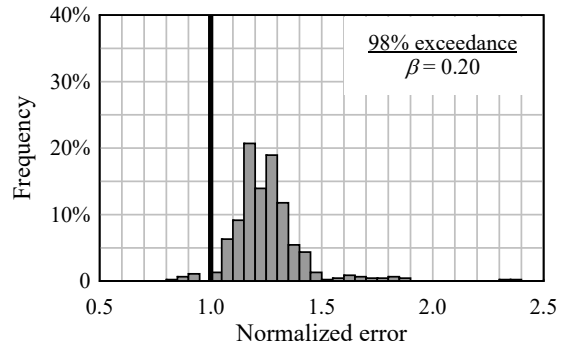
$$DF_{M\,EXT\,LG1} = (1 + \beta)\left[-0.23 + (0.47N)^{-0.33}(2.51L)^{-0.09}\left(27.00\frac{OH}{S}\right)^{0.09}\right]$$

where:

$M_{EXT\,LG1}$	=	Load Group 1 exterior girder maximum bending moment prediction
$M_{STATIC\,LG1}$	=	Maximum Load Group 1 moment using a static analysis (as shown above)
$DF_{M\,EXT\,LG1}$	=	Load Group 1 exterior girder maximum moment distribution factor
β	=	Exceedance factor (selected from figures below)
N	=	Number of girders
L	=	Span length (ft)
OH	=	Deck overhang width (ft)
S	=	Girder center to center spacing (ft)

Note: Normalized error defined as $\dfrac{M_{prediction}}{M_{FEA}}$, where normalized error ≥ 1.0 indicates a conservative prediction
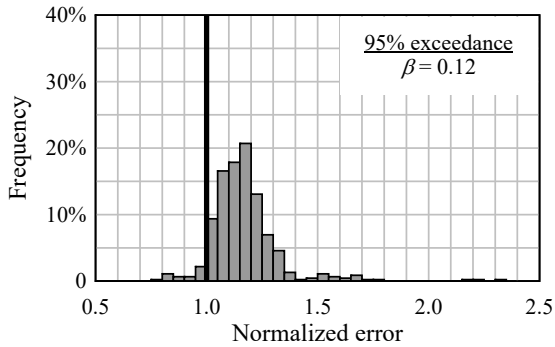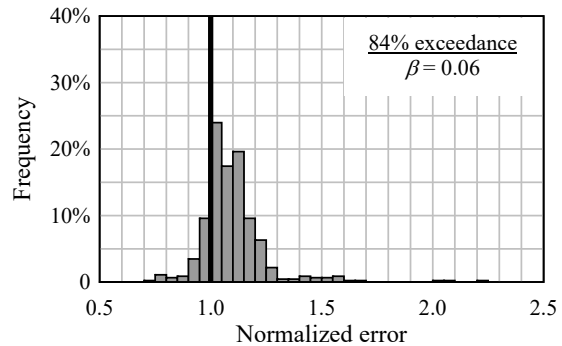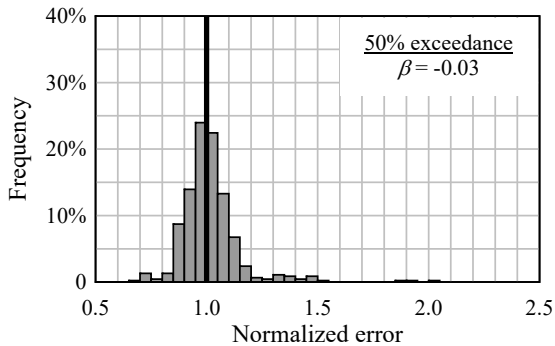
93

Load Group 1 – Interior girder maximum moment prediction

$$M_{INT\,LG1} = M_{STATIC\,LG1} \times DF_{M\,INT\,LG1}$$

$$DF_{M\,INT\,LG1} = \left(1 + \beta\right)\left[0.06 + \left(1.94N\right)^{-1.22}\left(0.53L\right)^{0.17}\left(8.63\frac{OH}{S}\right)^{-0.03}\right]$$

where:

$M_{INT\,LG1}$	=	Load Group 1 interior girder maximum bending moment prediction
$M_{STATIC\,LG1}$	=	Maximum Load Group 1 moment using a static analysis (as shown above)
$DF_{M\,INT\,LG1}$	=	Load Group 1 interior girder maximum moment distribution factor
β	=	Exceedance factor (selected from figures below)
N	=	Number of girders
L	=	Span length (ft)
OH	=	Deck overhang width (ft)
S	=	Girder center to center spacing (ft)

Note: Normalized error defined as $\dfrac{M_{prediction}}{M_{FEA}}$, where normalized error ≥ 1.0 indicates a conservative prediction
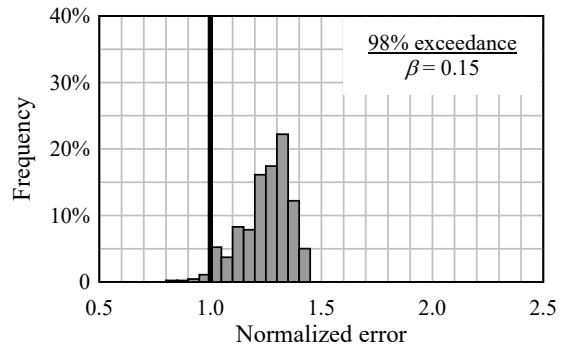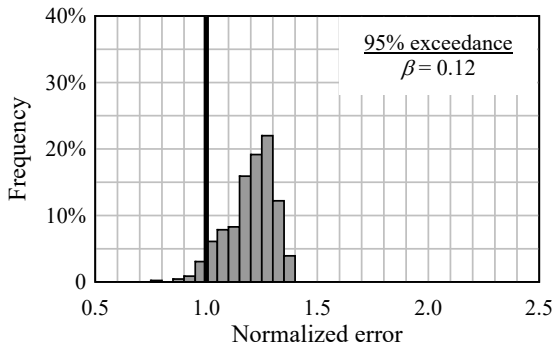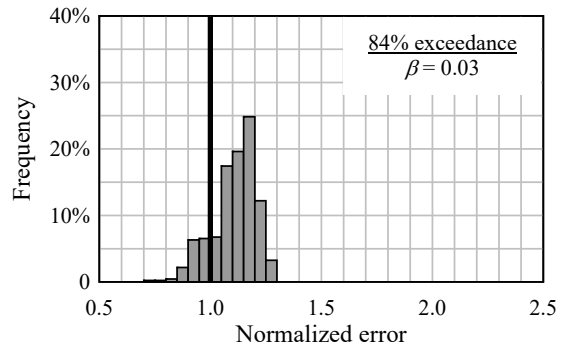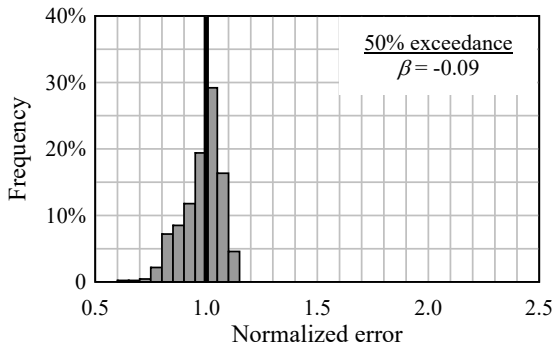
94

Load Group 2 – Exterior girder end shear force prediction

Load Group 2 loads

$V_{EXT\,LG2}$

$V_{EXT\,LG2}$

To predict $V_{EXT\,LG2}$

Convert 3D loads to equivalent one dimensional loads

Equivalent Load Group 2 loads

Span length

$V_{STATIC\,LG2}$

Note: Equivalent Load Group 2 loads include overhang bracket self-weight
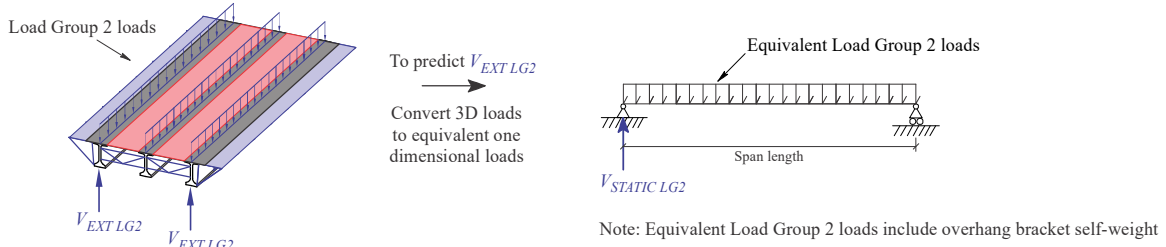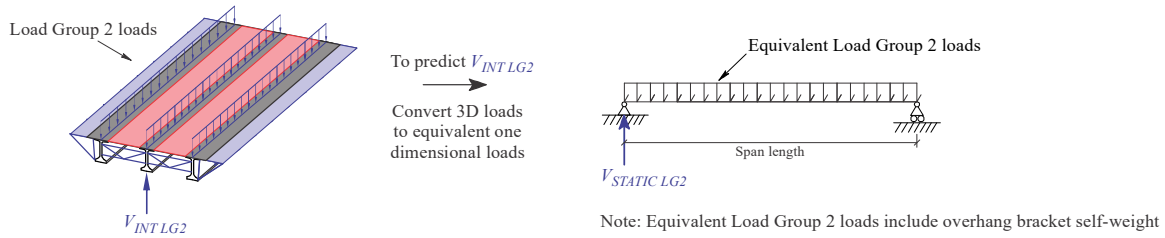
$$V_{EXT\,LG2} = V_{STATIC\,LG2} \times DF_{V\,EXT\,LG2}$$

$$DF_{V\,EXT\,LG2} = (1+\beta)\left[-0.01 + (0.78N)^{-0.93}(0.91L)^{0.06}\left(0.81\frac{OH}{S}\right)^{0.36}\right]$$

where:
	$V_{EXT\,LG2}$	=	Load Group 2 exterior girder end shear force prediction
	$V_{STATIC\,LG2}$	=	Maximum Load Group 2 end shear force using a static analysis (as shown above)
	$DF_{V\,EXT\,LG2}$	=	Load Group 2 exterior girder end shear force distribution factor
	β	=	Exceedance factor (selected from figures below)
	N	=	Number of girders
	L	=	Span length (ft)
	OH	=	Deck overhang width (ft)
	S	=	Girder center to center spacing (ft)

50% exceedance
$\beta = -0.09$

84% exceedance
$\beta = 0.03$

95% exceedance
$\beta = 0.12$

98% exceedance
$\beta = 0.15$

Note: Normalized error defined as $\dfrac{V_{prediction}}{V_{FEA}}$, where normalized error ≥ 1.0 indicates a conservative prediction

95

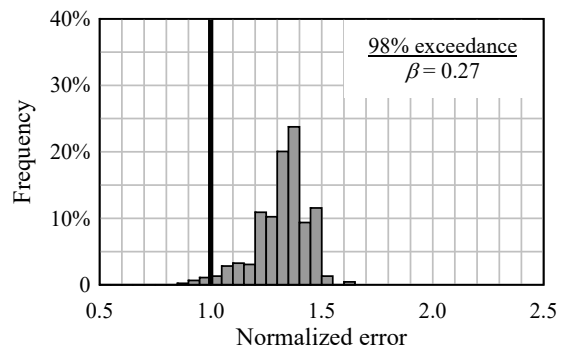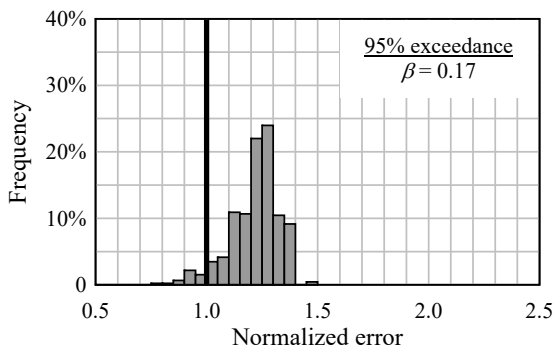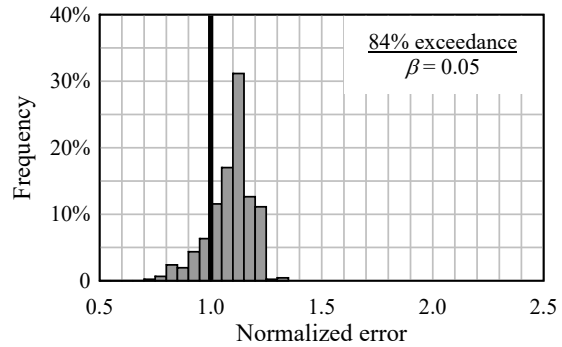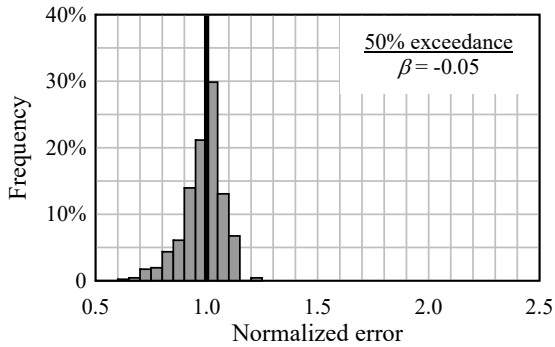# Load Group 2 – Interior girder end shear force prediction

To predict $V_{INT\,LG2}$

Convert 3D loads to equivalent one dimensional loads

Load Group 2 loads

$V_{INT\,LG2}$

Equivalent Load Group 2 loads

Span length

$V_{STATIC\,LG2}$

Note: Equivalent Load Group 2 loads include overhang bracket self-weight

$$V_{INT\,LG2} = V_{STATIC\,LG2} \times DF_{V\,INT\,LG2}$$

$$DF_{V\,INT\,LG2} = (1+\beta)\left[0.03 + (0.89N)^{-1.08}(1.04L)^{0.04}\left(10.16\frac{OH}{S}\right)^{-0.16}\right]$$

where:
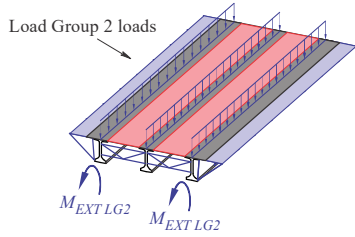|		
$V_{INT\,LG2}$	=	Load Group 2 interior girder end shear force prediction
$V_{STATIC\,LG2}$	=	Maximum Load Group 2 end shear force using a static analysis (as shown above)
$DF_{V\,INT\,LG2}$	=	Load Group 2 interior girder end shear force distribution factor
β	=	Exceedance factor (selected from figures below)
N	=	Number of girders
L	=	Span length (ft)
OH	=	Deck overhang width (ft)
S	=	Girder center to center spacing (ft)

50% exceedance
$\beta = -0.05$

84% exceedance
$\beta = 0.05$

95% exceedance
$\beta = 0.17$

98% exceedance
$\beta = 0.27$

Note: Normalized error defined as $\dfrac{V_{prediction}}{V_{FEA}}$, where normalized error ≥ 1.0 indicates a conservative prediction
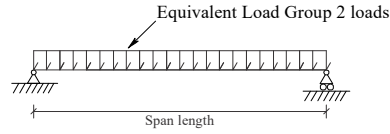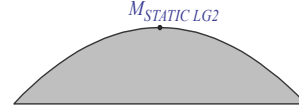
Load Group 2 – Exterior girder maximum moment prediction

To predict $M_{EXT\,LG2}$

Convert 3D loads to equivalent one dimensional loads

Load Group 2 loads

$M_{EXT\,LG2}$ $M_{EXT\,LG2}$

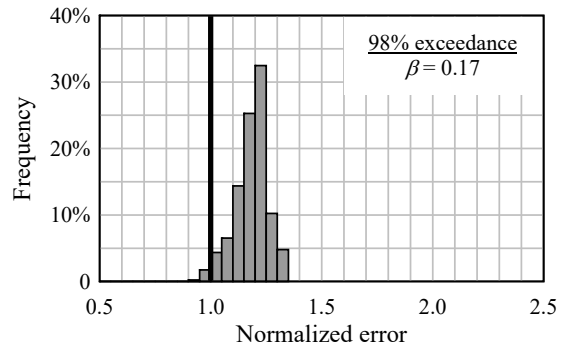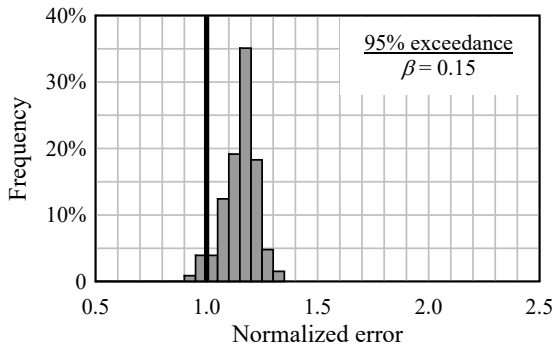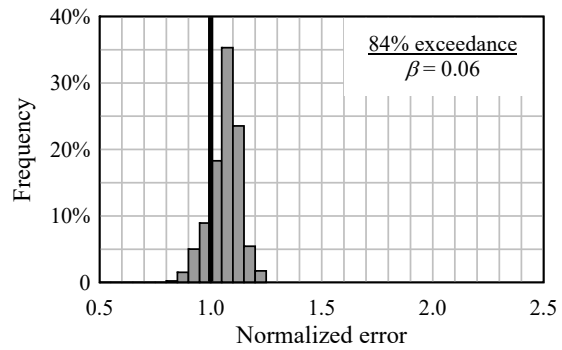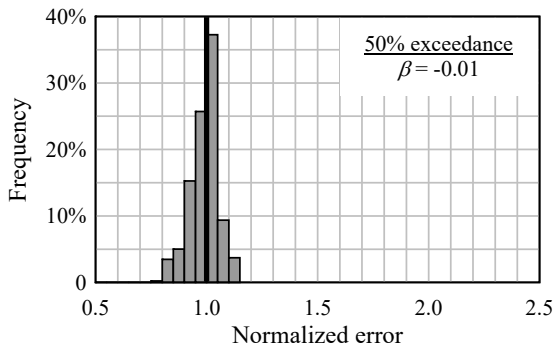Equivalent Load Group 2 loads

Span length

Note: Equivalent Load Group 2 loads include overhang bracket self-weight

$M_{STATIC\,LG2}$

$$M_{EXT\,LG2} = M_{STATIC\,LG2} \times DF_{M\,EXT\,LG2}$$

$$DF_{M\,EXT\,LG2} = \left(1 + \beta\right)\left[-0.06 + \left(1.66N\right)^{-0.77}\left(2.29L\right)^{-0.01}\left(24.58\frac{OH}{S}\right)^{0.17}\right]$$

where:

$M_{EXT\,LG2}$	=	Load Group 2 exterior girder maximum bending moment prediction	
$M_{STATIC\,LG2}$	=	Maximum Load Group 2 moment using a static analysis (as shown above)	
$DF_{M\,EXT\,LG2}$	=	Load Group 2 exterior girder maximum moment distribution factor	
β	=	Exceedance factor (selected from figures below)	
N	=	Number of girders	
L	=	Span length (ft)	
OH	=	Deck overhang width (ft)	
S	=	Girder center to center spacing (ft)	

50% exceedance
$\beta = -0.01$

84% exceedance
$\beta = 0.06$

95% exceedance
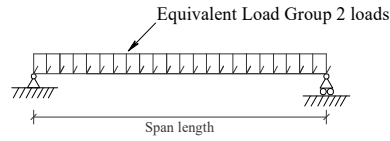$\beta = 0.15$

98% exceedance
$\beta = 0.17$

Note: Normalized error defined as $\dfrac{M_{prediction}}{M_{FEA}}$, where normalized error ≥ 1.0 indicates a conservative prediction

97

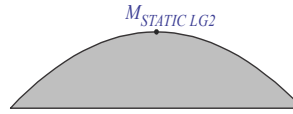# Load Group 2 – Interior girder maximum moment prediction

Load Group 2 loads

$M_{INT\,LG2}$

To predict $M_{INT\,LG2}$

Convert 3D loads to equivalent one dimensional loads
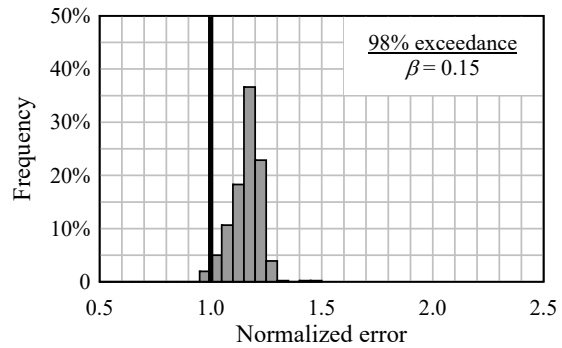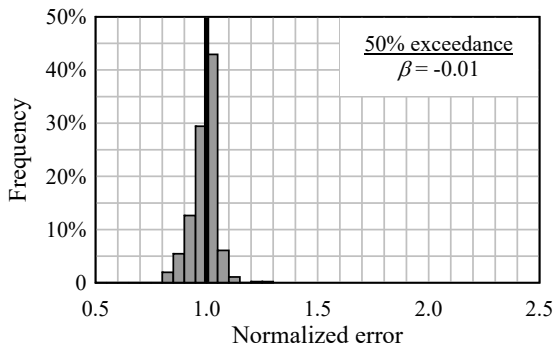
Equivalent Load Group 2 loads

Span length

Note: Equivalent Load Group 2 loads include overhang bracket self-weight

$M_{STATIC\,LG2}$

$$M_{INT\,LG2} = M_{STATIC\,LG2} \times DF_{M\,INT\,LG2}$$

$$DF_{M\,INT\,LG2} = \left(1 + \beta\right)\left[0.01 + \left(0.72N\right)^{-1.09}\left(18.19L\right)^{0.01}\left(14.01\frac{OH}{S}\right)^{-0.16}\right]$$

where:

$M_{INT\,LG2}$	=	Load Group 2 interior girder maximum bending moment prediction
$M_{STATIC\,LG2}$	=	Maximum Load Group 2 moment using a static analysis (as shown above)
$DF_{M\,INT\,LG2}$	=	Load Group 2 interior girder maximum moment distribution factor
β	=	Exceedance factor (selected from figures below)
N	=	Number of girders
L	=	Span length (ft)
OH	=	Deck overhang width (ft)
S	=	Girder center to center spacing (ft)

50% exceedance
$\beta = -0.01$

84% exceedance
$\beta = 0.06$

95% exceedance
$\beta = 0.11$

98% exceedance
$\beta = 0.15$

Note: Normalized error defined as $\dfrac{M_{prediction}}{M_{FEA}}$, where normalized error ≥ 1.0 indicates a conservative prediction

98
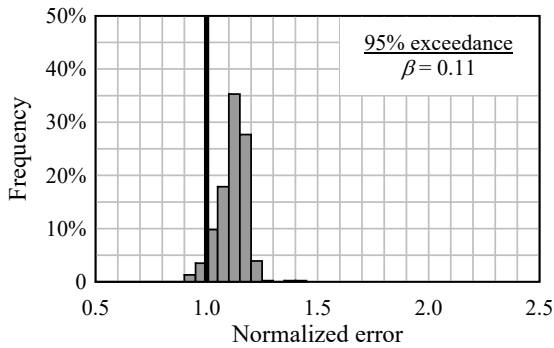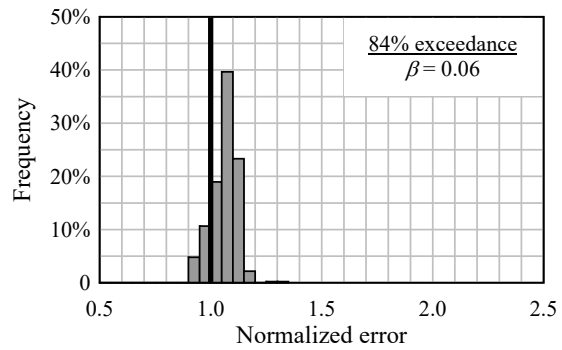
APPENDIX E
EXAMPLE CALCULATIONS:
QUANTIFYING EXTERIOR AND INTERIOR GIRDER END SHEAR FORCES AND
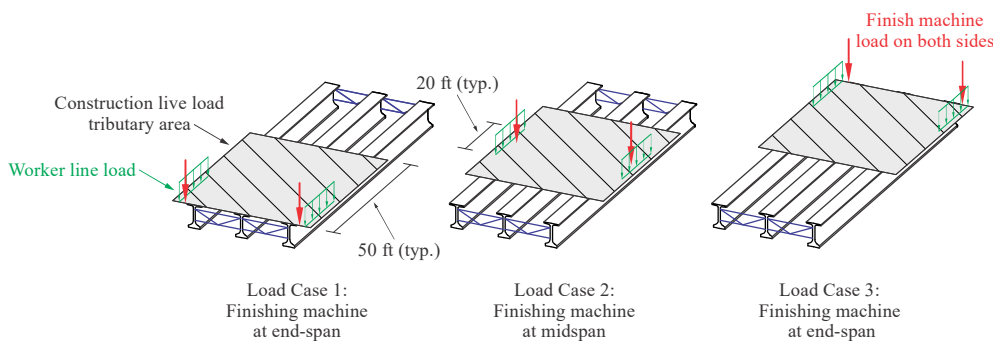**MAXIMUM MOMENTS WITH CONSTRUCTION LOADS APPLIED**

Presented in this appendix is an example calculation worksheet that demonstrates (by example) how the proposed distribution factor equations are used in conjunction with a simply supported static beam analysis to predict girder end shear forces and maximum girder moments.

Prediction of exterior and interior girder end shear forces and moments with construction Load Group 1 (LG1) loads applied

<u>System parameters...</u>

N = 5   ... Number of girders

L = 180   ... (ft) Span length

OH = 48 ÷ 12 = 4   ... (ft) Deck overhang (OH) width

S = 9   ... (ft) Girder center-to-center spacing

θ = 15   ... (deg.) Skew angle

<u>Considering construction LG1 loads applied ...</u>

Load Case 1:
Finishing machine
at end-span

Load Case 2:
Finishing machine
at midspan

Load Case 3:
Finishing machine
at end-span

<u>Compute additional bridge dimensions ...</u>

$$\text{DeckWidth} = [S \cdot (N - 1)] + (2 \cdot OH) = 44$$

... (ft) Width of the deck (edge to edge)

$$\text{TotalWidth} = [S \cdot (N - 1)] + \left[2 \cdot \left(OH + \frac{2.5}{12} + \frac{24}{12} \right) \right] = 48.42$$

... (ft) Width of the bridge (including overhang formwork)

<u>Quantify construction LG1 loads ...</u>

LiveLoad = 20   ... (lbf/ft^2) Live load (Load Group 1)

WorkerLine = 75   ... (lbf/ft) Worker line load (Load Group 1)

$$\text{MachineLoad(width)} = \begin{vmatrix} \text{MachineLoad} \leftarrow 7 & \text{if } 0 < \text{width} \le 32 \\ \text{MachineLoad} \leftarrow 11 & \text{if } 32 < \text{width} \le 56 \\ \text{MachineLoad} \leftarrow 13 & \text{if } 56 < \text{width} \le 80 \\ \text{MachineLoad} \leftarrow 16 & \text{if } 80 < \text{width} \le 120 \\ \text{return } \text{MachineLoad} \end{vmatrix}$$

MachineLoad = MachineLoad(DeckWidth) = 11   ... (kips) Machine load as a function of deck width (LG1)
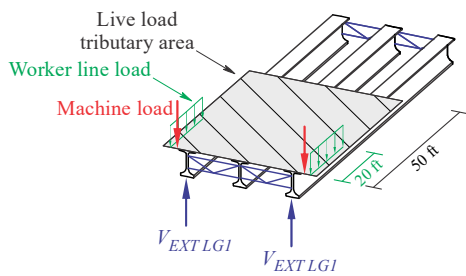
To predict $V_{EXT\,LG1}$
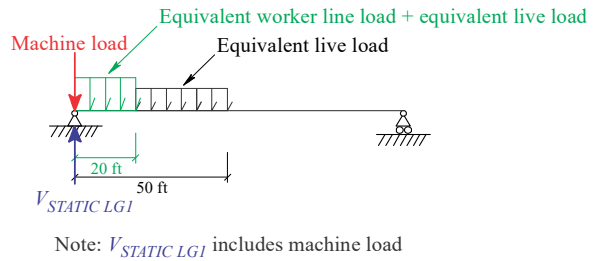
Convert 3D loads to equivalent one dimensional loads

Note: $V_{STATIC\,LG1}$ includes machine load

Equivalent worker line load + equivalent live load

Equivalent live load

Machine load

$V_{STATIC\,LG1}$

20 ft

50 ft

Live load tributary area

Worker line load

Machine load

$V_{EXT\,LG1}$

$V_{EXT\,LG1}$

20 ft

50 ft

<u>Quantify</u> $V_{STATIC\,LG1}$ <u>using a static analysis with the finishing machine load located at one end...</u>

MachineLocation $= 0$ ... (ft) Machine located at End A

<u>Collapse construction LG1 loads to equivalent one-dimensional loads ...</u>

EquivLive $=$ LiveLoad·TotalWidth $\div$ 1000 $=$ 0.968   ... (kip/ft) Converted pressure live load (psf) to equivalent line load

LiveLength $=$ 50   ... (ft) Length of applied live load

LiveArm $=$ LiveLength $\div$ 2 $=$ 25   ... (ft) Distance from End A to the center of the equivalent live load

EquivWorker $=$ 2·WorkerLine $\div$ 1000 $=$ 0.15   ... (kip/ft) Convert two worker line loads (psf), applied on each overhang, to equivalent (single) worker line load

WorkerLength $=$ 20   ... (ft) Length of the applied worker line load

WorkerArm $=$ WorkerLength $\div$ 2 $=$ 10   ... (ft) Distance from End A to the center of the equivalent worker line load

<u>Quantify reactions ...</u>

$$\text{RxnB} = \frac{(\text{EquivLive·LiveLength})\cdot\text{LiveArm} + (\text{EquivWorker·WorkerLength})\cdot\text{WorkerArm} + \text{MachineLoad·0}}{L} = 6.89$$

... (kips) Reaction at End B by summing the moments at End A

RxnA $=$ (MachineLoad $+$ EquivLive·LiveLength $+$ EquivWorker·WorkerLength) $-$ RxnB $=$ 55.53

... (kips) Reaction at End A

<u>Define ...</u> $V_{STATIC\,LG1}$

$V_{STATIC\,LG1} =$ RxnA $=$ 55.53   ... (kips) Maximum reaction using a static analysis

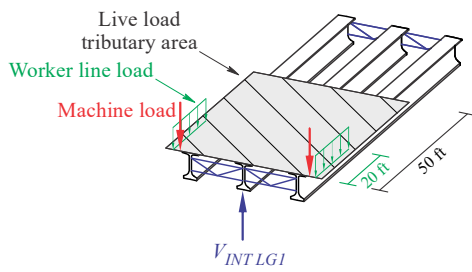<u>Quantify the exterior girder end shear force distribution factor ...</u>

Select a desired exceedance level: $\beta = 0.31$ to achieve a 95% exceedance level

$$DF_{V\,EXT\,LG1} = (1 + \beta)\cdot\left[-0.26 + (0.60\cdot N)^{-0.41}\cdot(0.03\cdot L)^{-0.03}\cdot\left(1.76\cdot\frac{OH}{S}\right)^{0.27} + 0.10\cdot(\theta)^{0.02}\right] = 0.541$$
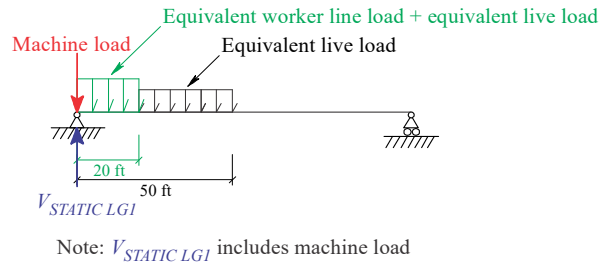
... LG1 exterior girder end shear force distribution factor

<u>Compute the exterior girder end shear force prediction ...</u>

$V_{EXT\,LG1} = V_{STATIC\,LG1}\cdot DF_{V\,EXT\,LG1} = 30.01$ ... (kips) LG1 exterior girder end shear force prediction

Live load tributary area

Worker line load

Machine load

20 ft

50 ft

$V_{INT\,LG1}$

To predict $V_{INT\,LG1}$

Convert 3D loads to equivalent one dimensional loads

Equivalent worker line load + equivalent live load

Equivalent live load

Machine load

20 ft

50 ft

$V_{STATIC\,LG1}$

Note: $V_{STATIC\,LG1}$ includes machine load

Quantify $V_{STATIC\,LG1}$ using a static analysis with the finishing machine load located at one end...

As shown above, $V_{STATIC\,LG1} = RxnA = 55.53$ ... (kips) Maximum reaction using a static analysis

Quantify the interior girder end shear force distribution factor ...

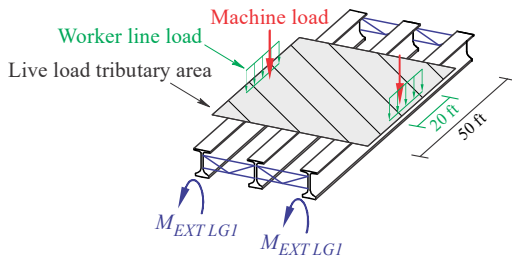Select a desired exceedance level: $\beta = 0.29$ to achieve a 95% exceedance level

$$DF_{V\,INT\,LG1} = (1 + \beta)\cdot\left[-0.90 + (0.13\cdot N)^{-0.11}\cdot(0.01\cdot L)^{0.02}\cdot\left(4.80\cdot\frac{OH}{S}\right)^{0.02} + 0.03\cdot(\theta)^{0.01}\right] = 0.268$$

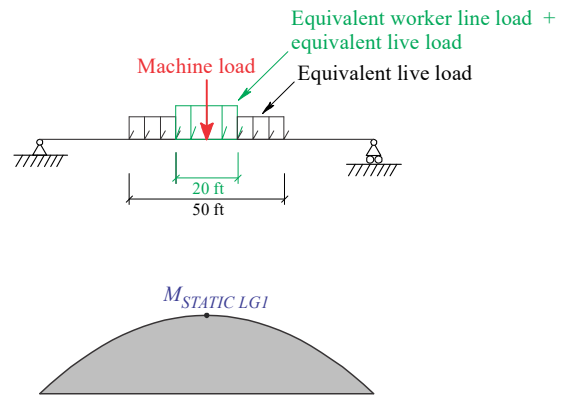... LG1 interior girder end shear force distribution factor

Compute the interior girder end shear force prediction ...

$V_{INT\,LG1} = V_{STATIC\,LG1}\cdot DF_{V\,INT\,LG1} = 14.89$ ... (kips) LG1 interior girder end shear force prediction

102

Quantify $M_{STATIC\ LG1}$ using a static analysis with the finishing machine load located at the midspan...

$$MachineLocation = L \div 2 = 90 \qquad \text{... (ft) Machine located at midspan}$$

Collapse construction LG1 loads to equivalent one-dimensional loads ...

$$EquivLive = LiveLoad \cdot TotalWidth \div 1000 = 0.968 \qquad \text{... (kip/ft) Converted pressure live load (psf) to equivalent line load}$$

$$LiveLength = 50 \qquad \text{... (ft) Length of applied live load}$$

$$EquivWorker = 2 \cdot WorkerLine \div 1000 = 0.15 \qquad \text{... (kip/ft) Convert two worker line loads (psf), applied on each overhang, to equivalent (single) worker line load}$$

$$WorkerLength = 20 \qquad \text{... (ft) Length of the applied worker line load}$$

Quantify maximum moment at the midspan...

$$RxnA = (MachineLoad + EquivLive \cdot LiveLength + EquivWorker \cdot WorkerLength) \div 2 = 31.21$$

... (kips) Reaction at End A

$$MaxMoment = RxnA \cdot MachineLocation - \left[\begin{array}{l} \left(EquivLive \cdot \dfrac{LiveLength}{2} \right) \cdot \dfrac{LiveLength}{4} \ ... \\ + \left(EquivWorker \cdot \dfrac{WorkerLength}{2} \right) \cdot \dfrac{WorkerLength}{4} \end{array} \right] = 2499$$

... (kip-ft) Maximum moment at midspan

Define ... $M_{STATIC\ LG1}$

$$M_{STATIC\ LG1} = MaxMoment = 2499 \qquad \text{... (kip-ft) Maximum moment using a static analysis}$$

Quantify the exterior girder maximum moment distribution factor ...
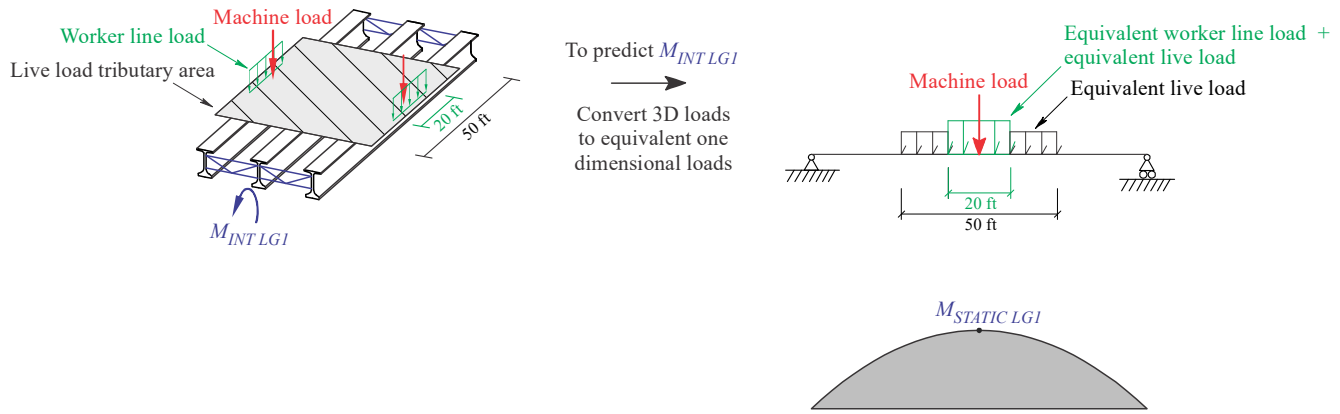
Select a desired exceedance level: $\beta = 0.08$ to achieve a 95% exceedance level

$$DF_{M\ EXT\ LG1} = (1 + \beta) \cdot \left[-0.23 + (0.47 \cdot N)^{-0.33} \cdot (2.51 \cdot L)^{-0.09} \cdot \left(27.00 \cdot \frac{OH}{S} \right)^{0.09} \right] = 0.339$$

... LG1 exterior girder maximum moment distribution factor

Compute the exterior girder maximum moment prediction ...

$$M_{EXT\ LG1} = M_{STATIC\ LG1} \cdot DF_{M\ EXT\ LG1} = 848 \qquad \text{... (kip-ft) LG1 exterior girder maximum moment prediction}$$

Quantify $M_{STATIC\ LG1}$ using a static analysis with the finishing machine load located at the midspan...

As shown above, $M_{STATIC\ LG1} = 2499$ ... (kip-ft) Maximum moment using a static analysis

Quantify the interior girder maximum moment distribution factor ...

Select a desired exceedance level: $\beta = 0.12$ to achieve a 95% exceedance level

$$DF_{M\ INT\ LG1} = (1 + \beta) \cdot \left[0.06 + (1.94 \cdot N)^{-1.22} \cdot (0.53 \cdot L)^{0.17} \cdot \left(8.63 \cdot \frac{OH}{S} \right)^{-0.03} \right] = 0.213$$

... LG1 interior girder maximum moment distribution factor

Compute the interior girder maximum moment prediction ...

$M_{INT\ LG1} = M_{STATIC\ LG1} \cdot DF_{M\ INT\ LG1} = 533$ ... (kip-ft) LG1 interior girder maximum moment prediction
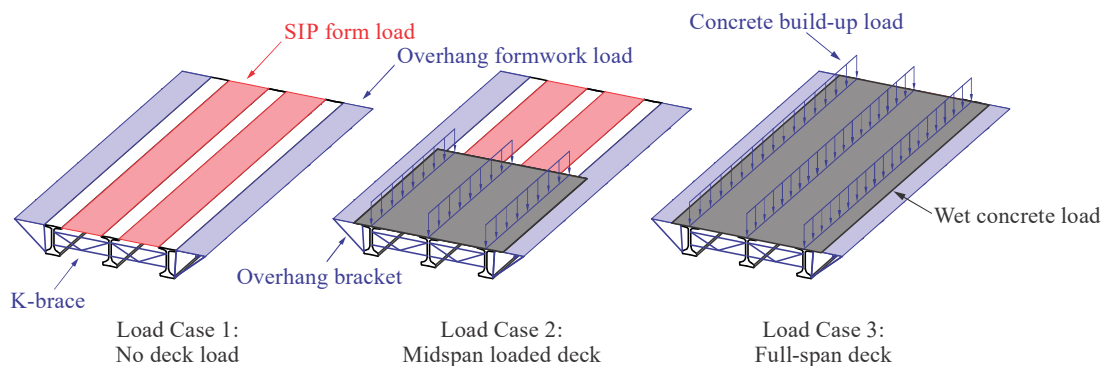
Prediction of exterior and interior girder end shear forces and moments with construction Load Group 2 (LG2) loads applied

System parameters...

$N = 5$ ... Number of girders

$L = 180$ ... (ft) Span length

$OH = 48 \div 12 = 4$ ... (ft) Deck overhang (OH) width

$S = 9$ ... (ft) Girder center-to-center spacing

$\theta = 15$ ... (deg.) Skew angle
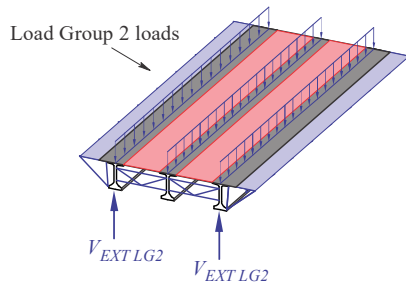
Considering construction LG2 loads applied ...

Load Case 1: No deck load   Load Case 2: Midspan loaded deck   Load Case 3: Full-span deck
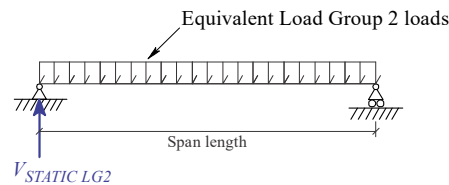
Compute additional bridge dimensions ...

$DeckWidth = [S \cdot (N - 1)] + (2 \cdot OH) = 44$ ... (ft) Width of the deck (edge to edge)

$FormWidth = \left[S - \left(\dfrac{48}{12} \right) \right] \cdot (N - 1) = 20$ ... (ft) Total formwork width (between girders)

$TotalWidth = [S \cdot (N - 1)] + \left[2 \cdot \left(OH + \dfrac{2.5}{12} + \dfrac{24}{12} \right) \right] = 48.42$ ... (ft) Width of the bridge (including overhang formwork)

Quantify construction LG2 loads ...

$WetConcrete = 150 \cdot \left(\dfrac{8.5}{12} \right) = 106.25$ ... (lbf/ft^2) Wet concrete load (Load Group 2)

$ConcreteBuildup = 50$ ... (lbf/ft) Concrete buildup (for each girder, LG2)

$SIPforms = 20$ ... (lbf/ft^2) Stay-in-place formwork pressure load (LG2)

$OverhangForms = 10$ ... (lbf/ft^2) Overhang formwork pressure load (LG2)

$OHbracketSelfWt = 167$ ... (lbf) Overhang bracket self-weight of a single bracket (LG2) (Note: based on material and overhang bracket dimensions)

Load Group 2 loads

To predict $V_{EXT\,LG2}$

Convert 3D loads to equivalent one dimensional loads

Equivalent Load Group 2 loads

Span length

$V_{STATIC\,LG2}$

$V_{EXT\,LG2}$ $V_{EXT\,LG2}$

Note: Equivalent Load Group 2 loads include overhang bracket self-weight

Quantify $V_{STATIC\,LG2}$ <u>using a static analysis with the deck fully placed...</u>

DeckLength $= L = 180$ ... (ft) Length of fully placed deck

<u>Collapse construction LG2 loads to equivalent one-dimensional loads ...</u>

EquivConcrete $=$ WetConcrete·DeckWidth $\div\ 1000 = 4.675$ ... (kip/ft) Converted pressure load (psf) to equivalent line load

EquivBuildup $=$ ConcreteBuildup·N $\div\ 1000 = 0.25$ ... (kip/ft) Concrete buildup for all girders to equivalent line load

EquivSIPforms $=$ SIPforms·FormWidth $\div\ 1000 = 0.4$ ... (kip/ft) Converted pressure load (psf) to equivalent line load

$$\text{EquivOverhangForms} = \text{OverhangForms}\cdot\left[2\cdot\left(\text{OH} - \frac{48}{2}\cdot\frac{1}{12} + \frac{2.5}{12} + \frac{24}{12}\right)\right]\div\ 1000 = 0.084$$

... (kip/ft) Converted pressure load (psf) to equivalent line load for overhang formwork (based on deck overhang width)

$$\text{NumBrackets} = 2\cdot\left(\frac{L}{5} + 1\right) = 74$$

... Total number of overhang brackets
(assumed at 5 ft spacing and at each end)

$$\text{EquivOHbrackets} = \frac{\text{NumBrackets}\cdot\text{OHbracketSelfWt}\div\ 1000}{L} = 0.069$$

... (kip/ft) Total bracket weight converted to equivalent line load

<u>Quantify reactions ...</u>

RxnA $=$ (EquivConcrete $+$ EquivBuildup $+$ EquivSIPforms $+$ EquivOverhangForms $+$ EquivOHbrackets)·L $\div\ 2 = 493$

... (kips) Reaction at End A

<u>Define ...</u> $V_{STATIC\,LG2}$

$V_{STATIC\,LG2} =$ RxnA $= 493$ ... (kips) Maximum reaction using a static analysis

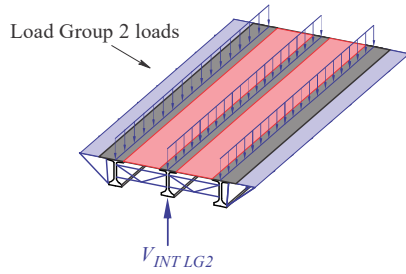<u>Quantify the exterior girder end shear force distribution factor ...</u>

Select a desired exceedance level: $\beta = 0.12$ to achieve a 95% exceedance level

$$\text{DF}_{V\,\text{EXT}\,LG2} = (1 + \beta)\cdot\left[-0.01 + (0.78\cdot N)^{-0.93}\cdot(0.91\cdot L)^{0.06}\cdot\left(0.81\cdot\frac{\text{OH}}{\text{S}}\right)^{0.36}\right] = 0.286$$
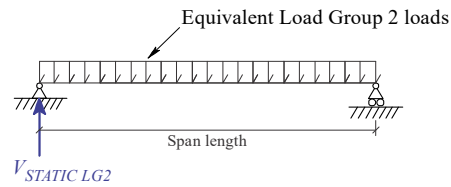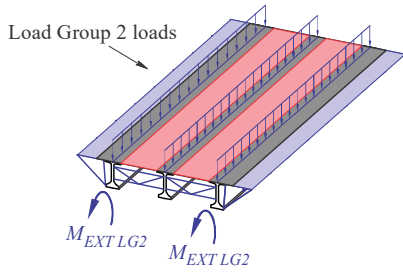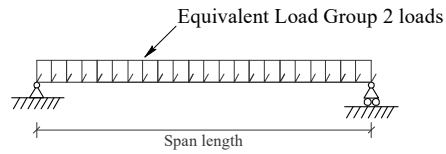
... LG2 exterior girder end shear force distribution factor

<u>Compute the exterior girder end shear force prediction ...</u>

$V_{EXT\,LG2} = V_{STATIC\,LG2}\cdot\text{DF}_{V\,\text{EXT}\,LG2} = 140.9$ ... (kips) LG2 exterior girder end shear force prediction

106

Load Group 2 loads

$V_{INT\,LG2}$

To predict $V_{INT\,LG2}$

Convert 3D loads to equivalent one dimensional loads

Equivalent Load Group 2 loads

Span length

$V_{STATIC\,LG2}$

Note: Equivalent Load Group 2 loads include overhang bracket self-weight

Quantify $V_{STATIC\,LG2}$ using a static analysis with the finishing machine load located at one end...

As shown above, $V_{STATIC\,LG2} = RxnA = 493$ ... (kips) Maximum reaction using a static analysis

Quantify the interior girder end shear force distribution factor ...

Select a desired exceedance level: $\beta = 0.17$ to achieve a 95% exceedance level

$$DF_{V\,INT\,LG2} = (1 + \beta)\cdot\left[0.03 + (0.89\cdot N)^{-1.08}\cdot(1.04\cdot L)^{0.04}\cdot\left(10.16\cdot\frac{OH}{S}\right)^{-0.16}\right] = 0.261$$

... LG2 interior girder end shear force distribution factor
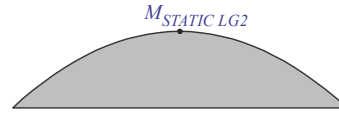
Compute the interior girder end shear force prediction ...

$V_{INT\,LG2} = V_{STATIC\,LG2}\cdot DF_{V\,INT\,LG2} = 128.7$ ... (kips) LG2 interior girder end shear force prediction

Load Group 2 loads

To predict $M_{EXT\,LG2}$

Convert 3D loads to equivalent one dimensional loads

Equivalent Load Group 2 loads

Span length

Note: Equivalent Load Group 2 loads include overhang bracket self-weight

$M_{EXT\,LG2}$ $M_{EXT\,LG2}$

$M_{STATIC\,LG2}$

Quantify $M_{STATIC\,LG2}$ using a static analysis with the deck fully placed...

DeckLength $= L = 180$ ... (ft) Length of fully placed deck

Collapse construction LG2 loads to equivalent one-dimensional loads ...

EquivConcrete $=$ WetConcrete·DeckWidth $\div 1000 = 4.675$ ... (kip/ft) Converted pressure load (psf) to equivalent line load

EquivBuildup $=$ ConcreteBuildup·N $\div 1000 = 0.25$ ... (kip/ft) Concrete buildup for all girders to equivalent line load

EquivSIPforms $=$ SIPforms·FormWidth $\div 1000 = 0.4$ ... (kip/ft) Converted pressure load (psf) to equivalent line load

EquivOverhangForms $=$ OverhangForms$\cdot\left[2\cdot\left(OH\cdot12 - \dfrac{48}{2} + 2.5 + 24\right)\cdot\dfrac{1}{12}\right] \div 1000 = 0.084$

... (kip/ft) Converted pressure load (psf) to equivalent line load for overhang formwork (based on deck overhang width)

NumBrackets $= 2\cdot\left(\dfrac{L}{5} + 1\right) = 74$

... Total number of overhang brackets
(assumed at 5 ft spacing and at each end)

EquivOHbrackets $= \dfrac{\text{NumBrackets·OHbracketSelfWt} \div 1000}{L} = 0.069$

... (kip/ft) Total bracket weight converted to equivalent line load

Quantify reactions ...

RxnA $=$ (EquivConcrete $+$ EquivBuildup $+$ EquivSIPforms $+$ EquivOverhangForms $+$ EquivOHbrackets)·L $\div 2 = 493$

... (kips) Reaction at End A

Define ... $M_{STATIC\,LG2}$

$w =$ EquivConcrete $+$ EquivBuildup $+$ EquivSIPforms $+$ EquivOverhangForms $+$ EquivOHbrackets $= 5.478$

... (kip/ft) Total equivalent LG2 line load

$M_{STATIC\,LG2} = (w)\cdot L^2 \div 8 = 22185$ ... (kip-ft) Maximum moment using a static analysis

<u>Quantify the exterior girder maximum moment distribution factor ...</u>

Select a desired exceedance level: $\beta = 0.15$ to achieve a 95% exceedance level
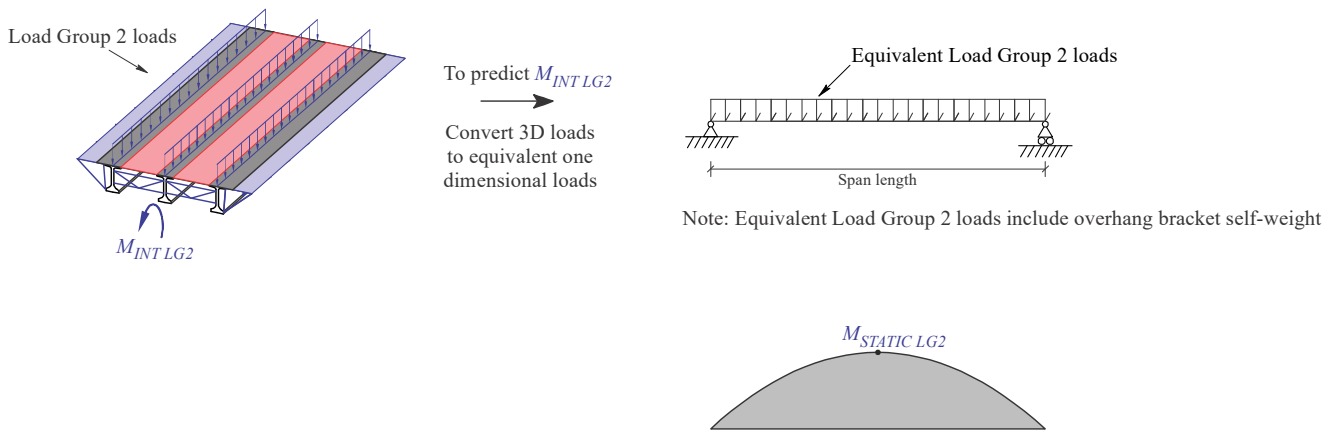
$$DF_{M\ EXT\ LG2} = (1 + \beta) \cdot \left[-0.06 + (1.66 \cdot N)^{-0.77} \cdot (2.29 \cdot L)^{-0.01} \cdot \left(24.58 \cdot \frac{OH}{S} \right)^{0.17} \right] = 0.250$$

... LG2 exterior girder maximum moment distribution factor

<u>Compute the exterior girder maximum moment prediction ...</u>

$M_{EXT\ LG2} = M_{STATIC\ LG2} \cdot DF_{M\ EXT\ LG2} = 5540$ ... (kip-ft) LG2 exterior girder maximum moment prediction

Load Group 2 loads

$M_{INT\ LG2}$

To predict $M_{INT\ LG2}$

Convert 3D loads to equivalent one dimensional loads

Equivalent Load Group 2 loads

Span length

Note: Equivalent Load Group 2 loads include overhang bracket self-weight

$M_{STATIC\ LG2}$

<u>Quantify</u> $M_{STATIC\ LG2}$ <u>using a static analysis with the deck fully placed...</u>

As shown above, $M_{STATIC\ LG2} = 22185$ ... (kip-ft) Maximum moment using a static analysis

<u>Quantify the interior girder maximum moment distribution factor ...</u>

Select a desired exceedance level: $\beta = 0.11$ to achieve a 95% exceedance level

$$DF_{M\ INT\ LG2} = (1 + \beta) \cdot \left[0.01 + (0.72 \cdot N)^{-1.09} \cdot (18.19 \cdot L)^{0.01} \cdot \left(14.01 \cdot \frac{OH}{S} \right)^{-0.16} \right] = 0.233$$

... LG2 interior girder maximum moment distribution factor

<u>Compute the interior girder maximum moment prediction ...</u>

$M_{INT\ LG2} = M_{STATIC\ LG2} \cdot DF_{M\ INT\ LG2} = 5179$ ... (kip-ft) LG2 interior girder maximum moment prediction

APPENDIX F
DETAILED ILLUSTRATIONS:
DISTRIBUTION FACTORS FOR CASES WITH INTERIOR BRACING

Presented in this appendix is an illustration of why the number of braces—which may influence the distribution of load between interior and exterior girders—was omitted from the final *DF* equation [i.e., Eqn. (7.17)] as a parameter. For Load Group 1, finishing machine and worker line loads are applied to the lateral extremities of the bridge by means of the overhang brackets. The Load Group 1 loads applied (indirectly) to the exterior girders are noticeably different from the uniform live load that is applied (indirectly) to the interior girders. Due to the eccentric nature of the finishing machine and worker line loads, the presence of additional interior bracing can influence the amount of load that is distributed from exterior to interior girders. That is, adding additional interior braces increases the transfer (distribution) of the lateral-extremity loads to interior girders. The loading condition where the number of braces is typically most influential occurs when the finishing machine load is applied at the midspan. In this condition, the finishing machine is at the furthest possible distance from the end-span bracing, thus reducing the influence of the end-span braces and increasing the influence of interior braces. To illustrate the influence of interior bracing on distribution factors, the calculation of maximum exterior girder moments for Load Group 1 (see Figure F.1) is given focus in this appendix.
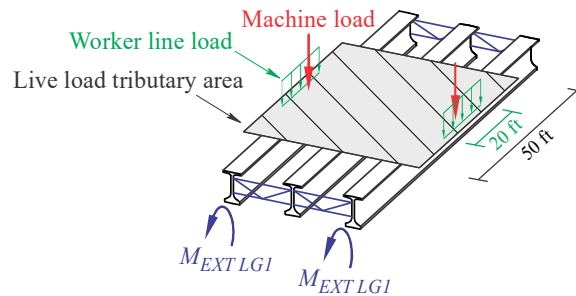
Figure F.1 Load Group 1 loads with the finishing machine located at the midspan to produce maximum girder moments

In the distribution factor parametric study carried out in this project, the number of brace points ranged from two (2) (i.e., only end-span bracing) to five (5) (i.e., quarter-point bracing). For each choice of 'number of braces', three (3) different bracing 'material-configuration' combinations were considered:

- Timber X-bracing
- Steel X-bracing
- Steel K-bracing

As a result, for a single bridge configuration (i.e., a system defined by single parameter values for span length, girder depth, skew angle, overhang width, girder spacing, and number of girders), twelve (12) possible bracing arrangements were considered in the distribution factor parametric study (see Figure F.2).
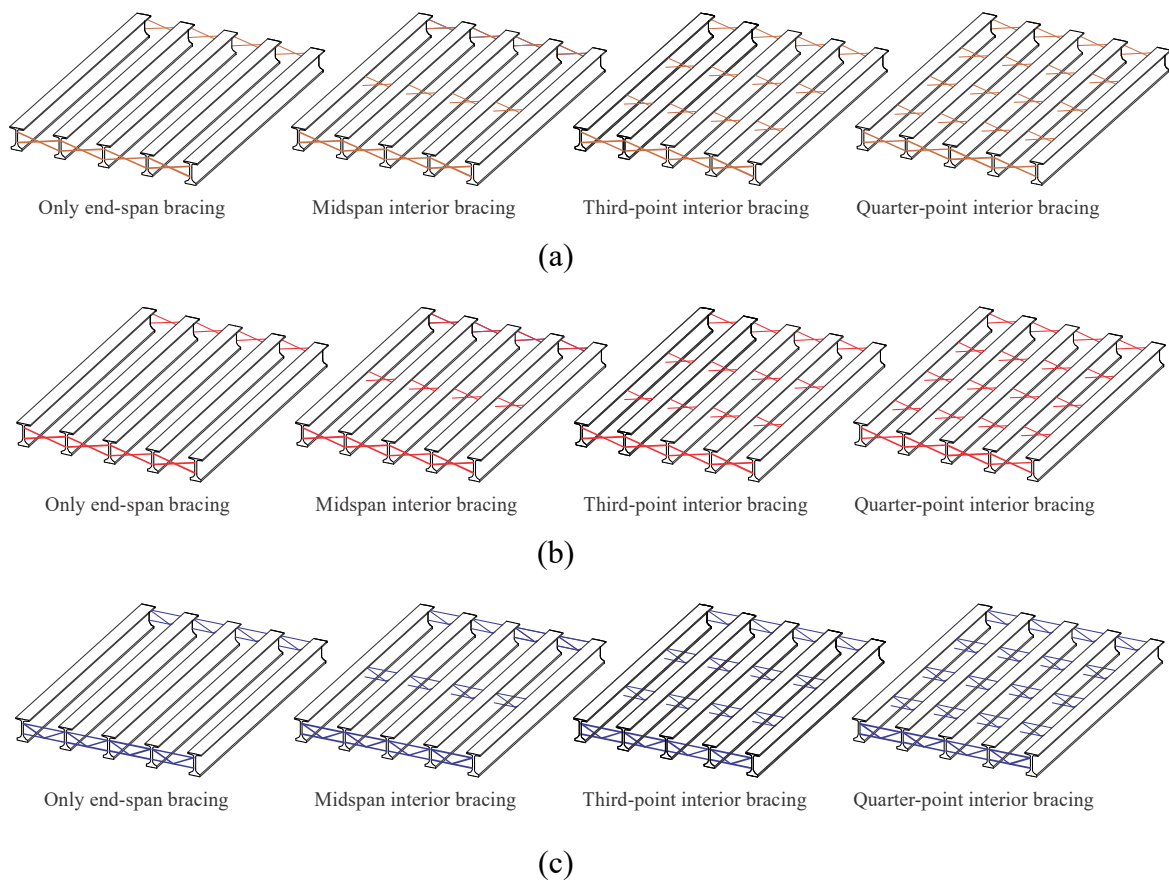
Only end-span bracing · Midspan interior bracing · Third-point interior bracing · Quarter-point interior bracing

(a)

Only end-span bracing · Midspan interior bracing · Third-point interior bracing · Quarter-point interior bracing

(b)

Only end-span bracing · Midspan interior bracing · Third-point interior bracing · Quarter-point interior bracing

(c)

Figure F.2 Brace configurations considered in the parametric study for 5-girder bridge systems with: (a) Timber X-bracing; (b) Steel X-bracing; (c) Steel K-bracing

To illustrate how load distribution within a bridge system varies as the number of braces is increased, the following baseline bridge configuration was selected:

- Five (5) 78" FIBs
- 180-ft span lengths
- 6-ft girder spacings
- 25-in. deck overhang widths
- 0-deg. skew angle
- Load Group 1 loads applied with the finishing located at the midspan

With these parameter choices fixed, four (4) different bracing conditions were selected for depiction:

- With only end-span bracing
- With *timber* end-span and midspan X-bracing
- With *steel* end-span and midspan X-bracing
- With *steel* end-span and midspan K-bracing

These cases are shown in Figures F.3-F.6 and the corresponding bridge system responses for each case—depicted as the midspan deflection for the girder system cross-section—are shown in Figures F.7-F.10. Midspan deflections for the end-span bracing case were found to be essentially the same for all three of the bracing material-configuration combinations, and as a result, the material (steel or timber) and bracing configuration (X- or K-brace) was not included in the description.

111

Theoretically, loads applied to a bridge girder system will be more evenly distributed among exterior and interior girders as interior bracing points are introduced. For the end-span-only bracing case, bracing stiffness provided to the girder system is not sufficient to distribute loads—which are located at the midspan and the lateral extremities—to interior girders. Therefore, loads at the extremities are carried solely by the exterior girders, and midspan deflections of the exterior girders are larger, relative to the interior girders (Figure F.7). With the addition of an interior midspan bracing point, exterior and interior girders are integrated together as a system. However, as shown in Figures F.8-F.10, significant load sharing only occurs when there is sufficient brace stiffness. That is, addition of a timber X-brace—the lowest stiffness brace type considered in the parametric study—at midspan provides a minimal change in load distribution and reduction of displacement for the exterior girders. In contrast, addition of a steel K-brace—the highest stiffness brace type considered in the parametric study—at midspan effectively redistributes loads at the extremities to interior girders, reducing the difference in displacement between exterior and interior girders (as shown in Figure F.10). In Figure F.11, responses are shown for all twelve (12) of the bracing arrangements considered in this study.

As noted in Chapter 7, a *culled dataset* was used in development of the recommended distribution factor equations. However, it is beneficial to illustrate the level of conservatism present in the empirical prediction of exterior girder maximum moment over the *full data set* as well. In Figure F.12, normalized errors of exterior girder moment (computed using the proposed $DF_{M\,EXT\,LG1}$ equation with: 95% exceedance; Table 7.3; β=0.08) are shown for the full data set, that is—all structural configurations; finishing machine at midspan; 36,288 cases. These data were then separated into groups corresponding to the three different bracing material-configuration combinations considered (i.e., steel K-bracing, steel X-bracing, and timber X-bracing (12,096 cases each). These data were further separated into sub-groups consisting of: *i*) cases with interior bracing at typical span lengths, and *ii*) cases with end-span bracing only, or with shorter-than-typical span lengths. At 'shorter-than-typical' span lengths (i.e., span lengths less than 90 ft), the uniform live load in Load Group 1 acts over nearly the entire span length (Figure F.13) resulting in a response that differs from that which occurs at more typical span lengths (see Figure F.14).

For the typical bridge configuration selected for illustration, and superimposed Load Group 1 (with finishing machine located at midspan), the distribution of maximum moment among exterior and interior girders is shown in Figures F.15-F.17. Normalized prediction errors in exterior girder moment, computed using the proposed $DF_{M\,EXT\,LG1}$ equation (95% exceedance; Table 7.3; β=0.08), are further separated into three groups based on brace stiffness. As illustrated in Figures F.15-F.17, a moderate increase in prediction-conservatism is observed for cases with interior bracing, but only for the steel bracing cases. Additionally, the degree of prediction-conservatism is smaller for steel X-bracing than steel K-bracing, due to the lower stiffness of steel X-braces as compared to steel K-braces. Overall, differences in the conservatism of moment prediction for timber X-braced bridges versus steel K-braced bridges was not sufficient (~10%-20%) to warrant introducing additional terms (number of braces, brace stiffness) into the recommended distribution factor equations.
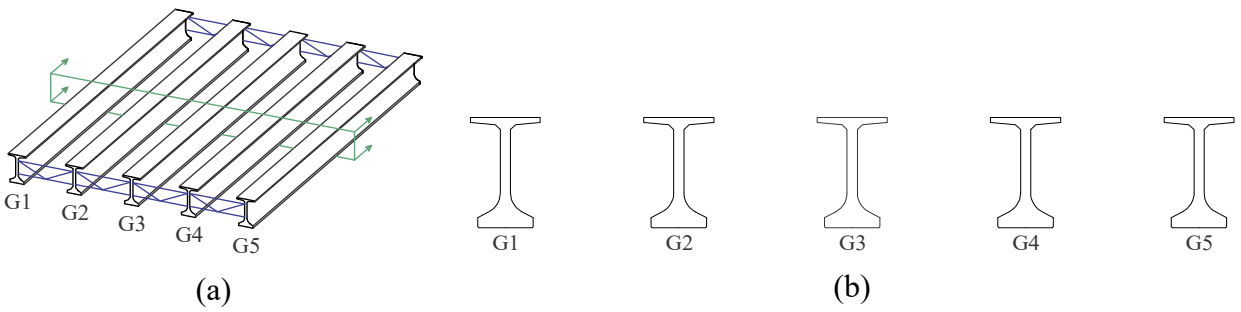
(a) (b)

Figure F.3 Bridge cross-section with only end-span bracing: (a) Isometric view;
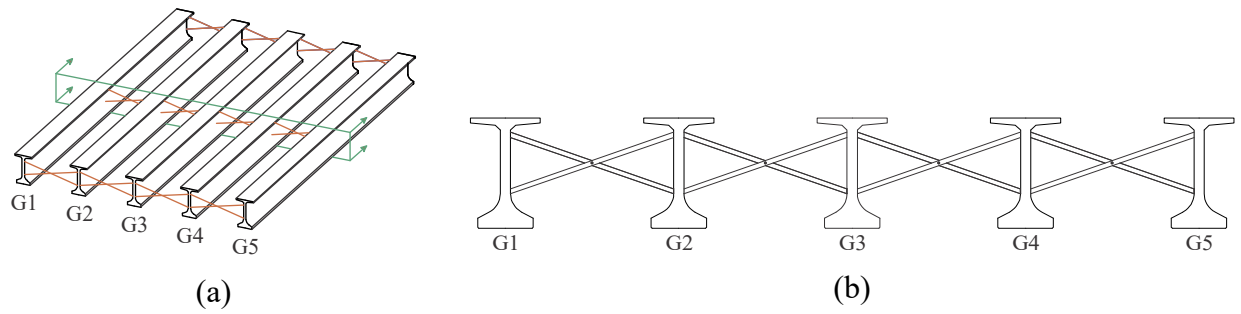(b) Cross-section at the midspan

(a) (b)

Figure F.4 Bridge cross-section with interior midspan *timber* X-bracing: (a) Isometric view;
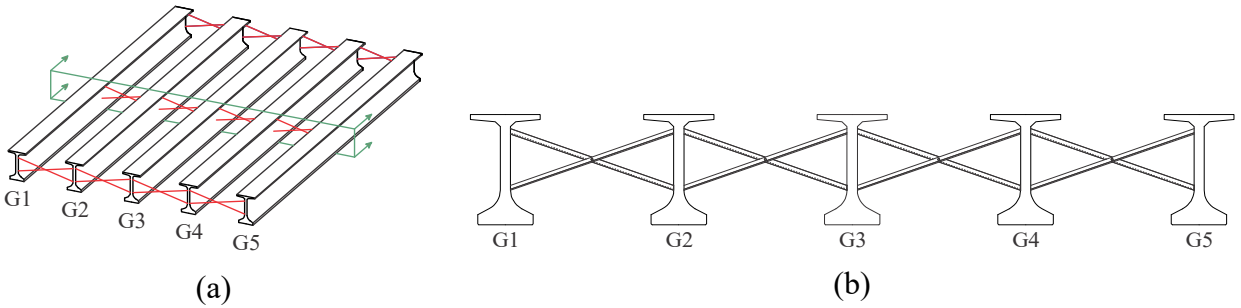(b) Cross-section at the midspan

(a) (b)

Figure F.5 Bridge cross-section with interior midspan *steel* X-bracing: (a) Isometric view;
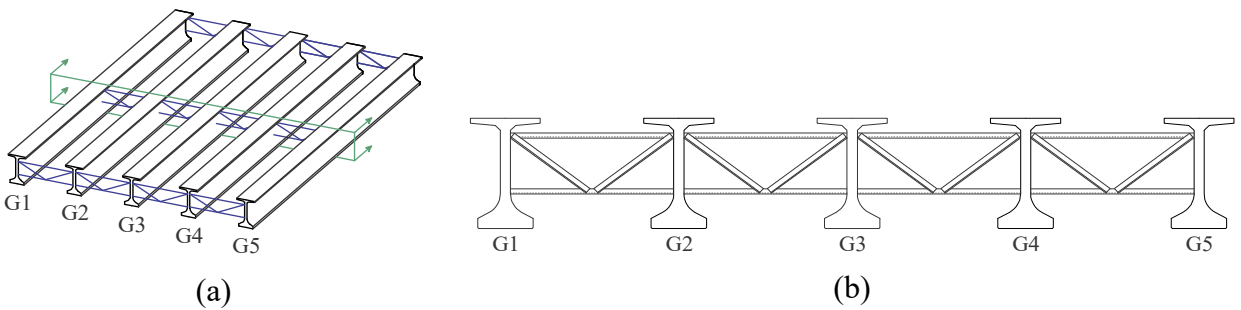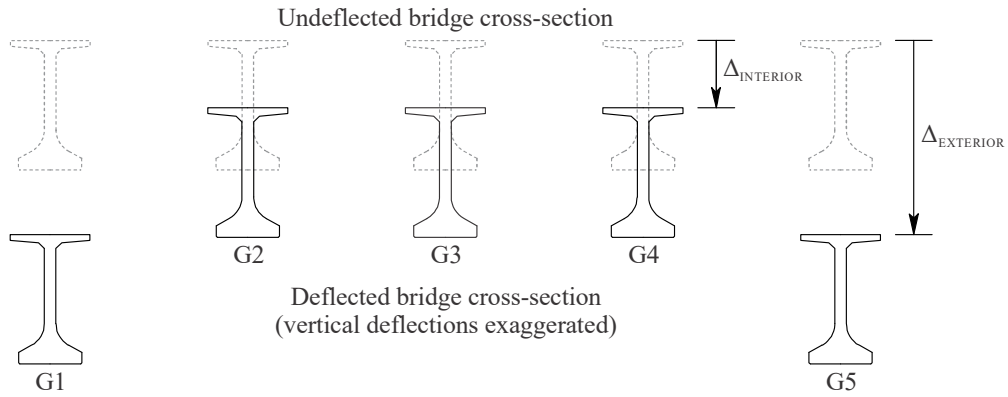(b) Cross-section at the midspan

(a) (b)

Figure F.6 Bridge cross-section with interior midspan *steel* K-bracing: (a) Isometric view;
(b) Cross-section at the midspan

Undeflected bridge cross-section

Figure F.7 Bridge cross-section midspan deflection without interior bracing
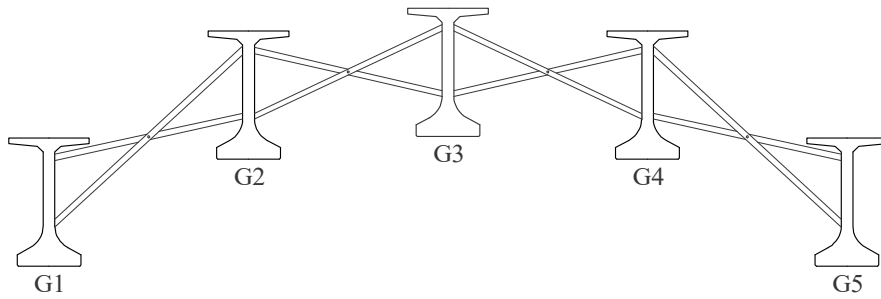
Figure F.8 Bridge cross-section midspan deflection with interior timber X-bracing
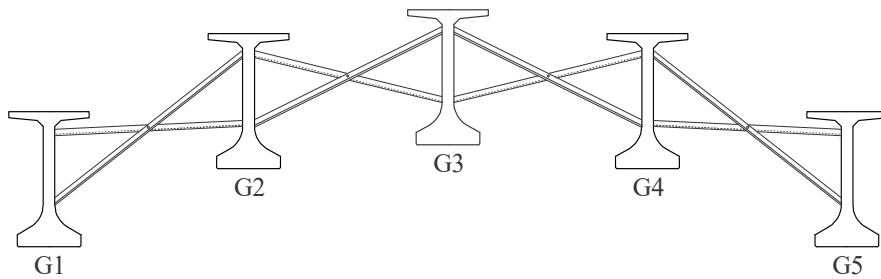
Figure F.9 Bridge cross-section midspan deflection with interior steel X-bracing
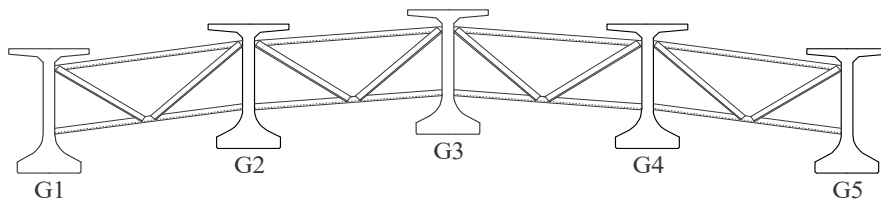
Figure F.10 Bridge cross-section midspan deflection with interior steel K-bracing
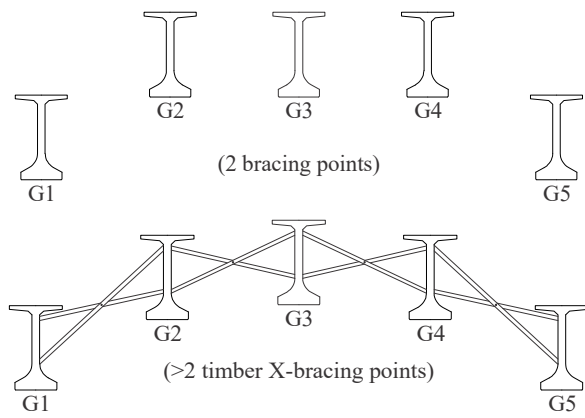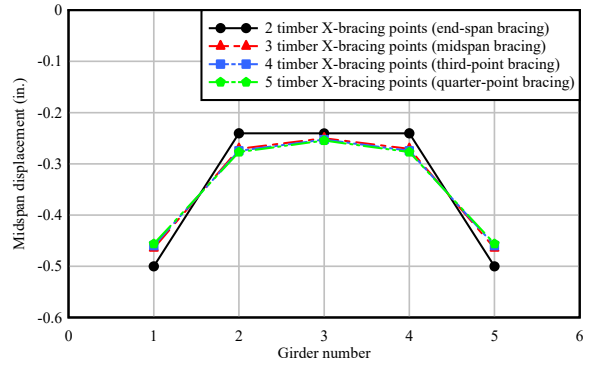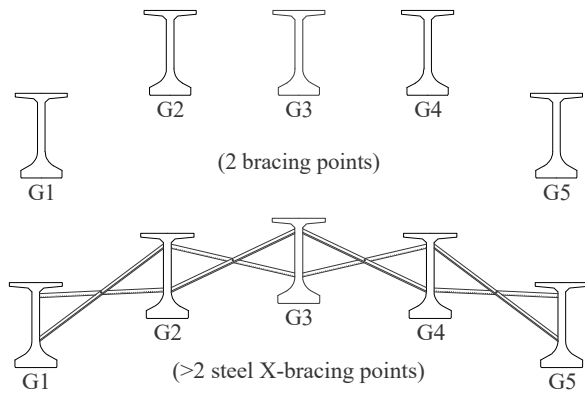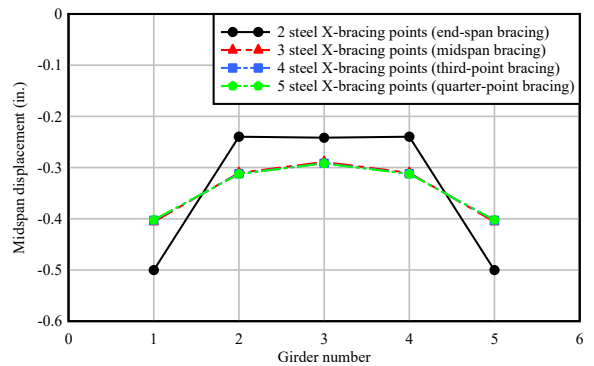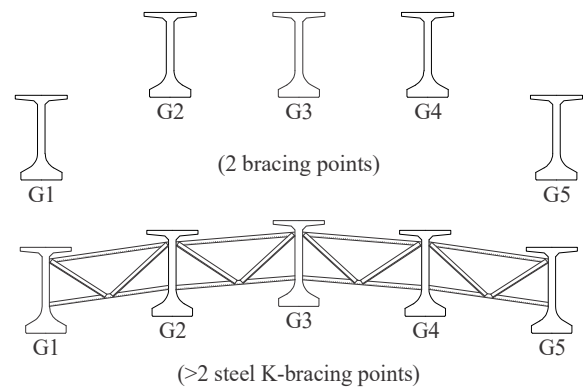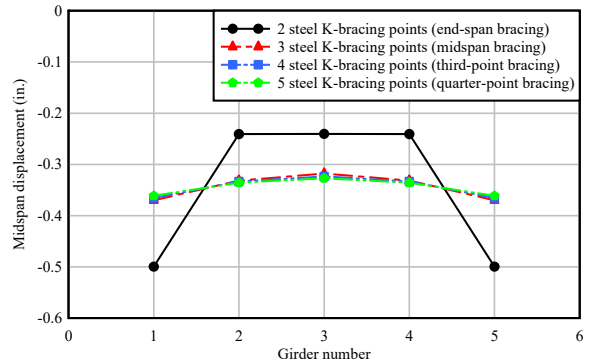
Figure F.11 5-girder, FIB78, 180-ft span, 6-ft girder spacing, 25-in. deck overhang, 0-deg. skew bridge configuration: (a) deformed shapes for timber X-bracing; (b) midspan displacement quantities for timber X-bracing; (c) deformed shapes for steel X-bracing; (d) midspan displacement quantities for steel X-bracing; (e) deformed shapes for steel K-bracing; (f) midspan displacement quantities for steel K-bracing
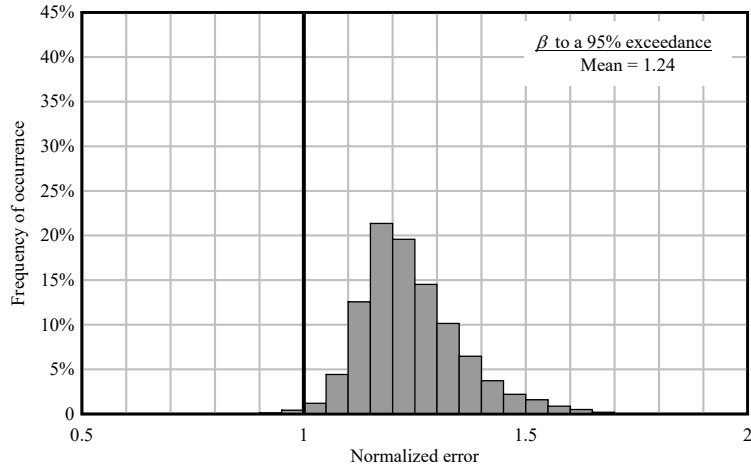
Figure F.12 Moment ($M_{EXT\ LG1}$) prediction error for all bridge configurations (36,288 cases) using $DF_{M\ EXT\ LG1}$ in conjunction with a static beam analysis, shifted with β to a 95% exceedance
Note: bridge configurations include different brace materials and configurations
(i.e., steel K-bracing, steel X-bracing, and timber X-bracing are separate bridge configurations)
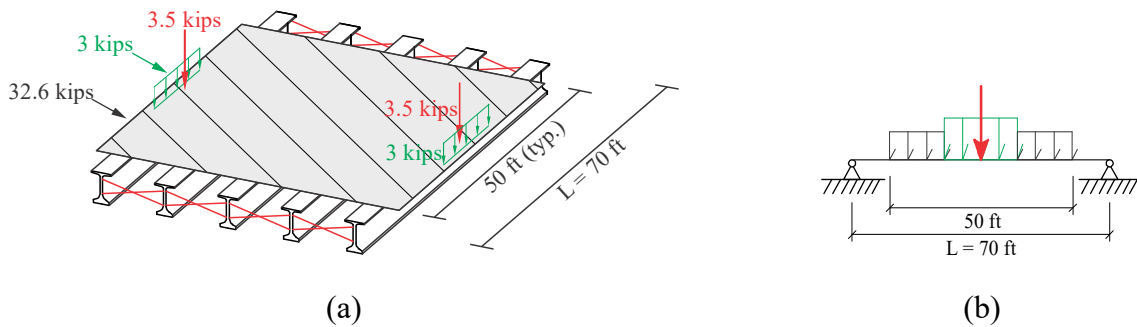
Figure F.13 Load Group 1 loads applied at the midspan for a 'shorter-than-typical' span length:
(a) Isometric view; (b) Elevation view
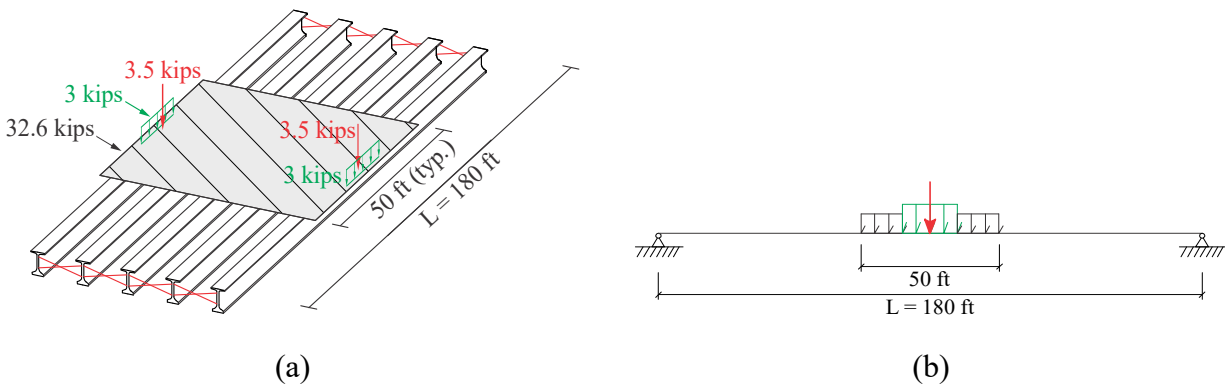
Figure F.14 Load Group 1 loads applied at the midspan for a typical span length:
(a) Isometric view; (b) Elevation view

116
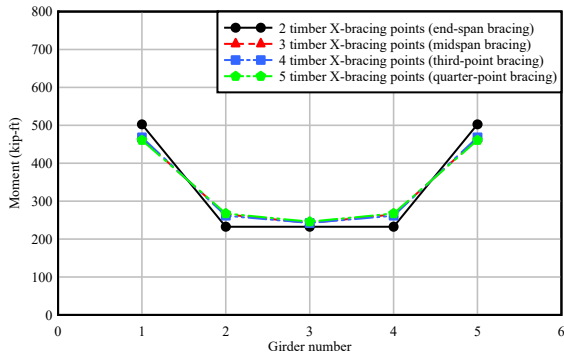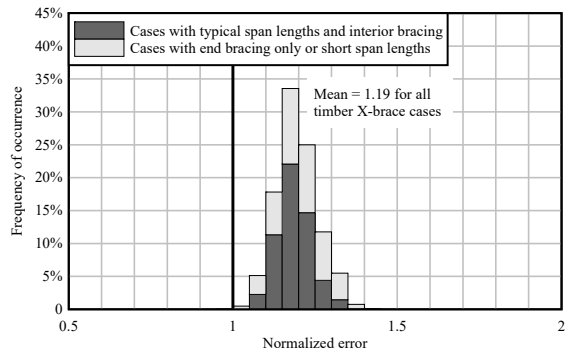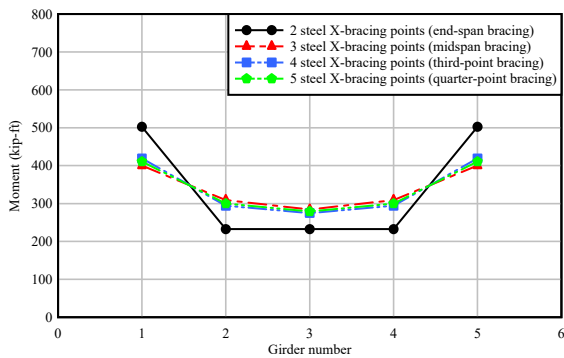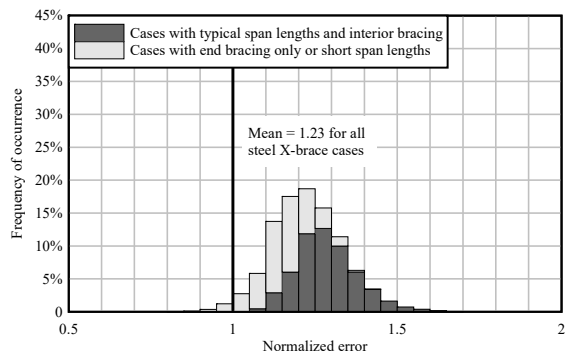
Figure F.15 Timber X-bracing cases: (a) Moment for each girder at the midspan for the typical bridge configuration; (b) Moment ($M_{EXT\,LG1}$) prediciton for the timber X-brace data set using $DF_{M\,EXT\,LG1}$ in conjunction with a static beam analysis, shifted with β to a 95% exceedance
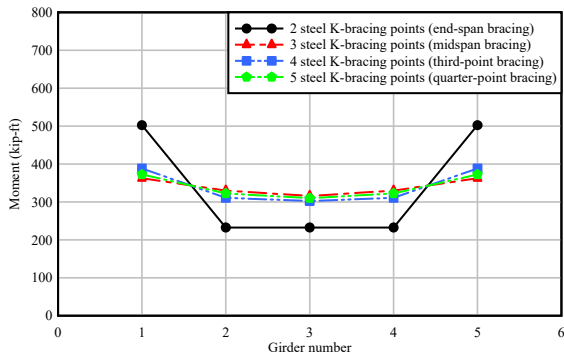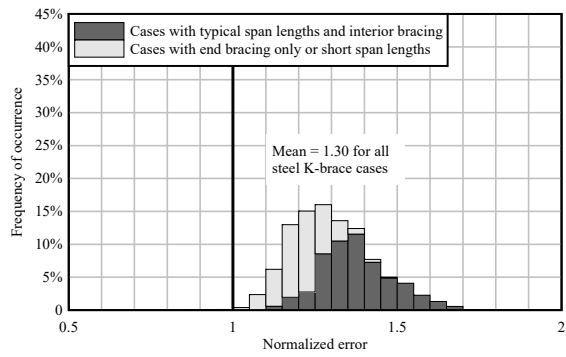

Figure F.16 Steel X-bracing cases: (a) Moment for each girder at the midspan for the typical bridge configuration; (b) Moment ($M_{EXT\,LG1}$) prediciton for the steel X-brace data set using $DF_{M\,EXT\,LG1}$ in conjunction with a static beam analysis, shifted with β to a 95% exceedance

Figure F.17 Steel K-bracing cases: (a) Moment for each girder at the midspan for the typical bridge configuration; (b) Moment ($M_{EXT\,LG1}$) prediciton for the steel K-brace data set using $DF_{M\,EXT\,LG1}$ in conjunction with a static beam analysis, shifted with β to a 95% exceedance